AD_296 176

63-2-4

COSMIC RAY GROUP

Department of Physics

UNIVERSITY OF CALIFORNIA

BERKELEY

A Study of Ionospheric Absorption Produced by Solar Cosmic Rays.

Robert Anthony Weir, Jr.

AF 49(638)-873

ABSTRACT

The absorption of cosmic radio noise in the lower inosphere due to the arrival of solar cosmic rays has been calculated for several locations at the high magnetic latitudes. The calculation was made in three parts; the volume production rate of electrons from ionization, the equilibrium electron density resulting from the competition between production and recombination processes, and the absorption of electro magnetic radiation passing through the ionized region. The calculation was made for proton energy spectra in the form of power law as observed by balloon-borne detectors following large solar flares. The calculated absorption was compared with observations obtained by riometers (relative ionospheric opacity meter) at Point Barrow, Fort Yukon, College, and Farewell, Alaska.

For the solar proton event of July 14, 1959, the calculated absorption based on balloon data does not agree in magnitude nor latitude variation with the observations obtained by the Alaskan riometers. The lack of agreement in absolute magnitude indicates that the atmospheric coefficients used in obtaining the equilibrium electron density are in error. In particular, the collisional detachment as well as electron attachment coefficients appear to require considerable revision. The lack of agreement in the latitude variation substantiates observations at rocket altitude which indicate that the power law energy spectrum flattens considerably at proton energies below 100 Mev.

TABLE OF CONTENTS

TABLE OF CONTENTS (continued)

CHAPTER I

Introduction

For years it has been known that a direct correlation exists between enhanced solar activity and changes in terrestrial radio wave propagation. A familiar effect is the increase in the critical frequencies of the E, F1 and F2 layers and stronger absorption in the D layer during the period of the sun spot maximum. More dramatic changes in terrestrial radio propagation are often associated with flare activity on the sun. The Short Wave Fadeout that occurs on the sunlit side of the earth following a solar outburst has been attributed to an increase in the free-electron content of the absorbing layer of the ionosphere. This, in turn, is caused by the ionizing action of a flux of electromagnetic radiation from the solar chromosphere having frequencies in the extreme ultraviolet and soft X-rays bands. Radio transmission "blackouts" occurring in the polar regions are often associated with magnetic storms. In some cases a transmission blackout may be caused by a lowering of the critical frequency of the reflecting layers with the consequent failure of the ionosphere to return signals earthward that orginarily would be reflected. Impaired radio transmission also can result from increased ionization in the absorptive regions of the polar ionosphere. Blackouts of this type are associated with magnetic storms which are due to solar flares, the primary ionizing agent in this case being a swarm of low-energy particles impinging upon the upper atmosphere. These particles are able to reach the earth's atmosphere because the normal Störmer cutoff mechanism has been rendered ineffective by the magnetic storm.

Magnetic storms due to solar flares usually commence one to two days following the onset time of the flare; however, it has been noticed that an increased ionospheric opacity can develop well before the terrestrial magnetic field shows signs of any severe disturbance. Because the geographical

distribution of the ionospheric region of enhanced absorptive power is limited to the geomagnetic polar regions in these events, the change in character of the upper atmosphere must be due to the ionizing action of charged particles. These particles, however, must be much more energetic than those which comprise the swarm associated with a magnetic storm, if a geomagnetic cutoff mechanism is operative. It has been found that the increase in ionospheric opacity and consequent radio blackout occurring after the optical sighting of the solar flare (but well before the onset of the magnetic storm) is due to the ionizing action of the influx of solar cosmic rays resulting from the flare. These cosmic rays are now known to consist mainly of protons and, to a much lesser extent, alpha particles having energies from about 50 Mev to 1 Bev. The role of solar cosmic rays in the production of radio blackout effects, in contrast to the action of the other agents mentioned, has been only recently recognized, and extensive study of this phenomenon has been confined to the past three or four years. (1,2,3,4)

In 1953 Mitra and Shain (5) originated the cosmic radio noise technique for obtaining a measure of the increase in opacity of the upper atmosphere resulting from various solar and terrestrial disturbances. A cosmic radio noise flux is incident continuously upon the earth from the galaxy and is subject to continuous monitoring. The cosmic radio noise serves in the capacity of a continuous probe of the ionosphere and the received cosmic noise power is a quantitative indicator of the electronic content of its lower reaches. A special receiving system has been devised to monitor the cosmic noise level at a given frequency. This instrument, called a riometer, will be discussed more fully in a later section of this thesis. It suffices to say at this point that the riometer can provide direct information as to the absorbing power of the upper atmosphere.

During the years 1957 to 1960, which spanned the last solar maximum, efforts were made to identify the energetic particles emitted by the sun as a result of a disturbance on its surface, and to obtain energy spectra of the corpuscular radiation. This task is considerably more difficult than the collection of cosmic radio noise absorption data as balloon-borne counters had to be aloft during the time of the event. The majority of particle-producing solar flares expel relatively low-energy cosmic rays. These stop at balloon heights or higher in the atmosphere and cannot be detected on the ground. Moreover, the influx is confined to the geomagnetic polar regions by the earth's magnetic field. Relatively few stations exist in these regions which are equipped with the necessary facilities to carry out this type of measurement. However, the solar cosmic ray energy spectrum is a directly measurable quantity. The interaction between the solar particles and the earth's atmosphere can be considered the cause of the observed cosmic noise absorption.

The facts set forth above may lead one to pose the following question: given the solar cosmic ray energy spectrum, a quantity directly derivable from measurement, can a calculation be performed that will yield the observed absorption of cosmic radio noise? Such a calculation, to be successful, must correctly predict the electron production rate in the atmosphere due to the ionizing action of the solar cosmic rays, and must correctly account for the various electron recombination processes present. In the sections that follow an account is given of such a calculation, the results obtained are discussed and compared with cosmic ray and cosmic radio noise absorption data taken during a solar proton event.

CHAPTER II

The calculation of the vertical attenuation of cosmic radio noise at a given geographic location during a solar flare event was performed in three

principal steps: The rate of production of free electrons in the atmosphere due to ionizing encounters between the solar cosmic rays and the constituent molecules of the atmosphere, the equilibrium electron density resulting from the interplay between the primary ionizing process and the several recombination and secondary electron production mechanisms, and the specific attenuation of cosmic radio noise for a given radio frequency due to electron-neutral collisions throughout the atmosphere. An integration of the specific attenuation over the range of atmospheric heights gives the total vertical attenuation of cosmic radio noise.

The Electron Production Rate

The strong attenuation of radio waves often observed following a solar flare suggests that the atmosphere is rendered conducting in regions where the electron collision frequency is relatively large. Because electromagnetic radiations from the sun capable of ionizing N_2 and O_2 are strongly absorbed at heights of 85 km or higher (6), the production of free electrons deep in the atmosphere is due almost exclusively to the action of penetrating corpuscular radiation.

The number of primary electron-positive ion pairs formed by a fast, heavy, ionizing particle is directly proportional to the energy loss the particle suffers traversing a path in the atmosphere. The factor of proportionality, according to Rossi (7), for protons and α particles, is approximately 3.6×10^{-5} Mev/ion pair, a constant over an extended range of particle energies. The number of electron-ion pairs formed by an ionizing particle per cm of path at a height h is given by:

$$\frac{\rho(h)}{Q} \frac{dE}{dx}(E), \tag{2.1}$$

where dE/dx is the energy loss in Mev/gm cm^{-2} of the ionizing particle in air, $\rho(h)$ is the atmospheric density in gm/cm^3, and Q is the average energy in Mev required to form an electron-ion pair. Implicit in Eq. (2.1) is the assumption

that at all heights of interest (below 85-90 km) the relative proportion of the principal constituents of the atmosphere remains unchanged. That this seems to be the case follows from rocket measurements made of the atmosphere below the D layer performed in 1952 over White Sands, New Mexico, by groups from the University of Michigan and the University of Durham (U.K.). (8)

For computational purposes the altitude variation of air density as well as the pressure and electron collision frequency were taken from the work of Nicolet (9). The values for $\rho(h)$ given in Nicolet's paper differ very little from those given by the Rocket Panel (10), some eight years earlier.

The energy-loss curve used in this thesis was taken from the review article (11) by Bethe and Ashkin. Bailey (12), employing a different method for calculating the rate of production of electrons by solar cosmic ray particles, used as an energy-loss estimate at a given level in the atmosphere the residual particle range divided by its energy. Figure 1 exhibits the difference between the two loss curves for protons. It is seen that, except for stopping protons, Bailey's energy-loss values represent an over-estimate of the effect, exceeding those used in this paper by approximately a factor of two.

The number of electron-ion pairs formed in a unit volume at a height h is given by Eq. (2.1) multiplied by a weighting factor, $Y(E;\theta,\varphi,h)$, which depends on the particle spectrum of the particular event being analyzed, and integrated over the appropriate energy interval and solid angle:

$$q\left(\frac{\text{electrons}}{\text{cm}^3\text{-sec}}\right) = \int_{\Omega}\int_{E_m}^{\infty} \frac{\rho(h)}{Q}\,\frac{dE}{dx}(E)\; Y(E;\theta,\varphi,h)\; dE\; d\Omega \; . \qquad (2.2)$$

The quantity $Y(E;\theta,\varphi,h)$ appearing in the integrand represents the number of particles crossing unit area per second, having directions of incidence lying in unit solid angle centered about a direction fixed by local zenith and azimuth angles θ, φ, and having residual energies in unit energy range about E after

having penetrated to an atmospheric height, h. If it can be assumed that the ionizing particles, on the average, follow approximately rectilinear trajectories in the atmosphere, then this quantity is related to the integral energy spectrum which, in turn, can be derived from an integral range spectrum measurable by balloon-borne particle counters.

Such counters, while ascending into the upper atmosphere during a particle bombardment, record the number of energetic charged particles per second impinging upon them at a given height h (or at a given atmospheric depth, R). From these data, one can ascertain the number of particles crossing unit area at a height h per steradian, per second, having ranges in air equal to or in excess of the corresponding atmospheric depth R. By using the range-energy relationship in air for a given particle, one can obtain the corresponding integral energy spectrum, i.e., the number of particles crossing unit area per steradian, per second, initially having energies equal to or in excess of an energy E_i. This quantity will be designated $J(E_i)$.

Differential energy spectra derived from these observations bear a simple relationship to the weighting factor, $Y(E;\theta,\varphi,h)$ appearing in the integrand of Eq. (2.2).

$$Y(E;\theta,\varphi,h) = N(E_i) \ , \qquad (2.3)$$

where $N(E_i) = - \partial J/\partial E_i$.

E_i, the energy initially possessed by the particle, is now considered a function of the particle's residual energy, E, at height h and directions θ and φ, and is easily obtained for a given E and h from the range-energy relationship for the particle in air (11), and the known dependence of atmospheric depth on the height. (9)

The assumption of strict rectilinearity of the particle trajectories implied in Eq. (2.3) cannot be justified completely owing to the action of the earth's

magnetic field on the particle motion. However, the degree to which Eq. (2.3) represents a good approximation depends on the curvature imposed on the particle paths by the geomagnetic field. Accordingly, a separate investigation was made of the actual paths of fast protons in the atmosphere in the presence of a magnetic field, which, in the small, would approximate the terrestrial field. The results of this investigation, which justify the approximation represented by Eq. (2.3), will be described in detail later in this thesis.

At present it will be assumed that the influence of the earth's field on the particle trajectories can be neglected and that the integral in Eq. (2.2) can be rewritten:

$$q = \int_{\Omega} \int_{E_m}^{\infty} \frac{\rho(h)}{Q} \frac{dE}{dx} (E)\, N(E_i)\, dE\, d\Omega \,, \tag{2.4}$$

where $E_i = E_i(E,h,\theta,\varphi)$.

From balloon measurements during solar proton events (13,14,15), it has been shown that the integral energy spectra of solar particles can be represented by a power law:

$$J(> E_i) = KE_i^{-S} \,, \tag{2.5}$$

where K and S are independent of the energy, E_i. This result is valid over the energy interval from 80 to 400 Mev for protons. Accordingly $N(E_i)$ has a similar form:

$$N(E_i) = \alpha E_i^{-\gamma} \,, \tag{2.6}$$

where $S = \gamma - 1$, and $K = \alpha/(\gamma - 1)$. In the electron production rate calculation, the lower limit of the energy integral, E_m, is a function of the local polar angles, θ and φ, as well as the geomagnetic latitude, Φ. It is assumed in this study that during the solar particle bombardment, at least until the onset of the magnetic storm that usually follows such outbursts, the Störmer geomagnetic

cutoff (as modified by Quenby and Webber (16)) holds. Thus, on the centered-dipole approximation, the geomagnetic cutoff rigidity is given by:

$$P = \frac{M \cos^4\Phi}{R^2[1 + (1 - \sin\theta \sin\varphi \cos^3\Phi)^{1/2}]^2} , \qquad (2.7)$$

where P is the cutoff rigidity for particles of momentum p and charge Ze at geomagnetic latitude Φ, θ is the local zenith angle, and φ the local azimuth angle increasing clockwise from geomagnetic north, M is the earth's magnetic moment, and R the radial distance from the dipole center to the point of observation. For $\theta = 0$ (particles incident from the zenith direction), $R = R_o$, at the earth's surface (6.4×10^3 km) and $M = 8.06 \times 10^{25}$ gauss cm^3, this reduced to the well-known expression:

$$P_o = \frac{M}{4R_o^2} \cos^4\Phi = 14.8 \cos^4\Phi \text{ (BV)} . \qquad (2.8)$$

On the right-hand side of Eq. (2.7), for geomagnetic latitudes greater than 60 degrees, the minimum value the square of the term in brackets in the denominator can assume is $(1 + 0.94)^2 = 3.8$. It is actually always very close to 4.0. To a good approximation, therefore, at high geomagnetic latitudes, the lower limit of the energy integral, E_m, is independent of the local polar angles but depends only on the geomagnetic latitude so far as the Störmer cutoff is concerned. The cutoff rigidity given for vertical incidence, Eq. (2.8), as modified by Quenby and Webber, is used throughout the calculation presented in this paper.

Another factor in the determination of E_m is the earth's shadow cone. This effect, as given by Kasper (17), is incorporated into the solid-angle integration in the form of weighting factors for large zenith angles ($\theta > 70^\circ$). In other words, for zenith angles greater than 70 degrees directions bounded by "forbidden" angular sectors given in diagrams in Kasper's paper are considered devoid of incident particles. The use of weighting factors to account for the

earth's shadow cone and the employment of the vertical geomagnetic cutoff to account for the Störmer cutoff introduces a negligible error in the result and avoids the necessity of an integration over the aximuth angle. Subject to the above approximations, the value of q for a solar proton flux given by Eq. (2.4) now becomes:

$$q = \frac{\rho(h)}{Q} \int_0^{\theta \to \pi/2} \omega(\theta) \sin\theta \int_{E_m(\Phi)}^{\infty} \frac{dE}{dx}(E)\, N(E_i)\, dE\, d\theta \,, \qquad (2.9)$$

with $N(E_i) = \alpha E_i^{-\gamma}$. α and γ are constants related to the incident proton flux, $\omega(\theta)$ is the shadow cone weighting factor for protons ($\omega(\theta) = 2\omega$ for $\theta \leq 70^\circ$ and $\omega(\theta) < 2\pi$ for $\theta > 70^\circ$), and Φ is the geomagnetic latitude.

The integration to obtain q was carried out numerically for three trial proton differential energy spectra, with exponents $\gamma = 3$, 5, and 7, corresponding to integral energy spectra of the power-law type with exponents smaller by one unit.

For each of these spectra q was computed for every four kilometers of height in the atmosphere, from 32 to 100 km.

Electron production rate calculations were carried out for geomagnetic latitudes corresponding to geographic locations at which polar blackout absorption measurements are available. Accordingly, the integration was performed for the following Alaskan stations: Pt. Barrow, Ft. Yukon, College, and Farewell. The geomagnetic latitudes and cutoff energies for these locations are given in the following table:

Pt. Barrow	$\Phi = 68.8^\circ$	$E_c = 20.8$ Mev
Ft. Yukon	$\Phi = 66.9^\circ$	$E_c = 54.0$ Mev
College	$\Phi = 64.7^\circ$	$E_c = 112.0$ Mev
Farewell	$\Phi = 61.6^\circ$	$E_c = 261.5$ Mev

For all three differential energy spectra the normalizing constant α was chosen such that the corresponding integral flux of protons at College, Alaska,

was 100 particles $ster^{-1}$ cm^{-2} sec^{-1}. Thus,

$$\frac{\alpha}{\gamma - 1} (112)^{-(\gamma-1)} = 100, \qquad \text{for } \gamma = 3, 5, 7,$$

so that

$$\alpha = 2.51 \times 10^{6}, \qquad \text{for } \gamma = 3,$$
$$\alpha = 6.29 \times 10^{10}, \qquad \text{for } \gamma = 5,$$
$$\alpha = 1.18 \times 10^{15}, \qquad \text{for } \gamma = 7.$$

By using the same spectrum for each of the four locations listed above, the total vertical attenuation as a function of geomagnetic latitude was obtained.

The electron production rate for $\gamma = 3, 5, 7$ and $E_c = 112$ Mev (College, Alaska) for $J(> 112 \text{ Mev}) = 100$ are shown in Fig. 2 as a function of atmospheric height. It can be seen immediately that the production rate curves are almost identical for heights exceeding that which corresponds to the stopping depth of the protons with energies near the Störmer cutoff. For $E_c = 112$ Mev, the corresponding depth is 10.7 gm/cm^2 which occurs at a height of 31 kilometers.

Recent observations (18) of heavy nuclei, principally alpha particles, in solar flare radiation suggest that the role of alpha particles might be important in the ionospheric absorption events such as considered in this problem. While the abundance of alpha particles relative to protons is not well known at present, a trial calculation was carried out using similar rigidity spectra for the flare particles and a proton-alpha ratio of 10. The results of this calculation are shown in Fig. 3, where the electron production rate is given for a proton spectrum with $\gamma = 5$ and $J_p(112) = 100$, and an alpha particle spectrum with $\gamma = 4.73$, and $J_\alpha(119.5) = 10$. The two electron production rates are shown separately as well as their sum, representing the total electron production rate during a solar flare event with a significant alpha-particle content.

CHAPTER III

In the atmosphere above the lower boundary of the D region (which, to be definite, will be assumed to lie at about 90 km), the recombination of electrons is chiefly radiative and production and recombination processes are direct and simply competitive. In contrast to this, the region below ninety km is characterized by nonradiative recombination processes and by the formation of negative molecular ions. This is due to the fact that the atmosphere above ninety km does more than simply shield the lower atmosphere from ionizing radiation. That part of the solar spectrum that causes molecular photodissociation is also heavily absorbed (6,8) and free electrons created in the course of a corpuscular bombardment find themselves in an atmosphere composed almost exclusively of the molecular species of its constituent elements. The ambient temperature of the atmosphere in the height range thirty to ninety km exhibits little variation around a mean value of about 250 degrees K. The collision frequency is quite large (10^{10} to 10^{6} sec^{-1} and thermalization of the nascent free electrons occurs in a matter of microseconds. An environment such as this, slow electrons in a molecular atmosphere, favors nonradiative recombination processes.

Mathematically, the temporal behavior of the electron density in regions above ninety km can be characterized by the familiar equation:

$$dN/dt = q - \alpha N^2 , \tag{3.1}$$

where q is the electron production rate, N is the electron density, and α is the recombination rate coefficient. The equilibrium electron density profile can be obtained from the relatively simple relationship:

$$N = (q/\alpha)^{1/2} . \tag{3.2}$$

The situation is not so simple in the region below the D layer. The presence of negative ions adds a new dimension to the overall interaction that establishes the equilibrium electron density. However, a relationship analogous to Eq. (3.2)

holds in this region also, but before it is presented, those individual contributory processes, believed to be the most important, will be reviewed separately along with the values assumed for their associated rate coefficients.

Electron Loss Mechanisms

In an atmosphere 78% N_2 and 22% O_2 with other trace constituents and at a temperature of 250 degrees K the following are considered to be the primary mechanisms for recombination:

(a) Dissociative Recombination: Rate Coefficient α_D. This process can be described by the equation

$$(XY)^+ + e \rightarrow X^* + Y^* ,$$

where X and Y represent the constituent atoms of the positive molecular ion, XY^+, and X^* represents one of the atoms in an excited state. In this process a free electron combines with a positive molecular ion, the excess energy serving to dissociate the molecule. This is a relatively fast process, rate coefficients for molecular nitrogen being quoted as lying between 10^{-6} to 10^{-7} cm^3/sec. Nicolet (6) gives $\alpha_D(N_2) = 5 \times 10^{-7}$ cm^3/sec, $\alpha_D(O_2) = 3 \times 10^{-8}$ cm^3/sec, and $\alpha_D(NO) = 3 \times 10^{-9}$ cm^3/sec. Crain (19), in a more recent paper, quotes various values for N_2 ranging from 10^{-6} to 4×10^{-7} and 3×10^{-7} to 10^{-8} for O_2. In addition to this, another process of unknown rate, namely

$$N_2^+ + O_2 \rightarrow N_2 + O_2^+ ,$$

occurs which makes it difficult to determine which molecular ion is the most important in the dissociative recombination process. Crain, however, states that a value of 10^{-7} for molecular oxygen is more reasonable than 10^{-8}. This, in effect, means that there is no real practical difference which molecular ion is chiefly responsible for this reaction with electrons. For purposes of calculation, Nicolet's value of $\alpha_D(N_2) = 5 \times 10^{-7}$ cm^3/sec has been assumed for the rate of dissociative recombination in air. Bailey, however, used $\alpha_D = 3 \times 10^{-8}$

cm^3/sec in his paper on cosmic ray induced radio wave absorption. (12)

(b) Nonradiative Attachment: Rate Coefficient η. The water vapor molecule and oxygen molecule have an affinity for free electrons. O_2 is far more abundant than H_2O in the upper atmosphere (19); the formation of O_2^- alone can be considered the one important process of this type. Molecular oxygen has an electron affinity of about 0.4 ev (20), but the attachment process itself has a pressure-dependent rate as has been shown by Chenin, Phelps and Biondi (21). This, therefore, means that a third body is involved in the reaction to conserve momentum and carry off excess energy. The process can be described by the equation

$$O_2 + e + (XY) \rightarrow O_2^- + (XY) ,$$

and the rate coefficient quoted by these authors is

$$\eta = 1.5 \times 10^{-30}\, n(O_2)\ cm^3/sec ,$$

where $n(O_2)$ is the number density of molecular oxygen, this species being assumed to be the third body in the interaction. Bailey (12) used a somewhat larger rate coefficient for this process. Although it is not explicitly given in his paper, he assumed η of approximately $2 \times 10^{-29}\, n(O_2)\ cm^3/sec$.

Secondary Electron Production Mechanisms

Besides the direct production of electrons by solar cosmic rays which initiates the secondary processes being described, there are two other important processes occurring within the atmosphere below 90 km which produce electrons. These are the photodetachment of electrons from negative ions (mainly O_2^-) and collisional detachment of electrons from the same ion.

Photodetachment of Negative Ions: Rate Coefficient ρS. As mentioned earlier, the portion of the solar spectrum which penetrates the atmosphere to depths greater than the D layer does not have quanta of sufficient energy to photodissociate neutral molecules or form electron-positive ion pairs. However, the negative ion, O_2^-, having been formed in the three-body process mentioned

earlier may undergo a further process described as follows:

$$O_2^- + h\nu \rightarrow O_2 + e \ .$$

The cross section for this reaction for various frequencies has been measured by Smith, Burch, and Branscomb (22). Their measurements lead to a photodissociation rate of O_2^- in the upper atmosphere of 0.44 cm^3/sec. This particular rate coefficient seems to be accepted by other workers (6,19), and in that sense can be said to be unique.

Collisional Detachment of Electrons from O_2^-: Rate Coefficient κ. Direct collisions between the negative ion, O_2^-, and neutral molecules in the atmosphere can result in the reaction

$$O_2^- + (XY) \rightarrow O_2 + (XY) + e \ .$$

The value of the rate coefficient of this process seems to be quite uncertain. Branscomb and Bailey (19), on the basis of ionosphere absorption measurements, quote a value of $\kappa = 2 \times 10^{-17}$ cm^3/sec. Nicolet and Aiken (6) give an upper limit of $\kappa = 4 \times 10^{-17}$ cm^3/sec, but Phelps and Pack (20), on the basis of drift tube swarm measurements, present a value of this rate coefficient three orders of magnitude lower than those quoted above. These latter authors give a rate of $\kappa = 4 \times 10^{-20}$ cm^3/sec at $230^\circ K$.

The value of the collisional detachment rate given by Phelps and Pack differs qualitatively as well as quantitatively from the others quoted in that it was derived from a direct laboratory measurement rather than inferred from the results of measurements made on other phenomena. Yet, unless there exists an important source of electrons in the upper atmosphere, operative during a proton event, that has been completely overlooked, this small collisional detachment rate cannot be reconciled with the observed nighttime absorption of cosmic radio noise. The cosmic radio noise absorption day-night ratio defined as

$$\frac{D}{N} = \frac{\text{Total Daytime Absorption (db)}}{\text{Total Nighttime Absorption (db)}}$$

is known from the College riometer data (23) to be in the neighborhood of 5. Accordingly, a calculation was made wherein the value of κ was varied between the extreme values quoted above and D/N as a function of flux at cutoff was calculated. The flux values assumed were

$$J(112 \text{ Mev}) = 100,\ 1000, \text{ and } 10{,}000\ ,$$

for $\gamma = 5$ differential proton energy spectrum. It was found that $\kappa = 5 \times 10^{-18}$ cm^3/sec gives $D/N \cong 5$ for all three values of J. The value for the collisional detachment rate used in this thesis is $\kappa = 5 \times 10^{-18}$ cm^3/sec.

Mutual Neutralization of Positive and Negative Ions: Rate Coefficient α_i. Such a process in the case of the oxygen molecular ion, can be described by the equation

$$O_2^- + (XY)^+ \rightarrow O_2 + (XY)\ .$$

This process, which does not directly affect the free-electron density but bears strongly on the negative-ion-to-electron ratio, was considered an important one by Bates and Massey (24). Nicolet (6) quotes a value of $\alpha_i = 10^{-7}$ cm^3/sec. This value of α_i is the one adopted in this thesis. Bailey (12), however, used a value of α_i of approximately two orders of magnitude less than the above, namely $\alpha_i = 3 \times 10^{-9}$ cm^3/sec.

In the following table the values of the various rate coefficients adopted for use in this thesis are summarized:

Dissociative Recombination	$\alpha_D = 5 \times 10^{-7}$ cm^3/sec
Nonradiative Attachment	$\eta = 1.5 \times 10^{-30}\ n(O_2)$ cm^3/sec
Photodetachment from O_2^-	$\rho S = 0.44$ sec
Collisional Detachment from O_2^-	$\kappa = 5 \times 10^{-18}$ cm^3/sec
Ionic Mutual Neutralization	$\alpha_i = 10^{-7}$ cm^3/sec

The Effective Recombination Coefficient

Having identified the principal processes by which free electrons interact with the various particles comprising the atmosphere in the height range thirty

to ninety km, one can express the over-all temporal variation of the electron and ion densities in terms of the rates of production and loss by these processes as follows:

$$dN/dt = q - \alpha_D N N^+ - \eta n(O_2) N + \kappa n N^- + \rho S N^- \; ; \tag{3.3}$$

$$dN^+/dt = q - \alpha_D N N^+ - \alpha_i N^+ N^- \; ; \tag{3.4}$$

$$dN^-/dt = \eta n(O_2) N - \kappa n N^- - \alpha_i N^+ N^- - \rho S N^- \; , \tag{3.5}$$

where N, N^+ and N^- are the electron, positive ion, and negative ion number densities, respectively; $n(O_2)$ is the number density of neutral oxygen molecules, n is the total neutral particle number density, and q is the production rate of electron-positive ion pairs due to the solar cosmic ray flux. The various rate coefficients are defined in the table at the end of the previous subsection.

It is immediately apparent that these equations are consistent with the physical requirement of charge neutrality; i.e., $N + N^- - N^+ = 0$. Therefore, if this condition is explicitly imposed, we have only two independent equations --the third being directly derivable from the other two.

The quantities N^+ and N^- can be expressed in terms of N and λ, the negative-ion-to-electron ratio, as follows:

$$N^- = \lambda N \; ; \tag{3.6}$$

$$N^+ = N^- + N = (1 + \lambda) N \; . \tag{3.7}$$

The important simplifying assumption is now made that the time derivatives in Eqs. (3.3), (3.4) and (3.5) differ significantly from zero during transitional periods that are relatively brief compared to the total time scale of the event. If the substitutions implied by Eqs. (3.6) and (3.7) are made in (3.3) and (3.4) and the assumption of quasi-equilibrium is made, two equations relating the unknowns, N and λ, to known quantites follow directly.

$$q - \alpha_D (1 + \lambda) N^2 - \eta n(O_2) N + \kappa n \lambda N + \rho S \lambda N = 0 \; ; \tag{3.8}$$

$$-\alpha_i \lambda (1 + \lambda) N^2 + \eta n(O_2) N - \kappa n \lambda N - \rho S \lambda N = 0 \; . \tag{3.9}$$

Adding these two equations, one obtains an expression for N, the electron density, entirely analogous to that holding for the atmospheric region above ninety km [Eq. (3.2)].

$$N = [q/(1 + \lambda)(\alpha_D + \lambda\alpha_i)]^{1/2} , \tag{3.10}$$

wherein the denominator, $(1 + \lambda)(\alpha_D + \lambda\alpha_i)$, can be identified with α, the recombination coefficient, in Eq. (3.2).

The complication introduced into the analysis by negative-ion formation expresses itself in terms of the unknown value of λ in Eq. (3.10). Bailey, in his analysis of solar cosmic ray induced absorption, obtained an expression for λ in terms of the rate coefficients and the neutral-particle densities only. This can be done if the term $\alpha_i\lambda(1 + \lambda)N^2$ is negligible compared to the other terms in Eq. (3.9). Assuming this to be the case, one immediately obtains

$$\lambda_B = \eta n(O_2)/(\kappa n + \rho S) . \tag{3.11}$$

The values of the rate coefficients appearing in the literature subsequent to the publication of Bailey's work tend to place this assumption on less firm ground. α_i has been increased two orders of magnitude while η and κ have new lower values. That this approximation may not be valid is particularly true for nighttime absorption in which case the photodetachment rate coefficient, ρS, vanishes. However, λ_B, as defined by Eq. (3.11), is an important parameter in obtaining the equilibrium negative-ion-to-electron ratio by the method used in this thesis. This present method requires no assumption as to the relative magnitude of the terms in Eqs. (3.8) and (3.9).

The following parameters are defined:

$$\beta \equiv \alpha_D/\alpha_i ;$$

$$\xi = 1/\lambda_B = (\kappa n + \rho S)/\eta n(O_2) ;$$

$$\zeta \equiv \alpha_i q/[\eta n(O_2)]^2 .$$

Following some straightforward but slightly lengthy algebraic manipulations, N can be eliminated between Eqs. (3.8) and (3.9) and the following cubic equation

obtained in λ:

$$\lambda^3 + u\lambda^2 + v\lambda + w = 0 , \tag{3.12}$$

where

$$u = [(\beta - 2/\xi)\xi^2 - \zeta]/(\xi^2 - \zeta) ,$$

$$v = (1 - 2\beta\xi)/(\xi^2 - \zeta) ,$$

$$w = \beta/(\xi^2 - \zeta) .$$

λ, which now appears as a root of a cubic equation (3.12), depends on q, the electron production rate of the particular event, as well as on the atmospheric parameters. However, it is of interest to note the behavior of the cubic as the parameter ζ tends to zero.

$$\zeta = \alpha_1 q/[\eta n(O_2)]^2 \to 0 ,$$

$$u \to (\beta - 2\lambda_B) ,$$

$$v \to \lambda_B^2 - 2\beta\lambda_B ,$$

$$w \to \beta\lambda_B^2 ,$$

and

$$\lambda^3 + (\beta - 2\lambda_B)\lambda^2 + (\lambda_B^2 - 2\beta\lambda_B)\lambda + \beta\lambda_B^2 = 0 ,$$

identically if $\lambda = \lambda_B$.

For various atmospheric heights it is found that the discriminant of the cubic is often negative. This guarantees the equation has three real roots; one root is negative, having no physical significance, but the other two are positive and invariably lie on either side of λ_B.

$$\lambda_1 < 0, \text{ but } 0 < \lambda_2 < \lambda_B < \lambda_3 .$$

Because λ_B is the limiting case for very small q, the root which represents the actual negative-ion-to-electron ratio must be less than λ_B, as q represents a source of electrons. This choice, based on physical reasoning, is supported by the fact that for cases of a positive discriminant wherein only one real root exists, its value is invariably less than that of the corresponding λ_B.

Calculations have shown that for the values adopted for the rate coefficients in this thesis, Bailey's approximation for λ holds up remarkably well for the nighttime case as well as the daytime for all reasonable cosmic ray flux values. It was only during the search for a value of κ consistent with the observed day-night ratio that significant differences were noted between λ_B and the proper root of the cubic. These differences were of an order of magnitude at heights of thirty to forty km for J(112 Mev) $\geq$ 500 particles ster^{-1} cm^2 sec^{-1} under nighttime conditions ($\rho S = 0$) for values of κ less than 10^{-19} cm^3/sec. For larger values of κ (assuming, of course, that the values of the other rate coefficients are not significantly revised), Bailey's approximation for λ can be made with confidence. It is to be noted further that the quantitative differences between Bailey's results and those obtained from the present analysis exist by virtue of the different values adopted respectively for the various rate coefficients. The difference in method of obtaining λ contributed little in this respect, although the method used in this thesis is on sounder theoretical ground.

In the literature of the lower ionosphere the quantity $(\alpha_D + \lambda\alpha_i)$ is termed the effective recombination coefficient rather than the more significant quantity $(1 + \lambda)(\alpha_D + \lambda\alpha_i)$. This convention is adhered to in this thesis. In conformity with this, Eq. (3.10) is rewritten:

$$N = [q/(1 + \lambda)\alpha_{eff}]^{1/2} , \qquad (3.13)$$

where

$$\alpha_{eff} \equiv (\alpha_D + \lambda\alpha_i) .$$

In Figs. 5, 6, 7, and 8 the quantities λ, α_{eff}, $(1 + \lambda)\alpha_{eff}$, as calculated in this thesis, are displayed along with their counterparts as computed by Bailey for day and night. Bailey's results are designated B, whereas those obtained herein are designated A. α_{eff} is plotted from right to left instead of in the conventional manner for the sake of clarity of presentation of the results

displayed in Figs. 5 and 6. The ratio

$$N_B(h)/N_A(h) = [(1 + \lambda_A)\alpha_{eff}/(1 + \lambda_B)\alpha_{effB}]^{1/2} ,$$

where λ_B here refers to Bailey's computed values for the negative-ion-to-electron ratio, is the ratio of electron densities for a given production rate as would be obtained using the rate coefficients of Bailey and those adopted in this thesis respectively. It is presented for day and night in Fig. 9.

The Equilibrium Electron Density

The equilibrium electron density, which is of central importance to this study, is obtained immediately from Eq. (3.10) or (3.13), assuming that the production rate and the negative-ion-to-electron ratio are known. Figure 4 gives the daytime and nighttime electron-density profiles due to a pure proton flux [$J(112\ \text{Mev}) = 100$; $\gamma = 5$] and a proton-alpha-particle flux in a particle ratio of 10 to 1 [$J_p(112\ \text{Mev}) = 100$; $\gamma_p = 5$ and $J_\alpha(119.5\ \text{Mev}) = 10$; $\gamma_\alpha = 4.73$]. Contours of the equilibrium electron density as a function of geomagnetic cutoff for constant atmospheric heights (daytime) are presented in Figs. 17, 18, and 19.

CHAPTER IV

Validity of the Equilibrium Assumption

One of the most important and useful approximations made in the development of the method presented in this thesis for the determination of the electron density height profile from the electron production rate resides in the assumption of equilibrium. Equilibrium in its strictest sense implies simultaneity with respect to changes of q and N. On the other hand, these changes must take place with extreme slowness, as only in this manner can dN/dt be strictly zero. Actually, dN/dt is not assumed to actually vanish but always to assume values that are negligibly small compared to the magnitudes of the various terms representing the several electron production and recombination processes. An assumption such as this might more properly be termed one of quasi-equilibrium. Here,

as q changes in time at some finite rate at a given height, N is assumed to pass through a sequence of equilibrium states corresponding, at each moment, to the particular value of q related to N through the equation of equilibrium. An estimate of the degree of validity one can ascribe to the quasi-equilibrium approximation can be obtained from the determination of the lag time (or the amount of departure from simultaneity) exhibited between changes in q and the concomitant changes in N. If the response time between N and q is small relative to some characteristic time interval of the event, changes in N brought about by changes in q can be considered almost simultaneous and quasi-equilibrium is a valid approximation. If, on the other hand, the response time is relatively large, a quasi-equilibrium process cannot be assumed.

The purpose of this subsection is to provide some quantitative information concerning the validity of the quasi-equilibrium approximation used in this thesis.

Two idealized sets of initial conditions are proposed that would result in the maximum departures from equilibrium between the electron density and the electron production rate at a given height h. Case (a) would result in the maximum lag time between the growth of the production rate and the increase of the electron density to its equilibrium values; Case (b) would result in the maximum lag time between the reduction of the production rate and the consequent decay of the electron density.

Case (a):

$$\begin{aligned} q(t) &= 0, \qquad N(h) = 0; \qquad f < 0; \\ q(t) &= q(h), \qquad N(h) = N(h,t); \qquad f \geq 0. \end{aligned} \tag{4.1}$$

In this case the production rate is zero prior to a certain reference time, $t = 0$. For times $t \geq 0$ the production rate proceeds at its full intensity as a function of height as it would be computed by the method given earlier. N(h) increases from zero and in some characteristic time, which is a function of height, assumes a value arbitrarily close to its theoretical equilibrium value.

Case (b):

$$\begin{aligned} q(t) &= q(h), \qquad N(h) = N_o(h); \qquad t < 0; \\ q(t) &= 0, \qquad N(h) = N(h,t); \qquad t \geq 0. \end{aligned} \tag{4.2}$$

In this case the equilibrium condition is assumed to hold between q and N. N_o is the equilibrium value of the electron density corresponding to q at a given height, h. At $t \geq 0$, $q = 0$, the primary production of electrons suddenly ceases and N decays from its equilibrium value.

The equations to be solved subject to the above initial conditions, Case (a) and Case (b), are (3.3) and (3.5),

$$dN/dt = q - \alpha_D N N^+ - \eta n(O_2)N + \kappa n N^- + \rho S N^-, \tag{3.3}$$

$$dN^-/dt = \eta n(O_2)N - \kappa n N^- - \alpha_1 N^+ N^- - \rho S N^-, \tag{3.5}$$

with $N + N^- = N^+$.

If λ, the negative-ion-electron ratio, could be considered a constant, special solutions of simple analytical form exist for the above system of equations and the initial conditions postulated. However, an assumption such as this is not justified without some evidence as to the range of heights over which it is valid, if indeed it is valid at all. Fortunately, some evidence bearing on the behavior of λ can be obtained from Eqs. (3.3) and (3.5) under the initial conditions of Case (b). Considering the special conditions of Case (b) first, one can write the system (3.3) and (3.5) as follows:

$$dN/dt = -\alpha_D N N^+ - \eta n(O_2)N + \kappa n N^- + \rho S N^- \; ; \tag{4.3}$$

$$dN^-/dt = \eta n(O_2)N - \kappa n N^- - \alpha_1 N^+ N^- - \rho S N^- \; ; \tag{3.5}$$

$N^- = \lambda N$ and $N^+ = (1 + \lambda)N$ for $t > 0$, and for $t = 0$

$$\lambda(t = 0) = \lambda_B = \eta n(O_2)/(\kappa n + \rho S) \; . \tag{3.11}$$

Multiplying (4.3) by N^-, (3.5) by N, subtracting the equations and dividing the difference by N^2, one obtains the following for the left-hand side of the resulting equation:

$$\frac{N(dN^-/dt) - N^-(dN/dt)}{N^2} = \frac{d}{dt}\left(\frac{N^-}{N}\right) = \frac{d\lambda}{dt} .$$

The complete equation becomes:

$$d\lambda/dt = (\alpha_D - \alpha_i)\lambda N^+ + \eta n(O_2)(1 + \lambda) - (\kappa n + \rho S)\lambda(1 + \lambda) . \quad (4.4)$$

If the first term on the right-hand side of Eq. (4.4), i.e., $[(\alpha_D - \alpha_i)\lambda N^+]$ is neglected, which is an approximation similar to that made by Bailey in his determination of the equilibrium value of λ, the equation can be written in the following form:

$$d\lambda/dt = \eta n(O_2)(1 + \lambda)(1 - \lambda/\lambda_B) , \quad (4.5)$$

for $t > 0$, with the initial condition $\lambda = \lambda_B = \eta n(O_2)/(\kappa n + \rho S)$ at $t = 0$. One can see immediately that the differential equation (4.5) with this initial condition on λ can only be satisfied by the trivial solution

$$\lambda = \lambda_B , \qquad \text{for } t \geq 0,$$

for if λ decreased from its equilibrium value, the right-hand side of Eq. (4.5) would be positive. This involves a contradiction, as a decrease in λ with time demands a negative first derivative which is inconsistent with the differential equation (4.5). The converse (λ increasing from λ_B with time) also involves the same contradiction. To an approximation of the order of that made by Bailey, λ is constant in time over height ranges of interest for a decaying electron density.

Unfortunately, a simple analytic solution corresponding to the initial conditions of Case (a) cannot be obtained due to the inhomogeneity introduced into the differential equation for λ by q. However, the solution corresponding to Case (b) indicates that λ changes little for large changes in the electron production rate and the electron density. It would seem reasonable to assume that λ can be considered a slowly changing parameter for an increasing electron density as well as a decaying one.

To obtain a differential equation for the electron density, one adds (3.3) and (3.5), remembering that $N^- = \lambda N$,

$$(d/dt)\ (1 + \lambda)N = q - (1 + \lambda)(\alpha_D + \lambda\alpha_i)N^2 \ . \tag{4.6}$$

Because λ is considered a constant and equal approximately to λ_B,

$$dN/dt = q/(1 + \lambda) - (\alpha_D + \lambda\alpha_i)N^2 \ . \tag{4.7}$$

Under the conditions assumed for Case (b), $q = 0$ for $t \geq 0$. Direct integration of Eq. (4.7) with $q = 0$ yields:

$$N = N_o/[1 + N_o(\alpha_D + \lambda\alpha_i)t] \ . \tag{4.8}$$

The electron density decreases essentially as t^{-1}.

To obtain a measure of the rate of recombination as a function of height, one may inquire as to the time required for the electron density to decay to 1/10 of its equilibrium value,

$$\begin{aligned} 0.1N_o &= N_o/[1 + N_o(\alpha_D + \lambda\alpha_i)\tau] \ , \\ \tau_1(h) &= 9/N_o(h)(\alpha_D + \lambda\alpha_i) \ , \end{aligned} \tag{4.9}$$

where $\tau_1(h)$ will be termed the "decay time." $\tau_1(h)$ vs h is shown in Fig. 12.

A more interesting quantity than the decay time is the rise time. For the conditions previously set forth in Case (a), i.e., $q = 0$, $N = 0$ for $t < 0$; $q = q(h)$, $N = N(t)$ for $t \geq 0$, what period of time must elapse for N(t) to increase from zero to 9/10) of its equilibrium value? As mentioned previously, we have no analysis in λ guaranteeing its approximate constancy as we have for Case (b). However, such an approximation seems reasonable in light of the behavior of λ for relatively large changes in N and q which occur in the case of decay from equilibrium. Accordingly one integrates Eq. (4.7) with $q = q(h)$.

The two identities, (I) $\operatorname{sech}^2 x = 1 - \tanh^2 x$ and (II) $(d/dx) \tanh x = \operatorname{sech}^2 x$, suggest a particular solution of the form $N = A \tanh (Bt)$. Inserting this into Eq. (4.7) and noting identity (I) one sees that the conditions

$$[(1 + \lambda)(\alpha_D + \lambda\alpha_i)/q]A^2 = 1 \ ,$$

and

$$(1 + \lambda)/q\ AB = 1$$

must hold.

Solving these simultaneously, one acquires a particular solution for Eq. (4.7):

$$N = [q/(1 + \lambda)(\alpha_D + \lambda\alpha_i)]^{1/2} \tanh [q(\alpha_D + \lambda\alpha_i)/(1 + \lambda)]^{1/2}t, \quad (4.10)$$

which satisfies the initial condition, $N = 0$ for $t = 0$, and

$$N \to [q/(1 + \lambda)(\alpha_D + \lambda\alpha_i)]^{1/2} = N_o , \qquad \text{for } t \to \infty .$$

The rise time will be defined as the time required for N to attain a $(9/10)E_o$,

$$\tau_2(H) = \left[\frac{(1 + \lambda)}{q(h)(\alpha_D + \lambda\alpha_i)} \right] \tanh^{-1}\left(\frac{9}{10}\right) = 1.47 \left[\frac{(1 + \lambda)}{q(\alpha_D + \lambda\alpha_i)} \right]^{1/2}, \quad (4.11)$$

where q and λ (equilibrium value) are functions of h. $\tau_2(h)$ is the "rise time" and as a function of h is shown in Fig. 12.

It will be noticed that both the decay and rise times are in the order of 20-40 minutes at heights which are important for the attenuation of cosmic radio noise. The duration of the steady particle bombardment which can be considered a characteristic time for the phenomena is measured in days. Moreover, the cases consid red here are not duplicated in nature--they are idealized extremes. Consequently it would seem that the quasi-equilibrium approximation is a suitable one in the present analysis.

CHAPTER V

Cosmic Noise Absorption

From the phenomenological view point, the effect of the solar particle bombardment on the atmosphere is the creation of a finite conductivity in a region which, under ordinary circumstances, behaves as a pure dielectric. Normally the non-ionized region below the D layer exhibits an index of refraction slightly greater than unity which varies directly as the air pressure and is frequency-independent over a very large frequency range (essentially from zero

to 10^{10} cycles/sec). The presence of a concentration of free electrons serves to depress the index of refraction to values less than unity and to introduce a dissipative process into the propagation of radio waves through the region. Furthermore, both the index of refraction and the absorption are frequency-dependent. The region in its ionized state, in contrast to its normal state, is dispersive. For waves of frequencies in the neighborhood of and less than the electron gyrofrequency (~ 1.5 mc/sec), the anisotropy introduced into the ionized atmosphere by the presence of the terrestrial magnetic field can have important effects on their propagation. At these frequencies the medium is birefringent and the amount of absorption depends on the mode of propagation. It is necessary, therefore, to examine the several effects that the solar particle bombardment may possibly induce in the propagation of radio waves in the height range of interest. The relative importance of the various propagation effects possible depend primarily on the radio frequency under consideration and the magnitude of the free-electron density and the electron-neutral collision frequency.

The radio frequency chosen for the analysis presented in this thesis is 27.6 mc/sec. This was the operating frequency of the riometers situated at various locations in the earth's polar latitudes to study the enhancement of the absorptive power of the atmosphere following various solar and geophysical events (25). This choice of frequency has the obvious virtue of allowing a direct comparison to be made between calculated results and available riometer data. It also permits a considerable simplification in the calculation of the specific absorption of the atmospheric region principally affected by the solar particle bombardment.

The earth's magnetic field at Farewell, Alaska, the location of lowest geomagnetic latitude considered in this study, is inclined from the zenith at

an angle of 16 degrees. At all other locations under consideration the inclination is less than this. Consequently the incoming cosmic noise is being propagated quasi-longitudinally with respect to the earth's field. For this type of propagation at 27.6 mc/sec, magneto-ionic double refraction can be neglected. Both modes of propagation follow similar paths and negligible difference exists in their respective absorptions.

Peak electron densities produced by solar particle bombardments are, at the most, of the order of that of the D layer. The index of refraction for radio waves having frequencies in the neighborhood of 30 mc/sec in this region is approximately equal to one. As a result of this, only the elementary theory of radio-wave absorption due to dissipative collisions between electrons and neutrals in a slightly ionized plasma is required to study the effect of the solar particle bombardment on the upper atmosphere. The absorption caused thereby is strictly nondeviative.

The specific absorption in decibels per km is given by

$$\chi = \frac{10^4}{nc} \frac{\omega_p^2 \nu}{\omega^2 + \nu} \log_{10} e \text{ db/km}, \tag{5.1}$$

where

$\omega_p^2 = \frac{Ne^2}{\epsilon m} \times 10^6$, the square of the plasma frequency,

N = electron density (electrons/cm^3),

e = electronic charge = 1.6×10^{-19} coulombs,

m = electron mass = 9.11×10^{-31} km,

ϵ = permittivity of free space = 8.85×10^{-12} farads/meter,

c = velocity of light = 3×10^8 m/sec,

n = index of refraction $\doteq$ 1,

ν = electron-neutral collision frequency,

ω = angular frequency of the radio waves = 1.63×10^8 radians/sec.

For computational purposes the specific absorption can be written:

$$\chi(h) = 4.6 \times 10^{4}[N(h)\nu(h)/[\omega^2 + \nu(h)^2]] \text{ db/km} . \qquad (5.2)$$

N(h) is the equilibrium electron density in the atmosphere height range 30-90 km obtained in the manner described in the preceding sections. The values used for the electron collision frequency in this thesis were those given by Nicolet (9). Nicolet arrived at the values presented in his paper by deducing the effective scattering cross section for electrons in air from data obtained experimentally by Kane (26). Kane, using a rocket-borne transmitter, measured the difference in absorption between a 7.75 mc/sec signal and its 6th harmonic traversing the atmosphere during a polar blackout. The launching was made at Ft. Churchill, Canada. The data acquired by Kane is presented in his paper as a collision frequency profile for the atmospheric height range 60-80 km. Nicolet made a theoretical extension of this range to include the 30-90 km range needed for the determination of the total vertical absorption due to the particle bombardment. The values of the collision frequency deduced by Nicolet from Kane's more limited results are less, by a factor of three, than those values obtained from the collision cross section of slow electrons with nitrogen determined from a laboratory experiment of Anderson and Goldstein (27). The atmosphere collision frequency profile obtained from Anderson's and Goldstein's laboratory measurement was used by Bailey in his paper on solar cosmic ray induced absorption.

The results of the present calculation are given in Fig. 10 which gives the specific attenuation as a function of height for daytime and nighttime conditions due to a flux of protons [J_p(112 Mev) = 100; $\gamma_p = 5$], and a heterogeneous flux of protons [J_p(112 Mev) = 100; $\gamma_p = 5$] and α particles [J_α(119.5 Mev) = 10; $\gamma_\alpha = 4.73$] of number ratio of 10 to 1. Contours of the specific attentuation as a function of geomagnetic cutoff due to protons under daytime conditions for constant heights are given in Figs. 20, 21, and 22.

The total vertical attenuation for a given geomagnetic particle cutoff

energy is obtained from the integral of the specific attenuation over the height range of the region of the atmosphere rendered absorbing by the solar particle influx

$$A(db) = 4.6 \times 10^{4} \int_{h_1}^{h_2} \frac{N(h)\nu(h)}{\omega^2 + \nu(h)^2}\, dh \ . \qquad (5.3)$$

The limits h_1 and h_2 have been taken to be 30 km and 90 km respectively. For heights greater than 90 km the particle energy loss in the atmosphere, due to its very low density, is negligible while primary electron production due to solar electromagnetic radiation becomes important. For heights less than 30 km, recombination is so rapid that an ambient electron density is virtually nonexistent.

The relative increase in vertical absorption of cosmic noise at 27.6 mc/sec during a solar proton event over that due to the atmosphere under normal conditions was calculated for Störmer proton cutoff energies of 261.5, 112, 54, and 20.8 Mev corresponding to geomagnetic latitudes 61.6, 64.7, 66.9, and 68.8 degrees respectively. The absorption as a function of proton flux is shown in Fig. 11 for power-law proton spectra with γ = 3, 5, and 7 for day and night. The variations of the absorption with the proton Störmer cutoff energy (E_c) for various total flux values normalized to E_c = 112 Mev (College, Alaska) are given for daytime and nighttime conditions for the same three values of γ as above. These results are presented in Fig. 23 through 28. Finally, the absorption is shown as a function of geomagnetic latitude, day and night in Fig. 29.

CHAPTER VI

The Effect of the Earth's Field on the Proton Stopping Heights

The earth's magnetic field exercises an influence of central importance in the establishment of the electron production rate height profile at a given geomagnetic latitude. Moreover, in its role as a rigidity spectrometer, the

terrestrial field, in conjunction with the solar particle spectrum, determines the latitude variation of the cosmic radio noise absorption over the polar cap. Yet, in the evaluation of the integral for the electron production rate, Eq. (2.9), the earth's field is assumed to exert a minor influence on the particle trajectories in air--in fact, an effect sufficiently small to be negligible. Accordingly, the solar particles could be thought of as traversing rectilinear paths through the atmosphere, as was assumed.

At first glance it seems paradoxical that the influence of the terrestrial field is of almost paramount importance in one stage of the analysis and can be neglected in the other. The reason, however, resides in the scale of the phenomena involved in the two stages of the calculation. The geomagnetic latitude variation of the cosmic ray cutoff rigidity derives from the over-all dipole structure of the terrestrial magnetic field and its influence on a particle over a relatively long path through space. On the other hand, the influence exerted by the earth's field on a particle slowing down in the atmosphere depends on the local structure of the field and its interaction with the particle over a relatively short path through the atmosphere. Thus, while considered in the large, the effect of the terrestrial field on the over-all particle trajectory might be great, it can also be true that under favorable conditions the influence of the field on the terminal portion of the particle trajectory can be entirely neglected.

The local terrestrial field in the north polar regions is directed downward and is inclined from the earth's normal at a rather small angle. It can be considered to be of uniform intensity over the height range 30 to 90 km above the earth's surface at the geographic locations for which the calculations contained in this thesis were performed. Presented in the following table are the local magnetic field strength, the field's inclination from the zenith direction,

and the minimum allowable particle energy (cutoff) for each of the geographic locations (28) of interest in this thesis.

Location	Local Field Strength (gauss)	Magnetic Inclination (degrees)	Cutoff Energy (Mev)
Pt. Barrow	0.57	9.6	20.8
Ft. Yukon	0.57	11.7	54
College	0.55	12.0	112
Farewell	0.55	15.8	261.5

It will be recalled that the quantity $Y(E;\theta,\varphi,h)$, appearing in the integral of Eq. (2.2), which represents the number of particles cm^{-2} $ster^{-1}$ sec^{-1} having energies in dE at E at height h, was obtained from the differential energy spectrum of the solar particles incident on the top of the atmosphere.

$$Y(E;\theta,\varphi,h) = N(E_1) \ . \qquad (2.3)$$

The connection between E at height h and E_1, the initial energy, was obtained through the known range-energy relationship (11) for protons in air. This method requires a knowledge of the particle trajectories, and, in the absence of a local magnetic field, the trajectories are known to be straight lines. If the magnetic field were absent, a vertically incident particle would have a range in air numerically equal to the atmospheric pressure at its stopping height. A particle of oblique incidence, traveling in a direction inclined at an angle θ from the zenith and haveing a range in air, R, would stop at a vertical height in the atmosphere corresponding to the pressure R cos θ. This is not true in the presence of a magnetic field. The field introduces a curvature into the particle trajectory the degree of which depends on the magnitude of the particle momentum, the strength of the field and direction of the magnetic field with respect to the particle momentum vector. The more energetic the particle, the more rigid is its trajectory and the more closely is the field-free situation approximated. The values given in the previous table for the quantities of importance in this res-

pect seem to indicate that the influence of the local field could be ignored safely. However, this assumption, if unwarranted, would introduce an error in the electron production rate calculation that could invalidate the results of the entire study. For this reason a separate investigation was made of the behavior of a set of particles slowing down in the atmosphere under the influence of the local magnetization field characteristic of the four geographic locations of interest and having initial conditions which would insure that their actual trajectories would exhibit the maximum deviation from rectilinearity. The results of this investigation are presented in Fig. 13. Four groups of particles were considered, each group initially having the minimum allowed energy at one of the geographic locations for which the calculation was made. The particles comprising each group were divided into subgroups, each subgroup being assigned an initial angle of incidence with respect to the zenith. Because the local magnetic field through its own inclination from the zenith destroys the rotational symmetry of the problem, the particles comprising a subgroup were assigned various initial azimuthal directions. The straight horizontal lines in Fig. 13 represent the stopping heights of particles having initial energies indicated in the figure and incident at the given zenith angles under the condition of zero magnetic field. The sinusoidal-like curves represent the stopping heights of the same particles as a function of their initial azimuthal directions at a given zenith angle of incidence under the influence of the earth's field associated with the location indicated. For Farewell, Ft. Yukon, and Pt. Barrow the stopping height curve for each zenith angle subgroup was drawn through points representing the stopping heights of four particles having initial azimuth directions of 0, 90, 180, and 270 degrees respectively. The plane of zero azimuth is defined as that containing the zenith direction and a unit vector pointing outward but parallel to the earth's field. Trajectories were calculated

for particles of eight initial azimuth directions for each zenith angle for College to assure the smoothness of the stopping height curves for that location. The equations of motion of the particles and the mathematical details of this study are given in the Appendix.

For each of the four geographic locations considered, the stopping heights of those particles having the minimum allowed energy at each location were computed. In all cases the assumption of rectilinearity, carried to the limit of particles stopping, appears to break down at large zenith angles, but holds up quite well out to 60 degrees. As might be expected, Farewell represents the worst case, as here the magnetic field has a substantial horizontal component, being inclined 16 degrees from the zenith. It must be borne in mind that the maximum effect produced by solar protons on the atmosphere with respect to increasing its opacity to cosmic radio noise occurs at heights considerably in excess of the particle stopping heights, with the exception of Pt. Barrow. This latter location, however, exhibits trajectories having the least deviation from the stopping heights obtained from the field-free analysis.

This analysis cannot in itself provide a direct estimate of the error in the final results incurred by the assumption of rectilinear particle trajectories in the atmosphere. But, because it shows that deviations from rectilinearity are not prohibitively large for the trajectories of those particles having initial conditions and path lengths most unfavorable to this assumption, it does indicate that the over-all error introduced into the final results thereby cannot be large, and, in fact, might well be entirely negligible considering the uncertainties surrounding other aspects of the calculation of the cosmic noise absorption. In addition, it should be noted that the earth's cosmic ray shadow establishes forbidden sectors affecting particles incident from large zenith angles (17) thus reducing the number of particles whose trajectories violate the assumption of rectilinearity.

CHAPTER VII

Discussion of the Results

There are two distinct aspects from which one can consider the various phenomena attendant upon a solar particle bombardment of the atmosphere. From the purely local point of view one may examine the various interaction processes occurring in the atmosphere as a result of the influx of solar cosmic rays as well as the distribution with height of the electron production rate, the electron density and the specific attenuation. Of special interest are the various "layer heights" or heights of maximum value of these quantities. A second and equally interesting aspect of the over-all particle-induced absorption phenomenon exists on a geographical scale. Here, one considers the geomagnetic latitude variation of the total attenuation of the cosmic radio noise, and the geomagnetic cutoff-energy contours of the electron production rate, electron density, and specific attenuation for a set of given atmospheric heights.

It can be stated at the outset that a distinguishing characteristic of the local height profiles of the various quantities of interest (production rate, electron density, and specific attenuation) is their virtual independence of the shape of the solar particle energy spectrum. The profiles seem to be determined solely by the atmosphere, while the absolute magnitudes assumed by the quantities are determined by the size of the particle flux in the neighborhood of the local cutoff energy. On the other hand, these same quantities, when viewed through their cutoff energy-constant height contours, show a strong dependence on the shape of the solar particle spectrum. Consequently, the latitude variation of the total attenuation of cosmic radio noise should be deducible from the primary solar cosmic ray spectrum provided a known geomagnetic cutoff mechanism is operative. This suggests the attractive possibility of obtaining the solar particle energy spectrum directly from ionospheric absorption

data gathered at various geomagnetic latitudes. Before this can be done with confidence, however, all details of the absorption phenomenon on the local level must be well understood. This applies in particular to the over-all recombination process through whose agency the ambient electron density is established. The numerical values of the rate coefficients of processes known to be important are controversial, and it well may be true that every important process has not been accounted for. It is to emphasize these differences that some of the results obtained by Bailey in his study on cosmic ray induced absorption (12) are compared in this thesis with those obtained from the present study. Moreover, the variation of the low-energy cutoff of the cosmic ray spectrum with latidude must be known. Does a Störmer-type mechanism operate following a solar flare before the onset of the inevitable magnetic storm, or is the geomagnetic field always grossly perturbed during the whole course of such an event? To obtain the solar particle spectrum from absorption data one must be able to predict the latitude behavior of the low-energy cutoff as well as account for the various atmospheric processes mentioned above.

The Local Aspect of the Terrestrial Effects of a Solar Flare

We begin the discussion of the results of the analysis described in previous sections of this thesis with a consideration of a solar event as viewed locally, with emphasis at present on the height profiles of the various important quantities connected with the event. The rate at which electrons are produced in the atmosphere by a particle bombardment is a proper first consideration. The curves representing the electron production rate presented in this thesis obviously depend on the magnitude of the bombarding flux assumed. The particular value chosen for normalizing the various solar proton energy spectra for which calculations were done was chosen as being representative of the flux magnitudes encountered in the aftermath of a large proton event. The locale chosen for

special study was College, Alaska (geomagnetic latitude 64.7°; geomagnetic cutoff E = 112 Mev). J(112 Mev) = 100 protons/cm^2-sec-ster agrees closely in magnitude with the actual integral spectrum obtained by Winkler et al. (15) at Minneapolis following the sudden commencement of a magnetic storm associated with the polar cap event of July 14, 1959. The spectrum obtained as reported by these authors was

$$J(E) = 1.05 \times 10^8 E^{-2.9} \text{ protons/cm}^2\text{-sec-ster}, \qquad (7.1)$$

for $88 < E < 300$ Mev.

At College, Alaska, the flux was

$$J(112) = (1.05 \times 10^8)/(112)^{2.9} = 119.8 \text{ protons/cm}^2\text{-ster-sec}. \qquad (7.2)$$

The first result of interest obtained from this study has already been mentioned, that is, the seeming lack of dependence of the height profile of the electron production rate on the cosmic ray energy spectrum. The reason for this becomes apparent when one glances at Fig. 1, the energy-loss curve for protons. Low-energy particles are more effective ionizing agents than those of high energy, and there are more of them if a power law of any negative order approximates the particle energy spectrum. Figure 2 displays this result. The electron production rate due to bombarding protons of three different differential energy spectra are shown for a geomagnetic proton energy cutoff of 112 Mev. The curves presented peak strongly at about 32 km, the atmospheric height corresponding to the stopping depth of 112 Mev protons (10.7 gm/cm^2). The curves fall steeply with increasing height from their peak values (which are almost equal due to the normalization imposed on the integral spectra) until a height of about 58 km is reached. Thereupon the descent, still steep, becomes a little more gradual. This is due to the growing importance of the laterally incident particles. At heights of 58 km and greater, the air is so thin that protons incident from all angles are contributing equally to the electron production rate.

This same pattern is followed for other values of the low-energy cutoff. A strong peak is obtained at the height corresponding to the stopping depth of the lowest energy particles. A steep fall-off follows the same general shape as that given in Fig. 2. This can be seen in Fig. 3. Three curves are displayed here: an electron production rate profile due to protons having a differential energy spectrum αE^{-5}, a profile due to alpha particles having an integral rigidity spectrum identical to that of the protons but in a particle ratio of one to ten with respect to the protons, and a profile due to the sum of the two. It will be noticed that the alpha-particle-electron production peak is displaced from that of the proton-electron production rate peak upward to 50 km. This height corresponds to the stopping depth of alpha particles vertically incident with an energy of 119.5 Mev, their geomagnetic cutoff corresponding to a proton cutoff of 112 Mev.

The alpha-particle-electron production rate profile also displays an interesting interplay between the geomagnetic cutoff and that due to the atmosphere. The electron production rate represented by the portion of Curve II (Fig. 3) to the left of its peak is entirely due to alpha particles initially having energies in excess of their geomagnetic cutoff value of 119.5 Mev. Because the minimum energy that an alpha particle must have to reach a given depth for these particles is a function of the depth and zenith angle of incidence only, the atmosphere cutoff and the particle spectrum determine this part of the electron production rate profile. This seems to be contrary to the statement made earlier concerning the lack of dependence of the electron production rate profile on the particle spectrum. It must be remembered, however, that this statement was based on the assumption of a flux predominantly made up of protons.

It is really more precise to say that the electron production rate height profile is independent of the incident particle spectrum for that range of

heights wherein ionization is predominently due to particles that entered the atmosphere having the geomagnetic cutoff energy characteristic of the given latitude. For protons at College, Alaska, these heights are 32 km and greater. For heights less than these, the electron production ray due to protons falls off sharply with increasing depth (decreasing height) and electron recombination is rapid and complete. The contribution to the total cosmic radio noise attenuation due to the ambient electron density distribution that would be spectrum-sensitive is negligible. Were alpha particles the primary ionizing agent, there would be a local dependence of the electron production rate on the particle spectrum.

The electron production rate, represented by the portion of Curve II (Fig. 3) to the right of its peak, is due primarily to the geomagnetic cutoff alpha particles. Like that portion of the proton-electron production rate profile analogous to it, this part of the production rate curve is independent of the alpha-particle spectrum.

The sum profile (Curve III, Fig. 3) shows an approximate twofold increase in the electron production rate resulting from the addition of one alpha particle per ten protons in the flux. This is not a drastic change, especially in view of the fact that the ambient electron density varies as the square root of the production rate [Eq. (3.13)]. It would seem that a contamination of a proton flux by alpha particles, unless it were very heavy, would not be readily discernable from cosmic radio noise measurements.

The electron density height profiles resulting from the action of a solar cosmic ray bombardment are shown in Fig. 4. Features of immediate interest are the locations of the peaks of the curves presented. Both the daytime and nighttime curves attain their maximum values at considerably greater heights than those at which the maximum primary production of electrons occurs. The height of peak electron density is greater at night than for the day which is character-

istic of the behavior of the normally occurring ionosphere layers. Curve II(b) (Fig. 4) represents the nighttime electron density profile due to an alpha-particle-proton flux and exhibits an irregularity at about 52 km due to the stopping alpha particles. Otherwise the curves are quite smooth.

The relative positions of the daytime peak and nighttime peak are opposite to those given by Bailey (12). The midday electron density, according to this author, peaks at about 85 km while the nighttime profile has its maximum at about 75 km. Bailey's results and the results derived from the present analysis agree in one respect, that being the approximate constancy of the layer height with change in geomagnetic latitude. Ortner, Egeland and Hulqvist (29), basing their statement on the results derived in an earlier paper by Hulqvist and Ortner (30), believe that the height of maximum electron density decreases with decreasing geomagnetic latitude. For a geomagnetic latitude of 59.7 they claim a layer is formed by a proton bombardment having a lower boundary situated at a height of 10 km and the "point of gravity" of the electron distribution resides at 15-20 km above ground level. They cite very low frequency and medium frequency propagation observations to support their position.

These differences with the results of the present study are qualitative; quantitative discrepancies are even more marked. Of all the limits in the chain of deduction connection the spectrum of the bombarding solar particles to the cosmic radio noise absorption, the one joining the electron density profile to the electron production rate in the atmosphere is surely the most doubtful. It has been brought out earlier that the electron recombination mechanism in the height range 30 to 90 km is a complex one, and there is disagreement concerning the values of the rate coefficients of the various component processes. It has also been mentioned that the numerical discrepancies appearing between Bailey's calculation of the negative-ion-to-electron ratio, λ, and those

presented here arise from the different rate coefficients used rather than from the differing methods employed in obtaining this quantity. This is true of all the discrepancies displayed in Figs. 5, 6, 7, and 8 which present profiles of important quantities relevant to the electron density distribution. It should be pointed out that the curves representing the effective recombination coefficient as a function of height should be read from right to left, the abscissa being on the top of the figure for α_{eff}. This was done to make Figs. 5 and 6 more easily legible. On examination of Figs. 5 and 6, one observes an almost constant order-of-magnitude difference in λ, for a given height, existing between Bailey's curve (B) and the curve derived in the course of the present investigation (A). This discrepancy reflects the order-of-magnitude difference in the respective choices of the values of η, the attachment rate coefficient. Whereas λ as computed by Bailey is larger than that derived in the present work, this is reversed in the case of the effective recombination coefficient. Figures 7 and 8 compare for day and night, respectively, the quantity $(1 + \lambda)\alpha_{eff}$ which, in fact, if not in name, is the equilibrium recombination coefficient in the 30-90 km height range. The rate coefficients used by Bailey dictate a smaller electron density for a given value of the electron production rate than possible for those used in the present study. This is explicitly shown in Fig. 9, wherein the ratio of the electron density, as would be calculated with Bailey's choice of coefficients (N_B) to that (N_A) computed with those rate values employed in the present study, is displayed. Except for heights in excess of 75 km under daytime conditions N_N/N_A is less than unity. Between 50 and 60 km, which is the most important height range as far as the actual absorption of cosmic radio noise is concerned (see Fig. 10), the daytime curve represents nearly an order of magnitude difference.

Figure 10 gives the specific attenuation (db/km) profiles for cosmic radio

noise at 27.6 mc/sec corresponding to the electron density profiles of Fig. 4. A rather striking feature displayed by these curves is the reversal of the height positions of the daytime and nighttime peaks with respect to their relative positions in the electron density profiles. The positions of the peak values of the specific attenuation occur at considerably greater heights than given by Hulqvist and Ortner (30) but are slightly lower than the maxima of Bailey's curves. It is also noteworthy that the peak values of the specific attenuation profiles occur at lesser heights than those of the corresponding electron density.

The total vertical attenuation as a function of the proton flux at geomagnetic cutoff of 112 Mev is given in Fig. 11. These curves show the almost negligible dependence of the attenuation on the shape of the proton integral spectrum. The daytime curves are straight lines on a log-log scale. The slight forward bend in the nighttime curves is due to the dependence of λ, the negative-ion-to-electron ratio, on the electron production rate for large flux values. This would not be observed were λ obtained by Bailey's method. The effect, however, is small which demonstrates the excellence of Bailey's approximation for λ [Eq. 3.11)].

The Absorption as a Function of the Particle Cutoff Energy

It has been pointed out several times in the course of this thesis that the low-energy part of the solar cosmic ray spectrum is responsible for most of the ionization occurring in the upper atmosphere during a solar particle bombardment. Consequently, the value of the low-energy cutoff is of decisive importance in determining the amount of absorption suffered by cosmic radio noise at a given geographic location.

The calculation of the cosmic radio noise attenuation was originally made for cutoff energies corresponding to the Quenby-Webber proton cutoff rigidities

of four geographic locations at which facilities were available for measuring the cosmic noise attenuation associated with a solar event. The minimum energy the solar particles must possess to reach the terrestrial atmosphere was thought of as being established in a known way by the earth's magnetic field. Hence, a particle cutoff energy variation with geomagnetic latitude would, through the solar cosmic ray spectrum, be reflected in a characteristic distribution of cosmic radio noise absorption. However, the validity of the results displayed in Figs. 14 through 28 which give constant height contours of the electron production rate, electron density and specific attenuation as well as the total cosmic noise absorption as a function of the solar proton cutoff energy for day and night, is not affected by the assumption made concerning the type of cutoff operative during an event. In a later section the measured geographic distribution of cosmic radio noise attenuation associated with the solar flare of July 14, 1959, is discussed.

Figures 14, 15, and 16 give constant height contours for the electron production rate versus cutoff energy due to protons distributed in energy according to the differential energy spectra indicated in the figures. These curves can be used to facilitate further electron production rate calculations using "broken" spectra, as E_c mathematically is but a lower limit, and other changes necessary for such a calculation merely involve adjustments in multiplicative constants. For instance, if one wished to ascertain the electron production rate at a given height to a trial spectrum of the type

$$N(E_i) = \alpha_1 E_i^{-3} , \qquad \text{for } E_{c_1} \leq E_{c_2} ,$$

and

$$N(E_i) = \alpha_2 E_i^{-7} , \qquad \text{for } E_{c_2} \leq E_i \leq \infty ,$$

the curves could be used in accordance with the relation

$$\int_{\Omega}\int_{E_{c_1}}^{\infty} N(E_i)\,\frac{dE}{dx}\,dE\,d\Omega = \int_{\Omega}\left[\int_{E_{c_1}}^{E_{c_2}} \alpha_1 E_i^{-3}\,\frac{dE}{dx}\,dE + \int_{E_{c_2}}^{\infty} E_i^{-7}\,\frac{dE}{dx}\,dE\right] d\Omega\,, \qquad (7.3)$$

but

$$\int_{\Omega}\int_{E_{c_1}}^{E_{c_2}} dE\,d\Omega = \int_{\Omega}\int_{E_{c_1}}^{\infty} dE\,d\Omega - \int_{\Omega}\int_{E_{c_2}}^{\infty} dE\,d\Omega\,, \qquad (7.4)$$

where the expression represented by the difference of the double integrals on the right-hand side of the above symbolic equation can be obtained from the curves presented in Fig. 14 (say) with a proper adjustment of constants. The contours are of sufficient regularity that interpolation is possible. This offers a method of obtaining q(h) with a minimum of labor for spectra other than those chosen for the present work.

Figures 17 through 22 present constant height contours for the daytime electron density and specific attenuation respectively as functions of the solar proton cutoff energy for the proton differential energy spectra indicated. Because both of these quantities, for a given cutoff energy, present profiles which assume maximum values at atmospheric heights of some intermediate value in the height range of interest, the contours are drawn in such a manner as to avoid the inevitable confusion that would result from a conventional display. Contours for heights less than the maximum are drawn from left to right--those for heights greater than the maximum are drawn oppositely. The possibility of drawing these contours, as presented, demonstrates the approximate constancy of the height of the layer maxima with geomagnetic latitude, were a Störmer mechanism effective in establishing a low-energy cutoff. This was mentioned earlier in this discussion in connection with a seemingly contrary opinion held by Ortner, Egeland, and Hulqvist (29).

Figures 23, 24, and 25, the daytime attenuation versus cutoff energy curves, display one of the most striking results obtained in the study, the rectilinear

nature of these curves when plotted on log-log paper. The nighttime curves are not quite straight. This is due, in their case, to the dependence of the negative-ion-to-electron ratio on the electron production rate at night. The regularity of the daytime curves suggests the possibility of a simple empirical formula which might give the total vertical attenuation provided the cosmic ray flux, the cutoff energy and γ, the slope of the differential energy spectrum (on a log-log plot) are known.

For the daytime case, Bailey's expression for λ, the negative-ion-to-electron ratio, [Eq. (3.11)] is valid. If λ is independent of the electron production rate, the square of the total vertical attenuation is proportional to the flux,

$$A^2 = J ,$$

where A is the total vertical attenuation in db and J is the integral flux (protons/cm^2-sec-ster) above cutoff. Moreover, for a given value of J, the total vertical attenuation, A, is nearly proportional to $E_c^{-\gamma/2}$,

$$A = L(\gamma) E_c^{-\frac{\gamma}{2} + \beta(E_c,\gamma)} , \qquad (7.5)$$

where E_c is the low-energy cutoff in Mev, $L(\gamma)$ is a proportionality factor, and $\beta(E_c,\gamma)$ is a slowly varying parameter.

These facts suggest an investigation of the quantity

$$\log_{10}[A^2 E_c^{\gamma}/J(112)] ,$$

where A is total vertical attenuation (db) of cosmic radio noise corresponding to a proton differential energy spectrum of $W(E) = \alpha E^{-\gamma}$ and a low-energy cutoff of E_c. $J(112)$ is the corresponding integral proton flux for E_c = 112 Mev.

In order to present numerical results, it is necessary to choose a "reference" cutoff energy for the integral spectrum. E_c = 112 Mev is the normal proton geomagnetic cutoff at College, Alaska. However, the formula which will be presented presently does not depend on this interpretation of the argument of $J(E_c) = J(112)$.

The following empirical relationship is obtained from the curves presented in Figs. 23, 24, and 25:

$$\log_{10}[A^2 E_c^{\gamma}/J(112)] = 2(\gamma - 1) + M(\gamma, E_c) , \qquad (7.6)$$

where $M(\gamma, E_c)$ is given in Fig. 30 for $\gamma = 3$, 5, and 7, a range in E_c of $20 \leq E_c \leq 260$ Mev, and a range of integral spectra $10 \leq J(112) \leq 500$ protons/cm^2-sec-ster.

Equation (7.6) and Fig. 30, to a very good approximation, embody the results of the calculations performed to obtain the total vertical daytime cosmic noise attenuation due to a known proton flux at a frequency of 27.6 mc/sec. The daytime curves in Figs. 23, 24, and 25 can be derived from them, and through interpolation, the cosmic noise attenuation as a function of the proton cutoff energy for cosmic ray spectra other than those for which the full calculation was made can be obtained. Equation (7.6), along with the curves in Fig. 30, can be thought of as representing an ultimate condensation of the results of the calculations for the total daytime attenuation of cosmic radio noise at 27.6 mc/sec due to a solar proton bombardment of the atmosphere.

Figure 29 shows the theoretical geomagnetic latitude distribution of cosmic radio noise attenuation under the assumption that the terrestrial magnetic field is undisturbed and that a power-law spectrum holds down to cutoff. The low-energy cutoff is obtained from the Quenby-Webber cutoff rigidity formulae which represent a further refinement of the simple dipole theory (16). The latitude variation displayed in Fig. 29 is quite steep. It will be seen in a following section that the measured cosmic radio noise attenuation does not display the strong latitude variation shown in Fig. 29, but instead tends to be almost constant over the whole polar cap.

CHAPTER VIII

The Riometer

The cosmic radio noise attenuation data, to which the results presented in this thesis are to be compared, are obtained from riometer measurements made during a solar particle event. However, before comparisons are drawn, a brief account should be given of the relevant operational characteristics of the recording instrument. For a more complete description of the riometer (Relative Ionosphere Opacity Meter) one is referred to the paper devoted to this instrument by Little and Leinbach (31). For the purposes of this thesis the following data are sufficient:

Receiver Characteristics

Center Frequency	27.6 mc/sec
Width of Frequency Sweep	100 kc
R. F. Bandwidth	0.5 mc

In operation, a 6-kc exploring band is swept at about 2.5 kc/sec. This band in turn traverses a 100-kc search band every 40 seconds. The minimum signal strength recorded is attributed to cosmic radio noise. The sweeping technique described is designed to discriminate against man-made narrow band interference at the operating frequency of the system.

Antenna--3-element Yagi with 1/2 power beamwidth $\begin{cases} 60^\circ \text{ E plane} \\ 110^\circ \text{ H plane} \end{cases}$

Dynamic Range--15 db (fixed gain); 30 db (variable gain).

It is apparent immediately that the single-frequency analysis performed for this thesis is adequate. The spectral components in the operating band of the system, as given above, would show entirely negligible differential attenuations. The same statement cannot be made with regard to the total vertical attenuation calculated and the attenuation actually recorded. The relatively large beamwidth of the antenna employed permits the reception of a significant amount of

radiation that has traversed the absorbing region of the upper atmosphere obliquely. This should result in a greater measured absorption for a given particle flux than that calculated. The difference can be accounted for in an approximate way by an integration over an hypothetical receiving pattern that simulates the actual pattern of the Yagi. The following brief analysis is admittedly rough, but demonstrates the fact that the results derived for vertical attenuation do not differ very significantly from those measured, provided the difference is due only to the receiving pattern of the riometer antenna.

Let the noise power received vertically during an undisturbed period be P_o, and that similarly received during flare conditions be P. Then their ratio is

$$P/P_o = e^{-a} , \tag{8.1}$$

where a is the integral of the specific attenuation over the vertical height (in km).

$$a = \frac{10^3}{c} \int_{h_1(km)}^{h_2(km)} \frac{\omega_p^2 \nu}{\omega^2 + \nu^2} \, dh . \tag{8.2}$$

The quantities in the right-hand side of the above equation have been defined previously. The total relative vertical absorption, A, is given by

$$A = a(10 \log_{10} e) = 4.32a \text{ (db)} . \tag{8.3}$$

On the other hand, the total relative absorption, taking the receiving pattern into account, is

$$A_p = 10 \log_{10} e \left[\frac{\int_o^{2\pi} \int_o^{\pi/2} G(\theta,\varphi) e^{-a \sec \theta} \sin \theta \, d\theta \, d\varphi}{\int_o^{2\pi} \int_o^{\pi/2} G(\theta,\varphi) \sin \theta \, d\theta \, d\varphi} \right] \text{(db)} , \tag{8.4}$$

where G is the absorption cross section of the antenna. A unidirectional power pattern of $\cos^2\theta$ approximates fairly well the Yagi pattern with the 1/2 power beamwidths given above. It has a directivity (gain) of 4 db over isotropic and a 1/2 power beamwidth of 90^o (about midway between the E and H plane beamwidths of the Yagi, as quoted from Little and Leinbach). The shape of the unidirec-

tional cosine-squared pattern is such as to slightly enhance the effect of obliquity over that due to the Yagi pattern. This can be seen by an inspection of a diagram of the two patterns together which appears in the Beam Antenna Handbook (32). The unidirectional cosine-squared power pattern can be expected to provide a fair estimate of the difference that can be expected between measurements made of an event with similar riometers, one being equipped with a very narrow beam antenna directed vertically upward, and the other with the three-element Yagi.

Letting $G = \cos^2\theta$, A_p is given by

$$A_p = 10 \log_{10} \left\{ e^{-a} \left[1 - \frac{a}{2} (1 - a) \right] - \frac{a^3}{2} E_1(a) \right\}, \qquad (8.5)$$

where

$$E_1(a) \equiv \int_a^\infty \frac{e^{-z}}{z} dz ,$$

the exponential integral.

In the following table is presented values of the total vertical attenuation A, the attenuation that would be recorded by a riometer equipped with an (hypothetical) antenna having a cosine-squared power pattern, A_p, and the ratio A/A_p for selected values of a, the integral of the specific absorption.

a	A(db)	A_p (db)	A/A_p
0.01	0.0434	0.065	1.50
0.05	0.217	0.323	1.49
0.10	0.434	0.639	1.47
0.50	2.17	3.05	1.40
0.75	3.26	4.48	1.38
1.0	4.34	5.88	1.35
1.5	6.51	8.60	1.32
2.0	8.69	11.24	1.29
3.0	13.03	16.36	1.26
5.0	21.71	26.26	1.21

For events producing attenuations less than 1 db, one could relate the vertical to the measured attenuation by $A_{measured} \approx 1.3A$. For

$$1 \leq A_{meas.} \leq 10 \text{ db}, \qquad A_{meas.} \sim 1.35A,$$

$$10 \leq A_{meas.} \leq 15 \text{ db}, \qquad A_{meas.} \sim 1.30A.$$

It may be stated confidently that any large discrepancies which might exist between the measured absorption and the calculated vertical absorption are not due to the receiving pattern of the riometer antenna.

CHAPTER IX

Comparison with Experimental Data

In order that an actual solar cosmic ray event be examined in light of the theoretical results shown in Figs. 23 through 29 and represented by Eq. (7.6) and Fig. 30, there must be available adequate latitude coverage of the cosmic radio noise absorption associated with the phenomena and a measured cosmic ray spectrum. Reid and Leinbach (25) have presented absorption data from riometers situated at College, Barrow and King Salmon, Alaska, and Thule, Greenland, for the solar outbursts occurring on May 10 and July 10, 14, and 16, 1959. Various radio propagation, geomagnetic, and other data related to these same events, but collected at Kiruna, Sweden, are given by Ortner, Egeland, and Hulqvist (29) in their paper cited earlier. As far as cosmic radio noise data is concerned, there is excellent polar cap coverage for the four great flares of the year 1959.

On the other hand, a cosmic ray spectrum derived from data collected by balloon-borne counters has been published for but one of the 1959 events, that of July 14, which was the second of the July series of three.

As reported by Winkler, Bhavsar, and Peterson (15), the sudden commencement magnetic storm associated with the July 14 solar flare began at 0802 UT, July 15. At approximately 0900 UT balloon-borne counters of their Flight IGC-14, aloft at ceiling altitude over Minneapolis, registered a very spectacular and rapid rise in counting rate. This high intensity persisted for about five hours and

then began to decay. However, Flight IHC-G was launched at 0804 UT, July 15, and ascended during the five-hour period of relatively uniform high intensity. The solar cosmic ray influx, therefore, was being monitored by one flight (IGC-14) at ceiling altitude while the particle range spectrum was being obtained by a subsequent flight (IGC-G). The cosmic ray energy spectrum derived from the data obtained through these flights is given by Winkler, Bhavsar, and Peterson as

$$J(E_i) = 1.05 \times 10^8 E_i^{-2.9} \text{ cm}^{-2}\text{-sec}^{-1}\text{-ster}^{-1} , \qquad (7.1)$$

where $88 \leq E_i \leq 300$ Mev.

Absorption data taken at various locales in the north polar regions during the July 14 event are shown in Fig. 31. The data from Pt. Barrow, Thule, College, and King Salmon were copied from Fig. 6 of the paper of Reid and Leinbach (25) on polar cap absorption events. These authors presented the absorption data as superimposed curves. In Fig. 31 of this thesis the absorption curves are presented separately and on a somewhat different scale than that used by Reid and Leinbach. The Kiruna data were abstracted from Fig. 6 of the paper on very low frequency propagation by Ortner, Egeland, and Hulqvist (29). These data, as presented in their paper, were plotted with respect to Mid-European Time, which leads Universal Time by one hour. This correction was not attempted in Fig. 31, the absorption data were copied as presented in all cases as faithfully as possible.

It is evident that the upper atmosphere was still being affected by a particle bombardment due to the solar disturbance of July 10 at 0325 UT, July 14, the onset time of the second solar event of the July series. This is indicated by the presence of a residual absorption of cosmic radio noise of about 5 db at all riometer stations listed except King Salmon. Shortly following this second great flare, a recrudescence of cosmic radio noise absorption occurred, and at about 1500 UT, July 14, the cosmic ray bombardment due to this second flare seems

to have reached its full development. This last statement is based on the fact that all stations show an increasing attenuation of cosmic radio noise up to about 1500 UT. The College riometer did record a further sharp reduction in received cosmic radio noise power at about 2000 UT. However, this appears to have been due to strong localized auroral activity, as it is observed at no other station. The College riometer record indicates that an absorption in excess of 20 db occurred in the time interval 2300 UT, July 14, to about 1200 UT, July 15. It must be pointed out, however, that such large absorption values lie at the very limit of the dynamic range of the instrument. Riometer estimates of cosmic noise attenuation in excess of 15 db are inaccurate and the actual numerical values given should not be taken literally.

The normal geomagnetic cutoff at the Thule, Greenland, is the lowest of all stations listed. Consequently, the Thule riometer should be expected to show the largest absorption during a solar proton event. Yet the composite record of the polar cap absorption (Fig. 31) indicates that the absorption recorded at Thule was consistently less than that recorded at all stations other than the most southern geomagnetically, King Salmon. For example, at 1500 UT, July 14, the following values for cosmic radio noise absorption were recorded at the several stations:

Thule, Greenland	9.5 db
Pt. Barrow, Alaska	16 db
Kiruna, Sweden	14 db
King Salmon, Alaska	0 db

Even if one were to attribute 3 to 4 db absorption to auroral activity at the intermediate stations (Pt. Barrow, Kiruna, and College), the whole Thule record, if accepted at face value, remains an anomaly. That the accuracy of this record should in fact be held suspect is indicated by the excess of absorption registered at King Salmon during the magnetic storm (~ 12 db) over that recorded at

the same time at Thule (~ 10 db). It should be mentioned in this respect that the Thule riometer was not under scientific surveillance during these July events, situated as it was at a rather remote outpost, but was checked from time to time by U. S. Army personnel. During most of the period of its operation, it was unattended. It would not be unreasonable to suppose that the Thule riometer was operating under a bias error of at least 2 db during the July series. One may compare the absorption record of the Polar Blackout following the solar flare of May 10, 1959, from the Thule riometer with its record of the July events. The absorption at Thule during the May event was, according to the record, consistently greater than that recorded at the other polar stations. It would seem that a systematic malfunction of the Thule riometer during July is a likely explanation of this otherwise unexplicable behavior.

Were one to attempt to ascertain the cosmic radio noise absorption due to solar protons at 1500 UT, July 14, taking into account auroral contamination of the absorption data and a likely bias error in the Thule riometer record, one would arrive at the following values for solar cosmic ray induced cosmic radio noise absorption for the various polar cap riometer stations listed.

Station	Riometer Reading	Correction	Absorption due to solar cosmic rays
Thule	9.5 db	2 db (bias error)	11.5 db
Pt. Barrow	16 db	-3,-4 db (aurora)	13, 12 db
Kiruna	15.5 db	-3,-4 db (aurora)	12.5, 11.5 db
College	14 db	-3,-4 db (aurora)	11, 10 db
King Salmon	0 db	--	0 db

Is there any corroborative evidence that these adjusted absorption figures are in fact correct? To find such evidence, one may search the composite absorption record, Fig. 31, for a time period of minimum auroral activity, but during which one could assume, with some justification, that the same solar proton flux was responsible for the cosmic noise absorption recorded then as in the adjusted

record in question. The period shortly following the time that the maximum cosmic noise absorption was recorded at King Salmon seems to be one of reduced auroral activity. All three auroral zone stations (College, Kiruna, and Pt. Barrow) show rather sudden recoveries at about 1300 UT, July 15. The abruptness of these recoveries and the lack of change in the corresponding Thule record indicate a diminution of auroral activity rather than a change in the solar cosmic ray flux. The changes that had occurred at College, Kiruna and Pt. Barrow at this time are to be contrasted with those evidenced at all stations somewhat later (commencing at about 1800 UT, July 15) which were much more systematic and regular. These latter changes seem to represent a recovery due to a decay in the solar cosmic ray intensity rather than a decrease in auroral activity.

At 1500 UT, July 15, about two hours following the sudden recoveries recorded at College, Kiruna and Pt. Barrow just alluded to, the following values of cosmic radio noise absorption were recorded at the various riometer stations:

Thule	10.5 + 2 (bias error) = 12.5 db
Pt. Barrow	10 db
Kiruna	11 db
College	10 db
King Salmon	9 db

The cosmic radio noise absorption values presented above show consistency with the adjusted values of 1500 UT, July 14, appearing earlier in this section, but with King Salmon showing 9 db cosmic noise absorption. This latter reading is indicative of a breakdown of the geomagnetic cutoff that existed before the onset of the magnetic storm associated with the July 14 flare.

In summary, the above observations seem to support the following assumptions concerning the solar event of July 14, 1959:

(1) The fully developed solar proton influx bombarding the upper atmosphere

during the time interval 1500 UT, July 14, to about 1800 UT, July 15, 1959, can be represented by the integral spectrum obtained by Winkler, Bhavsar, and Peterson from balloon-borne counters at Minneapolis, Minnesota, shortly after the sudden commencement of geomagnetic storm of July 15, 1959. This spectrum can be presented in the form of a power law as follows:

$$J(E) = 1.05 \times 10^{8} E_i^{-2.9} \text{ protons/cm}^2\text{-sec-ster}, \qquad (7.1)$$

where $88 < E_i < 300$ Mev.

(2) Accounting as far as possible for absorption induced by auroral activity during the solar cosmic ray event and inaccuracies in the riometer data, one would conclude that the cosmic radio noise absorption due to the solar proton bombardment during the height of the July 14 event was virtually constant over the polar cap, and had a numerical magnitude of 10 to 12 db.

(3) A geomagnetic cutoff was operative from the onset time of the July 14 event to the time of the sudden commencement of the geomagnetic storm of July 15. This is directly adducible from the cosmic radio noise absorption record from King Salmon, Alaska, which shows no cosmic radio noise absorption up to the time of the S.C.

It is immediately obvious that the theoretical variation of cosmic radio noise absorption with geomagnetic latitude (Fig. 29) is not reflected in the absorption data of this event even when allowances are made for auroral contamination and riometer malfunction. It must be remembered in this respect that the theoretical variation of cosmic radio noise absorption as determined in this thesis is predicated on the assumption that extrapolation of the solar cosmic ray spectrum to low-energy values is permissible. The lack of variation of cosmic radio noise absorption over the polar cap in the presence of a geomagnetic cutoff is direct evidence of the inadmissibility of this assumption in this case at least. The solar proton integral spectrum must have begun to

flatten somewhere in the neighborhood of 90 or 100 Mev to produce the distribution of polar cap absorption inferred from the data. This statement may seem to conflict with the claim of Winkler et al. that their power-law spectrum is valid to 88 Mev. However, it is the only explanation that accounts for the observed variation of cosmic noise absorption in the presence of the normal (Quenby-Webber) cosmic ray cutoff. Were one to suppose that the geomagnetic cutoff actually operative on July 14, 1959, was quite different from that normally imposed by a dipole-like geomagnetic field, he would find that this would not obviate the theoretical necessity for a flattening of the cosmic ray spectrum. It would, however, permit a lower estimate to be made of the energy value at which the flattening of the spectrum began. Unfortunately there is no direct evidence that the cosmic ray cutoff was anything other than that normally operative over the polar cap. For protons the cutoff at College is 112 Mev. That there had been virtually the same cosmic noise absorption observed at Pt. Barrow and Thule as that recorded at College requires a flattening of the solar proton integral spectrum at energy values at least comparable to the geomagnetic cutoff for protons at College.

Can a correct estimate of the cosmic noise absorption during the event at a given station be made from the results of calculation, based as they are on the values of the various recombination rate coefficients adopted in this thesis? To answer this question, the solar proton integral spectrum obtained by Winkler, Bhavsar and Peterson can be used with the cutoff for protons obtained from the theory of Quenby and Webber in Eq. (7.6) to obtain the total vertical attenuation at College, Alaska, at 1500 UT, July 14. The composite absorption record, Fig. 31, indicates that the solar proton bombardment was fully developed at that time and the King Salmon record shows the existence of a geomagnetic low-energy cutoff for protons.

Substituting the proper numerical values for J(112 Mev), γ, and E_c into Eq. (7.6), one obtains:

$$J(112 \text{ Mev}) = 1.05 \times 10^8 (112)^{-2.9} = 119.7 ,$$

$$\gamma = 1 + 2.9 = 3.9 ,$$

$$E_c = 112 \text{ Mev} ,$$

$$M(E_c, \gamma) = 0.80 \text{ (from interpolation in Fig. 30)} ,$$

and

$$\log_{10}[A^2 (112)^{3.9}/119.7] = 2(3.9 - 1) + 0.80 ,$$

where A is the total vertical absorption in db. This yields

$$\boxed{A = 2.18 \text{ db} .}$$

The cosmic radio noise absorption recorded by the College riometer at 1500 UT, July 14, was 14 db. If one takes into account the absorption due to auroral activity, as was suggested earlier in this section, he must subtract 3 to 4 db from the value 14 db given in the record. A further correction for the finite beam width of the antenna, discussed in an earlier section, reduces the absorption figure by about 2 more db. This leaves a total vertical absorption of about 9 db, or a discrepancy of about 7 db between the actual total vertical attenuation of cosmic radio noise that can be directly attributed to the influx of solar protons during the July 14 event and that deduced from the cosmic ray spectrum measured in the course of the event. That less attenuation is predicted by a calculation from the cosmic ray spectrum than is actually observed is due either to the use of an incorrect electron-neutral collision frequency profile in the calculation, or to an underestimation of the equilibrium electron density. The second alternative is almost certainly the case, since the numerical determination of the electron density due to a solar proton bombardment depends rather critically on the values adopted for the various atmosphere rate coefficients. It was indicated in an earlier section of this thesis that

uncertainties of an order of magnitude or more can exist in the values one might choose to assign to these coefficients.

The curves representing the specific attenuation given in Fig. 10 show that the atmospheric height range of greatest importance for the absorption of cosmic radio noise is that of 50 to 65 km. At these heights the most important reaction occurring to establish the ultimate value of the electron density caused by the production of a free electron by solar cosmic rays is the attachment of electrons to oxygen molecules. The rate coefficient of this three-body process has recently been revised downward from a value of approximately $2 \times 10^{-29} n(O_2)$--[$n(O_2)$ is the number density of molecular oxygen] used by Bailey, to that of $1.5 \times 10^{-30} n(O_2)$, quoted by Nicolet and adopted for use in the present work. The results of the investigation of cosmic radio noise attenuation caused by solar cosmic rays presented in this thesis, indicate that a reinvestigation of this electron attachment process is needed. A further downward revision of the value of the rate coefficient of this process would bring agreement between the calculated and observed cosmic radio noise absorption due to a solar corpuscular bombardment of the earth's atmosphere.

CHAPTER X

Summary and Conclusions

In the course of this thesis there has been described a method of determining the changes produced in the upper atmosphere by an influx of solar cosmic rays. Such a bombardment brings into being a condition of abnormal ionization in a region below the normally occurring D layer. This is directly discernable as a change in the radio-wave propagation characteristics of the upper atmosphere, the region affected becoming one of relatively strong nondeviative absorption. This absorption is confined to the earth's polar regions. A quantitative measure of the absorbing power of the upper atmosphere under the influence of a

solar cosmic ray bombardment can be obtained through continuous monitoring of the intensity of the galactic radio noise reaching the earth's surface by special receiving systems (riometers) distributed over the geographical area affected.

The intensity and distribution of cosmic radio noise absorption is determined theoretically in this thesis under the following basic assumptions:

(1) The solar cosmic ray differential energy spectrum can be represented by a power law of the form

$$N = \alpha E_i^{-\gamma} ,$$

where α and γ are constants and E_i is the free-space particle energy. (This implies an integral spectrum of similar form which is consistent with results derived from balloon measurements).

(2) A low-energy cutoff, E_c, is imposed on the spectrum by the earth's magnetic field. The value of the cutoff energy for a given pair of geomagnetic coordinates is obtained from the theory of Quenby and Webber.

(3) The theoretical electron density profile existing in the region of abnormal ionization can be deduced from the assumption that a state of quasi-equilibrium exists between the production and recombination of free electrons. The individual electron production and recombination processes assumed to be of importance in the establishment of the electron density profile are dissociative recombination and electron attachment to molecular oxygen (loss mechanisms) and photodetachment and collisional detachment of electrons from heavy negative ions (secondary production mechanisms). A process of mutual neutralization between positive and negative ions also occurs. This process is important in establishing the negative-ion-to-electron ratio.

Calculations of the total vertical absorption of cosmic radio noise were performed using three trial solar proton spectra for four low-energy cutoff

values used correspond to the geomagnetic cutoffs at Pt. Barrow, Ft. Yukon, College, and Farewell, Alaska, respectively. The results of the calculations were sufficiently well ordered to permit the construction of absorption curves which are given in Figs. 23 through 28. Furthermore, it was possible to obtain an empirical formula of simple form relating the total vertical absorption of cosmic radio noise to the solar cosmic ray spectrum and the low-energy cutoff. This formula represents a continuation of the total vertical absorption for values of γ and E_c other than those used originally.

The results obtained from the theory are compared with observations made on the solar cosmic ray event of July 14, 1959. After reasonable allowances are made for auroral effects and possible riometer malfunction during the event, the following discrepancies between the theoretical results and observation are shown to exist:

(1) The distribution of cosmic radio noise absorption over the polar cap did not conform in this event with that derived under the assumptions given above. The absorption observed was virtually constant while the calculated distribution of absorption indicates that a strong variation with geomagnetic latitude should exist.

(2) The theory yields considerably less absorption for a known solar cosmic ray flux at a given location than that actually observed.

The discrepancy in latitude variation is indicative of a failure of the power-law spectrum to hold for solar proton energies much below 100 Mev in this particular event. This means that extrapolations of the spectrum to energy values less than those directly measurable can be an invalid procedure. A lack of variation of cosmic radio noise absorption with geomagnetic latitude implies a flattening of the solar cosmic ray spectrum in the neighborhood of the highest cutoff energy displaying the constant absorption.

The failure of the theory to account for the magnitude of the cosmic radio

noise absorption observed must be attributed to one or more incorrect values of the atmospheric recombination rate coefficients. The particular coefficient most suspect is that of the three-body electron attachment process to molecular oxygen.

This process is the most important one occurring in the atmospheric region of greatest absorption; therefore, an erroneous value of its rate coefficient would introduce an appreciable error in the final results of the absorption calculation. Furthermore, this rate coefficient has recently undergone an order-of-magnitude revision in its numerical value. A large degree of uncertainty still exists in the numerical value one should ascribe to this quantity.

APPENDIX

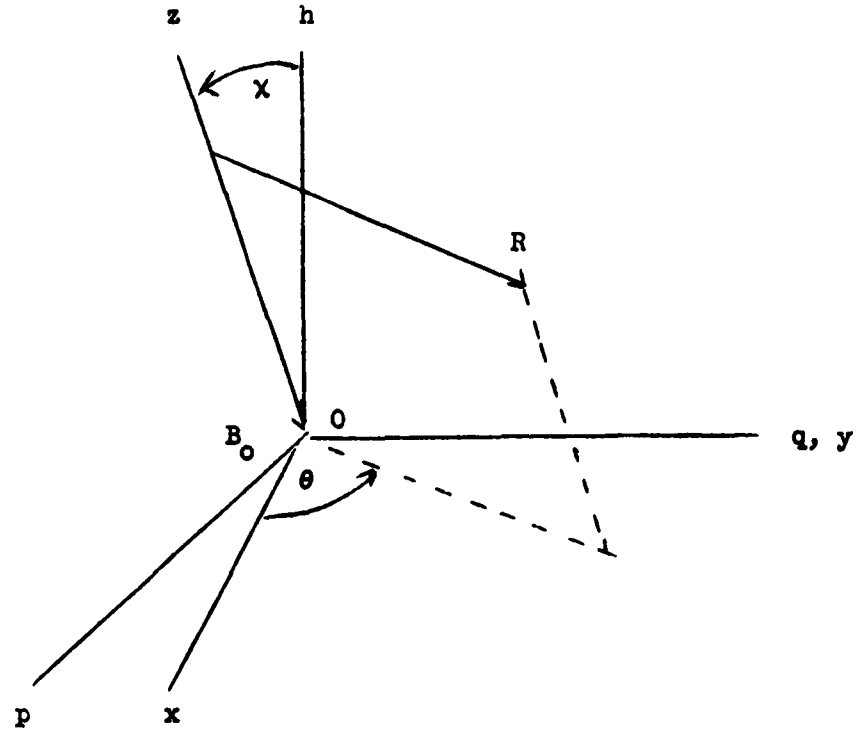

The particle whose trajectories and atmospheric stopping heights were determined in the analysis to be described were considered to be protons having

initial energies, E_i, in the range

$$20 < E_i < 260 \text{ Mev} .$$

Relativistic effects were neglected and the classical equations of motion were used throughout.

Let p, q, h be a cartesian coordinate system situated on the earth at a given geomagnetic latitude; h is positive upward in the direction of the local zenith. This system will be called the earth coordinate system.

Let x, y, z be a cartesian coordinate system so situated that z is parallel but oppositely directed to the local terrestrial magnetic field which is considered (in the small) to be of constant magnitude and direction. This system will be called the magnetic field coordinate system. The axes $\overline{Oh}$, $\overline{Oz}$, and $\overline{Op}$ are coplaner, and χ is the angle between the zenith direction (h) and the direction of the z axis (opposite to the earth's field direction). The q and y coordinates for the two systems, respectively, are collinear.

The cylindrical coordinate system, in whose terms the equations of motion of a proton of mass m and charge e traveling through the atmosphere are expressed, is related to the magnetic field coordinate system through the following equations.

$$\begin{aligned} x &= R \cos \theta , \\ y &= R \sin \theta , \\ z &= z . \end{aligned} \tag{A.1}$$

The equations of motion themselves are

$$\begin{aligned} m\ddot{R} - mR\dot{\theta}^2 + eR\dot{\theta}B_o &= Q_R , \\ mR\ddot{\theta} + 2m\dot{R}\dot{\theta} - e\dot{R}B_o &= Q_\theta , \\ m\ddot{z} &= Q_z , \end{aligned} \tag{A.2}$$

where m is the mass and e the charge of the particle, B_o is the earth's field and $\vec{Q}$ is a dissipative force given in terms of the energy-loss function for protons (Fig. 1, Curve A). The dot denotes differentiation with respect to the

time. The components of $\vec{Q}$ are given as follows:

$$Q_R = -\rho \frac{dE}{dS} \hat{e}_R \cdot \hat{e}_S = -\rho \frac{dE}{dS} \frac{v_R}{|v|} ,$$

$$Q_\theta = -\rho \frac{dE}{dS} \hat{e}_\theta \cdot \hat{e}_S = -\rho \frac{dE}{dS} \frac{v_\theta}{|v|} , \qquad (A.3)$$

$$Q_z = -\rho \frac{dE}{dS} \hat{e}_z \cdot \hat{e}_S = -\rho \frac{dE}{dS} \frac{v_z}{|v|} ,$$

where ρ is the air density at a height h; dE/dS is the energy-loss function (with a small change in notation) given in Fig. 1, Curve A; $\hat{e}_R$, $\hat{e}_\theta$, $\hat{e}_z$ are unit vectors pointing in the positive radial, azimuthal and axial directions in the magnetically centered cylindrical coordinate system; $\hat{e}_S$ is a unit vector pointing in the instantaneous direction of the particle motion; v_R, v_θ, v_z are the components of the particle velocity in the R, θ, and z directions, and $|v|$ is the absolute value of the total velocity.

The following substitutions are made for the dependent variables R and θ and for the independent variable, t (the time),

$$R = R_o + \xi ,$$

$$\theta = \varphi + \omega_H t , \qquad (A.4)$$

$$\tau = \omega_H t .$$

R_o is the initial radius of the circular spiral along which the proton is moving before being slowed down in the atmosphere, and ω_H is the initial gyrofrequency.

$$\omega_H = eB_o/m . \qquad (A.5)$$

Making these substitutions into the equations of motion [Eq.(A.2)], one obtains the following, after a certain amount of reduction and simplification:

$$\frac{d^2\xi}{d\tau^2} - (R_o + \xi)\left(\frac{d\varphi}{d\tau}\right)\left(\frac{d\varphi}{d\tau} + 1\right) = -F \frac{d\xi}{d\tau} ,$$

$$\frac{d^2\varphi}{d\tau^2} + \frac{[2(d\varphi/d\tau) + 1]\, d\xi/d\tau}{(R_o + \xi)} = - F\left(\frac{d\varphi}{d\tau} + 1\right), \qquad (A.6)$$

$$\frac{d^2z}{d\tau^2} = - F \frac{dz}{d\tau},$$

where

$$F = \frac{\alpha\rho(h)(dE/dS)(E)}{m\omega H^2[(d\xi/d\tau)^2 + R_o + \xi)^2[(d\varphi/d\tau) + 1]^2 + (dz/d\tau)^2\}^{1/2}} . \qquad (A.7)$$

In the actual numerical work, the following units were used: length in kilometers, $\rho(h)$, the density, in grams/cm^3, m, the mass, in grams, e, the charge, in coulombs, ω, the gyrofrequency, in radians/sec, $(dE/dS)(E)$, the energy loss, in Mev per gm/cm^2, α is a numerical constant whose value depends on the units used. (It was assigned a value of 1.60×10^{-11} which is consistent with the units employed in the calculation.) τ, dimensionless, F, dimensionless.

The initial conditions imposed on the equations of motion (Eq. A.6) to determine a trajectory are: h_i = the initial (starting height of the proton above the earth; $\dot{p}_i$, $\dot{q}_i$, $\dot{h}_i$ = the components of the particle velocity at height h_i in the earth coordinate system. These quantities along with a value for the angle χ are sufficient to specify the trajectory. The actual physical location of the trajectory is irrelevant. In the magnetic cylindrical coordinate system the initial conditions on R_i, $\dot{R}_i$, θ_i, and $\dot{\theta}_i$ are: $R_i = R_o$ (R_i = the initial spiral radius); $\dot{R}_i = 0$ (initially the particle trajectory is a circular spiral); $\theta_i = \varphi_i$ $(\tau = 0)$; $\dot{\theta}_i = \omega_H$ (the free-space gyrofrequency).

In terms of the transformed variables we have

$$\xi_i = 0 ,$$

$$\left.\frac{d\xi}{d\tau}\right|_i = 0 , \qquad (A.8)$$

$$\left.\frac{d\varphi}{d\tau}\right|_i = 0 .$$

Equations (A.8) hold for any trajectory. A particular trajectory is determined by the initial values of z, $\dot{z}$, R_o, and φ, which are derived from the initial values h_i, $\dot{p}_i$, $\dot{q}_i$, $\dot{h}_i$.

The initial value of z can be expressed in terms of R_o, h_i, and φ_i.

$$z_i = R_o \cos \varphi_i \tan \chi + h_i \sec \chi \ . \tag{A.9}$$

Now

$$R_o = (2mE_{o\perp})^{1/2}/B_o e = (m/B_o e)[(v_i^2 - v_{i\parallel})]^{1/2} \ ,$$

where $E_{o\perp}$ is the kinetic energy associated with the motion transverse to the magnetic field at height h_i, and $V_{i\parallel}$ is the component of the initial velocity (the velocity at height h_i) parallel to the magnetic field. After a certain amount of algebraic manipulation, it can be shown that

$$R_o = (1/\omega_H)[(\dot{p}_i \cos \chi - \dot{h}_i \sin \chi)^2 + \dot{q}_i^2]^{1/2} \ . \tag{A.10}$$

Thus Eq. (A.10) expressed R_o in terms of initial values of the velocity in the earth coordinate system.

$$z = p \sin \chi + h \cos \chi \ ,$$

so

$$\left.\frac{dz}{d\tau}\right|_{\tau=0} = \frac{1}{\omega_H} (\dot{p}_i \sin \chi + \dot{h}_i \cos \chi) \ , \tag{A.11}$$

and finally, because the initial velocity vector must be normal to the initial radius vector, R_o, we have

$$\varphi_i = \tan^{-1}(-\dot{x}_i/\dot{y}_i) \ ,$$

$$\varphi_i = \tan^{-1}[(\dot{h}_i \sin \chi - \dot{p}_i \cos \chi)/\dot{q}_i] \ . \tag{A.12}$$

Care must be exercised in choosing the correct branch of this function [Eq. (A.12)]. Thus all initial quantities of importance are given in terms of the necessary initial conditions in the earth coordinate system.

To determine a trajectory, one must solve the equations of motion, Eqs. (A.6), numerically with the above initial conditions. The changes of variable in the differential equations, especially in the independent variable, were made

primarily for scaling purposes to facilitate the numerical integration. Final values computed were ξ_f, φ_f, and z_f for stopping particles, i.e., for the condition that the particles' kinetic energy equals zero. A further transformation of coordinates gives the stopping height h_f,

$$h_f = z_f \cos \chi - x_f \sin \chi \ . \tag{A.13}$$

The contents of this Appendix can be summarized as follows:

$$\frac{d^2\xi}{d\tau^2} - (R_o + \xi)\frac{d\varphi}{d\tau}\left(\frac{d\varphi}{d\tau} + 1\right) = - F \frac{d\xi}{d\tau} ,$$

$$\frac{d^2\varphi}{d\tau^2} + \frac{[2(d\varphi/d\tau) + 1]\, d\xi/d\tau}{R_o + \xi} = - F\left(\frac{d\varphi}{d\tau} + 1\right) , \tag{A.6}$$

$$\frac{d^2z}{d\tau^2} = - F \frac{dz}{d\tau} ;$$

$$F = \frac{1.60 \times 10^{-11} \rho(h)(dE/dS)(E)}{m\omega_H^2\{(d\xi/d\tau)^2 + (R_o + \xi)^2[(d\varphi/d\tau) + 1]^2 + (dz/d\tau)^2\}^{1/2}} . \tag{A.7}$$

The particle kinetic energy in Mev is given by

$$E(\text{Mev}) = 6.25 \times 10^{15} \frac{m\omega_H^2}{2}\left[\left(\frac{d\xi}{d\tau}\right)^2 + (R_o + \xi)^2\left(\frac{d\varphi}{d\tau} + 1\right)^2 + \left(\frac{dz}{d\tau}\right)^2\right] .$$

Initially

$$\xi_i = 0 , \qquad \left.\frac{d\xi}{d\tau}\right|_i = 0 , \qquad \left.\frac{d\varphi}{d\tau}\right|_i = 0 , \tag{A.8}$$

and in terms of the initial values h_i, $\dot{p}_i$, $\dot{q}_i$, $\dot{h}_i$ the other necessary initial values are given as follows:

$$R_o = (1/\omega_H)[(\dot{p}_i \cos \chi - h_i \sin \chi)^2 + q_i^2]^{1/2} , \tag{A.10}$$

$$z_i = R_o \cos \varphi_i \tan \chi + h_i \sec \chi , \tag{A.9}$$

$$\left.\frac{dz}{d\tau}\right|_i = \frac{1}{\omega_H}(\dot{p}_i \sin \chi + \dot{h}_i \cos \chi) , \tag{A.11}$$

$$\varphi_i = \tan^{-1}[(\dot{h}_i \sin \chi - \dot{p}_i \cos \chi)/\dot{q}_i] . \tag{A.12}$$

The coordinate transformations used were

$$x = p \cos \chi - h \sin \chi ,$$
$$y = q , \qquad (A.15\Delta$$
$$z = p \sin \chi + h \cos \chi ,$$

and its inverse. Also, the cylindrical system is related to the cartesian magnetic system through

$$x = R \cos \theta ,$$
$$y = R \sin \theta , \qquad (A.1)$$
$$z = z ,$$

and

$$h_f = a_f \cos \chi - x_f \sin \chi . \qquad (A.13)$$

In addition to the trajectory and stopping height calculations, a particle range calculation was made,

$$R_y = 10^5 \int_{traj} \rho(h) \left[\left(\frac{d\xi}{d\tau} \right)^2 + (R_o + \xi)^2 \left(\frac{d\varphi}{d\tau} \right)^2 + \left(\frac{dz}{d\tau} \right)^2 \right] d\tau \ ga/cm^2 . \qquad (A.16)$$

This was done to provide a check on the correctness of the numerical work. The range in air of a particle with initial energy E_i is known and the computed range can be directly compared with known values.

The equations of motion and initial conditions used in the forms given above allowed one to study the structure of particle trajectories as well as to determine particle stopping heights. Of considerable interest was the amount of spiraling the particle performed in its journey down through the atmosphere. The initial height (h_i) chosen to begin the numerical integration was 105 km. The initial velocities were chosen in accordance with various stipulated initial directions with respect to the earth's field and initial kinetic energies. The numerical results displayed negligible proton energy loss occurring at heights

greater than about 65 km, but at heights less than this the rate of loss becomes great, the particles being stopped rather abruptly. The numerical solutions also indicate that for solar cosmic rays there is no spiraling in the atmosphere--the rectilinear approximation to the actual particle trajectory is almost always adequate.

REFERENCES

1. P. Meyer, E. Parker, and J. A. Simpson, Phys. Rev. 104, 768 (1956).

2. B. Peters, J. Geophys. Res. 64, 155, (1959).

3. E. P. Ney, Ann. Rev. Nucl. Science 10, 461 (1960).

4. I.G.Y. Bulletin, Natl. Acad. Sciences, No. 35, May, 1960.

5. A. P. Mitra and C. A. Shain, J. Atmos. Terrest. Phys. 4, 204 (1953).

6. M. Nicolet and A. C. Aikin, J. Geophys. Res. 65, 1469 (1960).

7. B. Rossi, High Energy Particles, (Prentice-Hall, Inc., New York, 1952).

8. R. L. F. Boyd and M. J. Seaton, eds., Rocket Explorations of the Upper Atmosphere (Pergamon Press Ltd., London, 1954).

9. N. Nicolet, Phys. Fluids 2, 95 (1959).

10. Rocket Panel, Phys. Rev. 88, 1027 (1952).

11. E. Segrè, ed., Experimental Nuclear Physics (John Wiley and Son, New York, 1955) Vol. I.

12. D. K. Bailey, Proc. I.R.E. 47, 255 (1959).

13. R. R. Brown and R. G. D'Arcy, Phys. Rev. Letters 3, 390 (1959).

14. K. A. Anderson, R. Arnoldy, R. Hoffman, L. Peterson, and J. R. Winckler, J. Geophys. Res. 64, 1133 (1959).

15. J. R. Winckler, P. D. Bhavsar, and L. Peterson, J. Geophys. Res. 66, 995 (1961).

16. J. J. Quenby and W. R. Webber, Phil. Mag. 4, 90 (1959).

17. J. E. Kasper, Suppl. Nuovo Cimento 11, 1 (1959).

18. E. P. Ney, Proc. International Conference on Cosmic Ray Physics, Kyoto, Japan (1961) (in press).

19. C. M. Crane, J. Geophys. Res. 66, 1117 (1961).

20. A. V. Phelps and J. L. Pack, Phys. Rev. Letters 6, 111 (1961).

21. L. M. Channin, A. V. Phelps, and M. A. Biondi, Phys. Rev. Letters 2, 344 (1959).

22. S. J. Smith, D. S. Burch, and L. M. Branscomb, Ann. Geophys. 14, 225 (1958).

23. H. Leinbach, Private communication.

24. D. R. Bates and H. S. W. Massey, Proc. Roy. Soc. (London) A187, 261 (1946).

25. G. C. Reid and H. Leinbach, Report, Geophysical Institute, University of Alaska, April, 1960.

26. J. A. Kane, J. Geophys. Res. 64, 133 (1959).

27. J. M. Anderson and L. Goldstein, Phys. Rev. 102, 388 (1956).

28. Geomagnetic Survey Maps, Nos. 1701, 1703, U. S. Hydrographic Office (1955).

29. J. Ortner, A. Egeland, and B. Hultqvist, I.R.E. Trans. Antennas and Propagation AP-8, 621 (1960).

30. B. Hultqvist and J. Ortner, Planetary and Space Science 1, 193 (1959).

31. C. G. Little and H. Leinbach, Proc. I.R.E. 47, 315 (1959).

32. W. I. Orr, Beam Antenna Handbook, Radio Publications Inc., Danbury Road, Wilton, Conn.

FIGURE LEGENDS

Fig. 1. Proton Energy Loss in Air vs Proton Energy

Fig. 2. Electron Production Rate vs Atmospheric Height for Three Solar Proton Spectra.

Fig. 3. Electron Production Rate vs Atmospheric Height for Solar Protons and Alpha Particles.

Fig. 4. Equilibrium Electron Density vs Atmospheric Height under Daytime and Nighttime Conditions.

Fig. 5. The Negative-Ion-to-Electron Ratio and the Effective Recombination Coefficient vs Atmospheric Height under Daytime Conditions.

Fig. 6. The Negative-Ion-to-Electron Ratio and the Effective Recombination Coefficient vs Atmospheric Height under Nighttime Conditions.

Fig. 7. $(1 + \lambda)\alpha_{eff}$ vs Atmospheric Height under Daytime Conditions.

Fig. 8. $(1 + \lambda)\alpha_{eff}$ vs Atmospheric Height under Nighttime Conditions.

Fig. 9. The Electron Density Ratio, N_B/N_A, vs Atmospheric Height under Daytime and Nighttime Conditions.

Fig. 10. The Specific Attenuation of Cosmic Radio Noise at 27.6 mc/sec vs Atmospheric Height under Daytime and Nighttime Conditions.

Fig. 11. Total Vertical Absorption of Cosmic Radio Noise at 27.6 mc/sec vs Solar Cosmic Ray Flux for Three Spectra under Daytime and Nighttime Conditions.

Fig. 12. Atmospheric Rise Time and Decay Time vs Height.

Fig. 13. Stopping Heights in the Atmosphere for Protons vs Angle of Incidence from Zenith for Various Initial Energies and Azimuths.

Fig. 14. Constant Height Contours of Electron Production Rate vs Solar Proton Cutoff Energy for $\gamma = 3$ Solar Cosmic Ray Spectrum.

Fig. 15. Constant Height Contours of Electron Production Rate vs Solar Proton Cutoff Energy for $\gamma = 5$ Solar Cosmic Ray Spectrum.

Fig. 16. Constant Height Contours of Electron Production Rate vs Solar Proton Cutoff Energy for $\gamma = 7$ Solar Cosmic Ray Spectrum.

Fig. 17. Constant Height Contours of Equilibrium Electron Density (Daytime) vs Solar Proton Cutoff Energy for $\gamma = 3$ Solar Cosmic Ray Spectrum.

Fig. 18. Constant Height Contours of Equilibrium Electron Density (Daytime) vs Solar Proton Cutoff Energy for $\gamma = 5$ Solar Cosmic Ray Spectrum.

Fig. 19. Constant Height Contours of Equilibrium Electron Density (Daytime) vs Solar Proton Cutoff Energy for $\gamma = 7$ Solar Cosmic Ray Spectrum.

Fig. 20. Constant Height Contours of Specific Attenuation (Daytime) vs Solar Proton Cutoff Energy for $\gamma = 3$ Solar Cosmic Ray Spectrum.

Fig. 21. Constant Height Contours of Specific Attenuation (Daytime) vs Solar Proton Cutoff Energy for $\gamma = 5$ Solar Cosmic Ray Spectrum.

Fig. 22. Constant Height Contours of Specific Attenuation (Daytime) vs Solar Proton Cutoff Energy for $\gamma = 7$ Solar Cosmic Ray Spectrum

Fig. 23. Total Attenuation vs Solar Proton Cutoff Energy (Daytime), $\gamma = 3$.

Fig. 24. Total Attenuation vs Solar Proton Cutoff Energy (Daytime), $\gamma = 5$.

Fig. 25. Total Attenuation vs Solar Proton Cutoff Energy (Daytime), $\gamma = 7$.

Fig. 26. Total Attenuation vs Solar Proton Cutoff Energy (Nighttime), $\gamma = 3$.

Fig. 27. Total Attenuation vs Solar Proton Cutoff Energy (Nighttime), $\gamma = 5$.

Fig. 28. Total Attenuation vs Solar Proton Cutoff Energy (Nighttime), $\gamma = 7$.

Fig. 29. Total Attenuation vs Geomagnetic Latitude (Daytime and Nighttime) for Three Solar Cosmic Ray Spectra.

Fig. 30. $M(E_c, \gamma)$ vs Solar Proton Cutoff Energy (see text).

Fig. 31. Cosmic Radio Noise Absorption Data from the Event of July 14, 1959.

ACKNOWLEDGMENTS

The author gratefully acknowledges the encouragement and guidance given him by Dr. Robert R. Brown under whose direction this thesis was written. Thanks are extended to the personnel of the University of California Computer Center for the help and cooperation received from them in the employment of the IBM 704 Data Processing System for the computational work contained herein.

The research was supported by the U. S. Air Force under Contract AF 49(638)873.

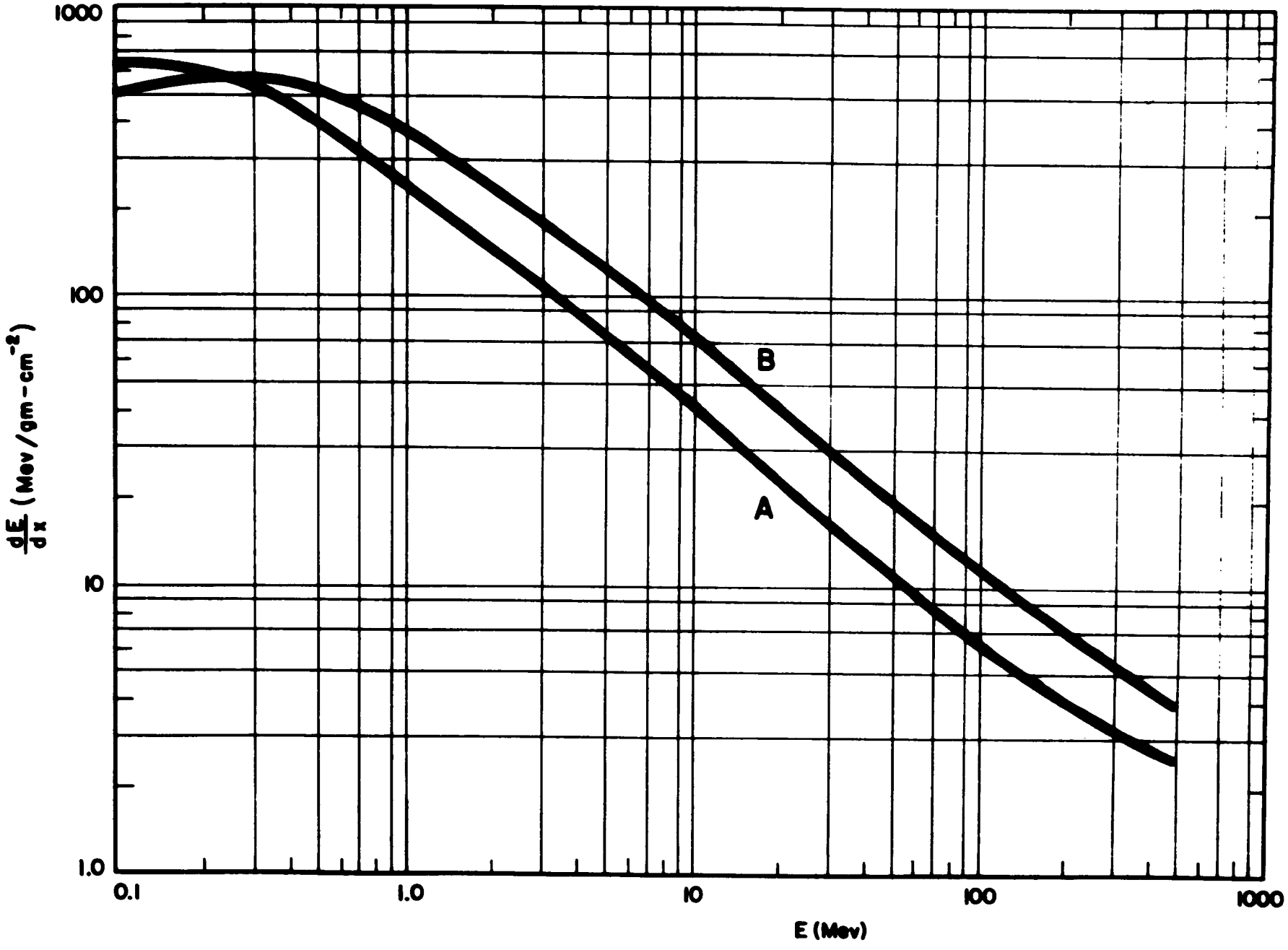

FIGURE 1

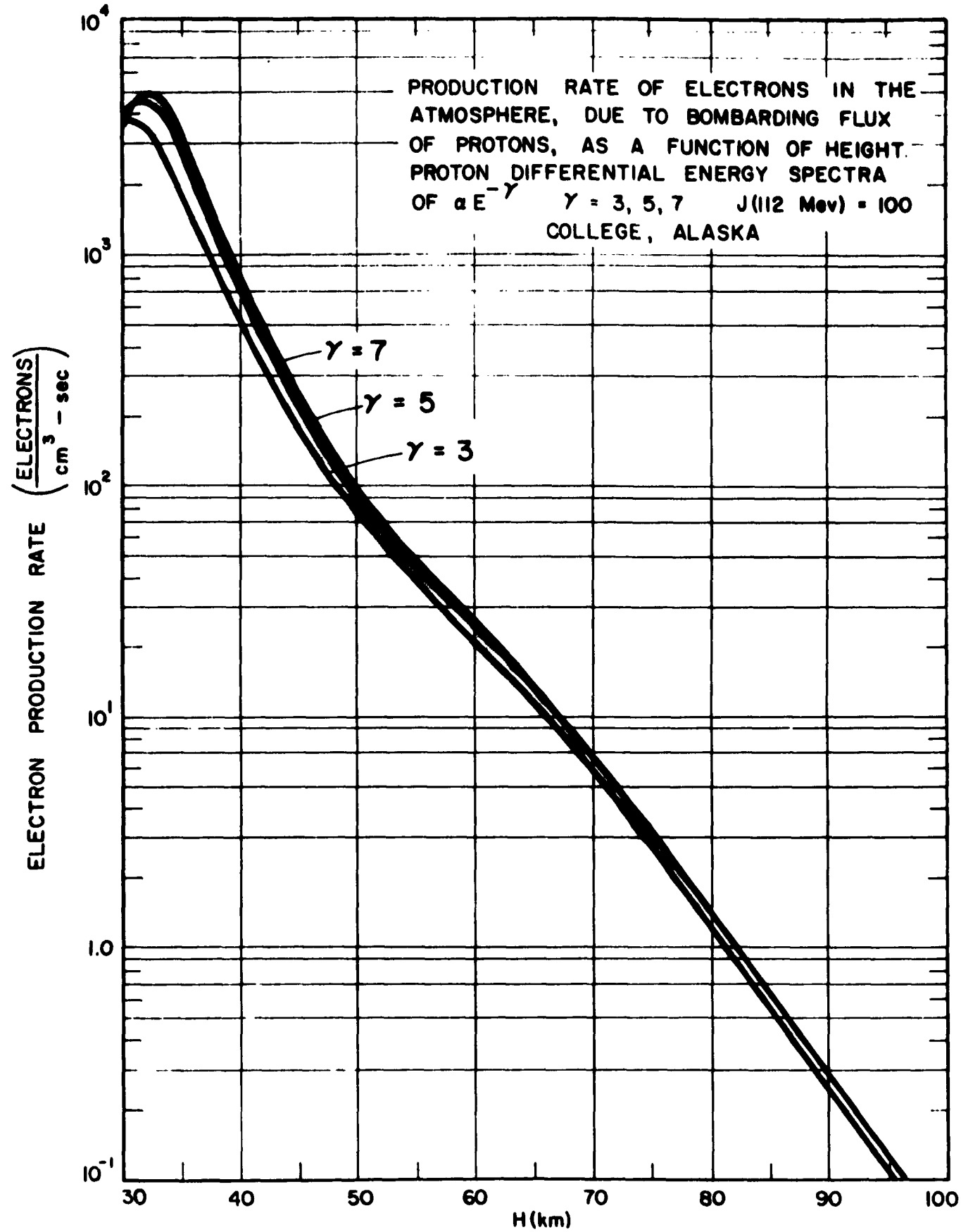
PRODUCTION RATE OF ELECTRONS IN THE ATMOSPHERE, DUE TO BOMBARDING FLUX OF PROTONS, AS A FUNCTION OF HEIGHT.
PROTON DIFFERENTIAL ENERGY SPECTRA OF $\alpha E^{-\gamma}$ γ = 3, 5, 7 J(112 Mev) = 100
COLLEGE, ALASKA
$\gamma = 7$
$\gamma = 5$
$\gamma = 3$
ELECTRON PRODUCTION RATE $\left(\frac{\text{ELECTRONS}}{\text{cm}^3 - \text{sec}}\right)$
10^4
10^3
10^2
10^1
1.0
10^{-1}
30
40
50
60
70
80
90
100
H(km)

FIGURE 2

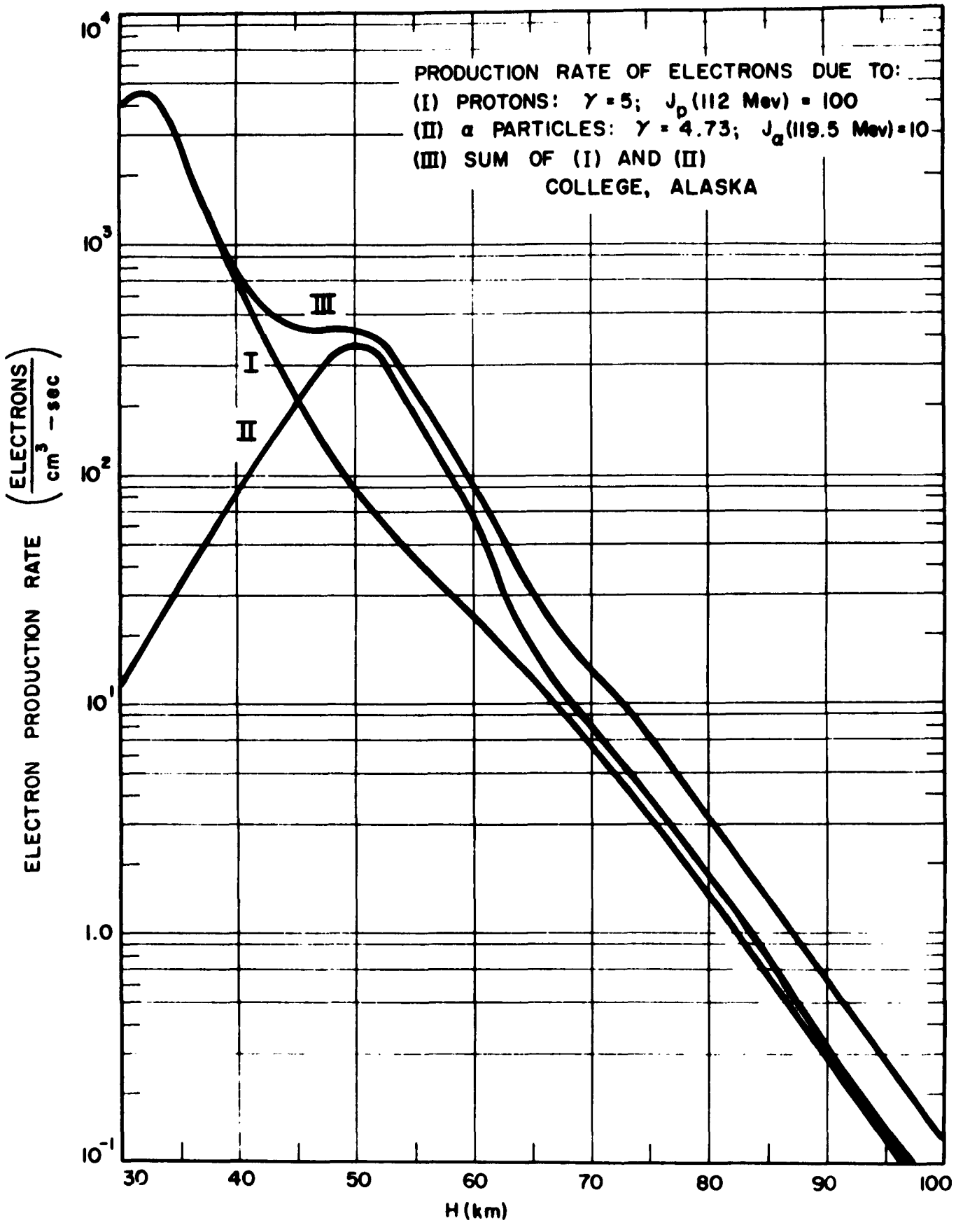
PRODUCTION RATE OF ELECTRONS DUE TO:
(I) PROTONS: γ = 5; J_p(112 Mev) = 100
(II) α PARTICLES: γ = 4.73; J_α(119.5 Mev) = 10
(III) SUM OF (I) AND (II)
COLLEGE, ALASKA
ELECTRON PRODUCTION RATE (ELECTRONS / cm³ - sec)
10⁴
10³
10²
10¹
1.0
10⁻¹
I
II
III
30
40
50
60
70
80
90
100
H (km)

FIGURE 3

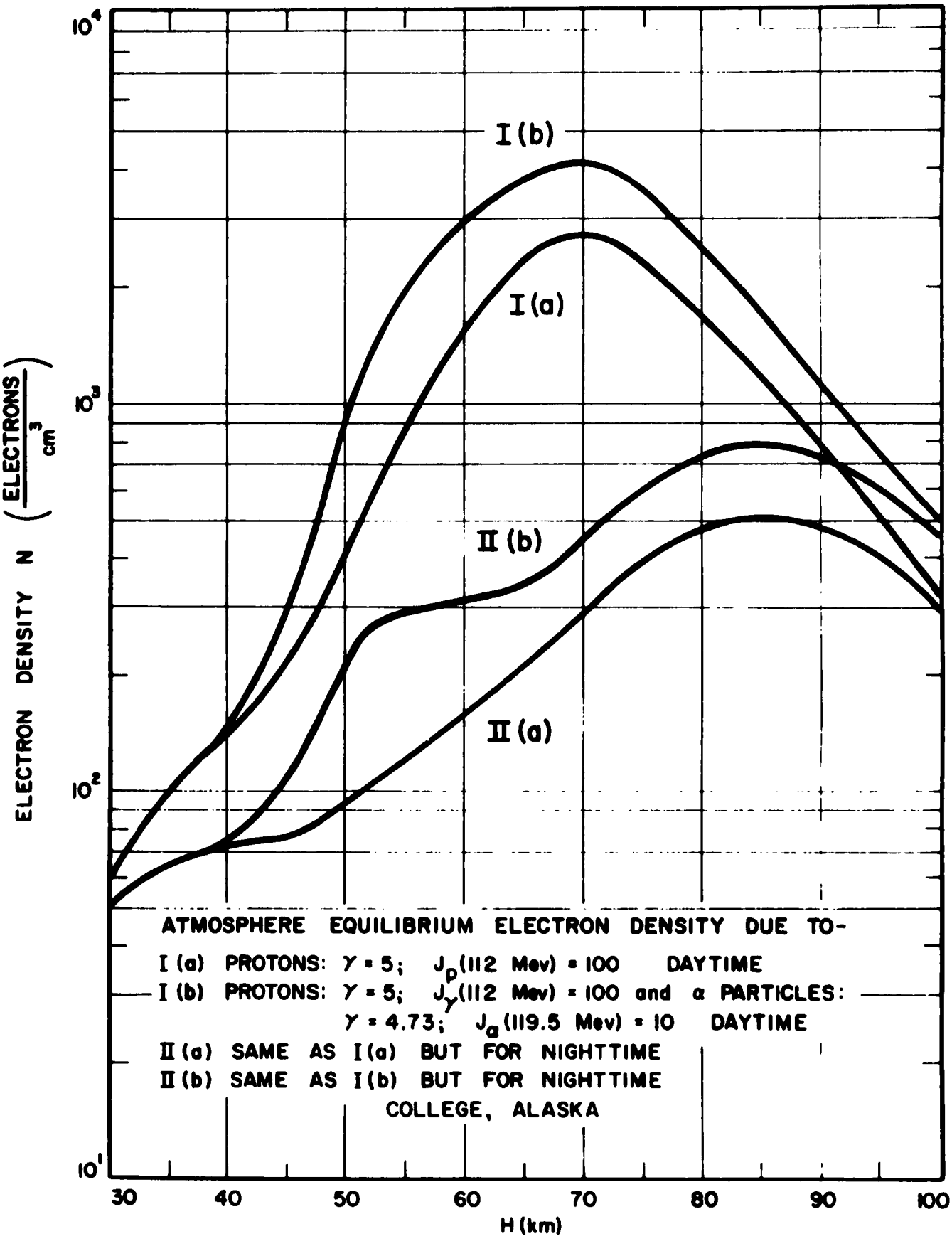
ELECTRON DENSITY N $\left(\frac{\text{ELECTRONS}}{\text{cm}^3}\right)$
10^4
10^3
10^2
10^1
I (b)
I (a)
II (b)
II (a)
ATMOSPHERE EQUILIBRIUM ELECTRON DENSITY DUE TO-
I (a) PROTONS: $\gamma = 5$; J_p(112 Mev) = 100 DAYTIME
I (b) PROTONS: $\gamma = 5$; J_γ(112 Mev) = 100 and α PARTICLES:
$\gamma = 4.73$; J_α(119.5 Mev) = 10 DAYTIME
II (a) SAME AS I (a) BUT FOR NIGHTTIME
II (b) SAME AS I (b) BUT FOR NIGHTTIME
COLLEGE, ALASKA
30
40
50
60
70
80
90
100
H (km)

FIGURE 4

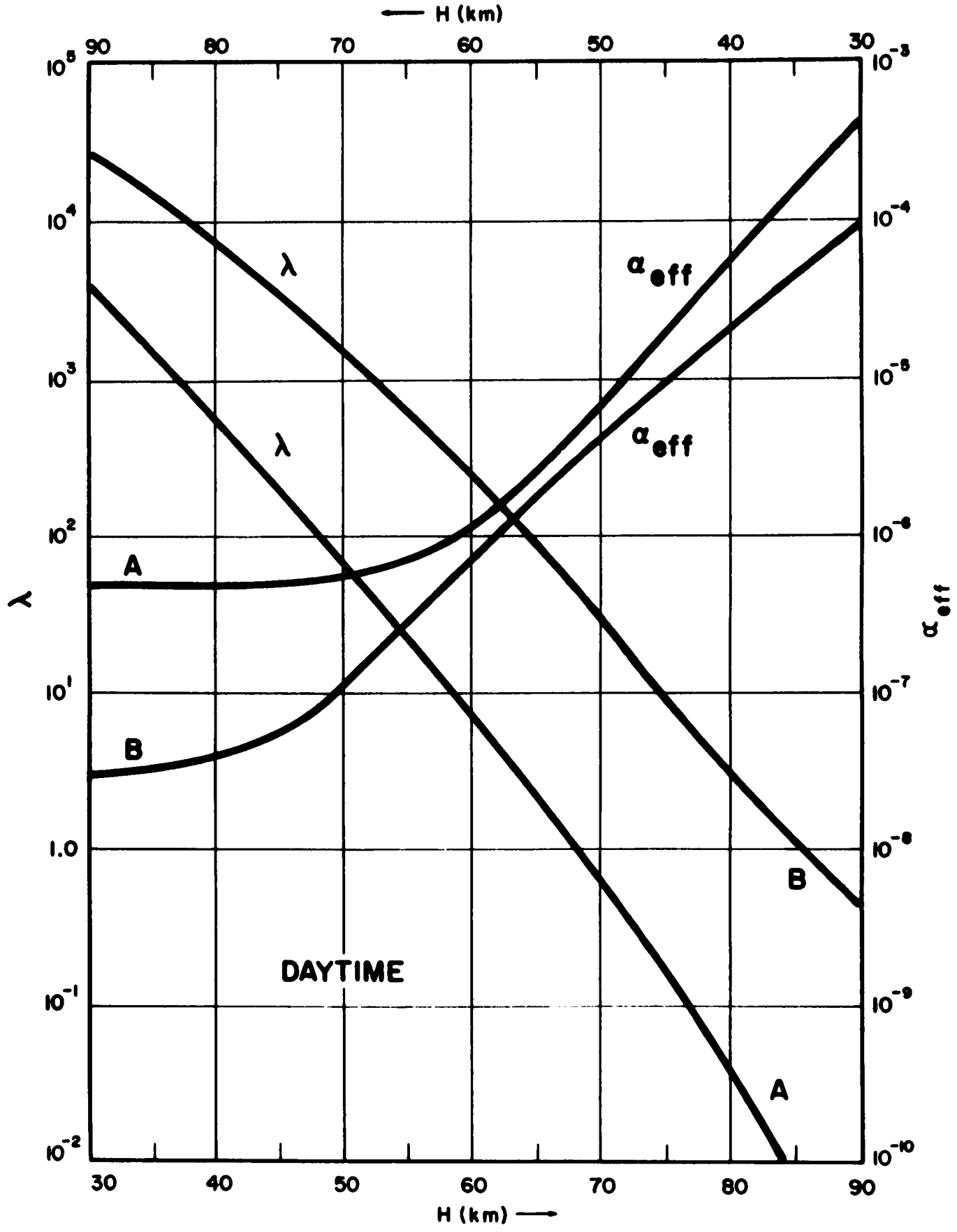
H (km)
90
80
70
60
50
40
30
10^5
10^4
10^3
10^2
10^1
1.0
10^{-1}
10^{-2}
10^{-3}
10^{-4}
10^{-5}
10^{-6}
10^{-7}
10^{-8}
10^{-9}
10^{-10}
λ
α_{eff}
λ
α_{eff}
A
B
B
A
DAYTIME
λ
α_{eff}
H (km)

FIGURE 5

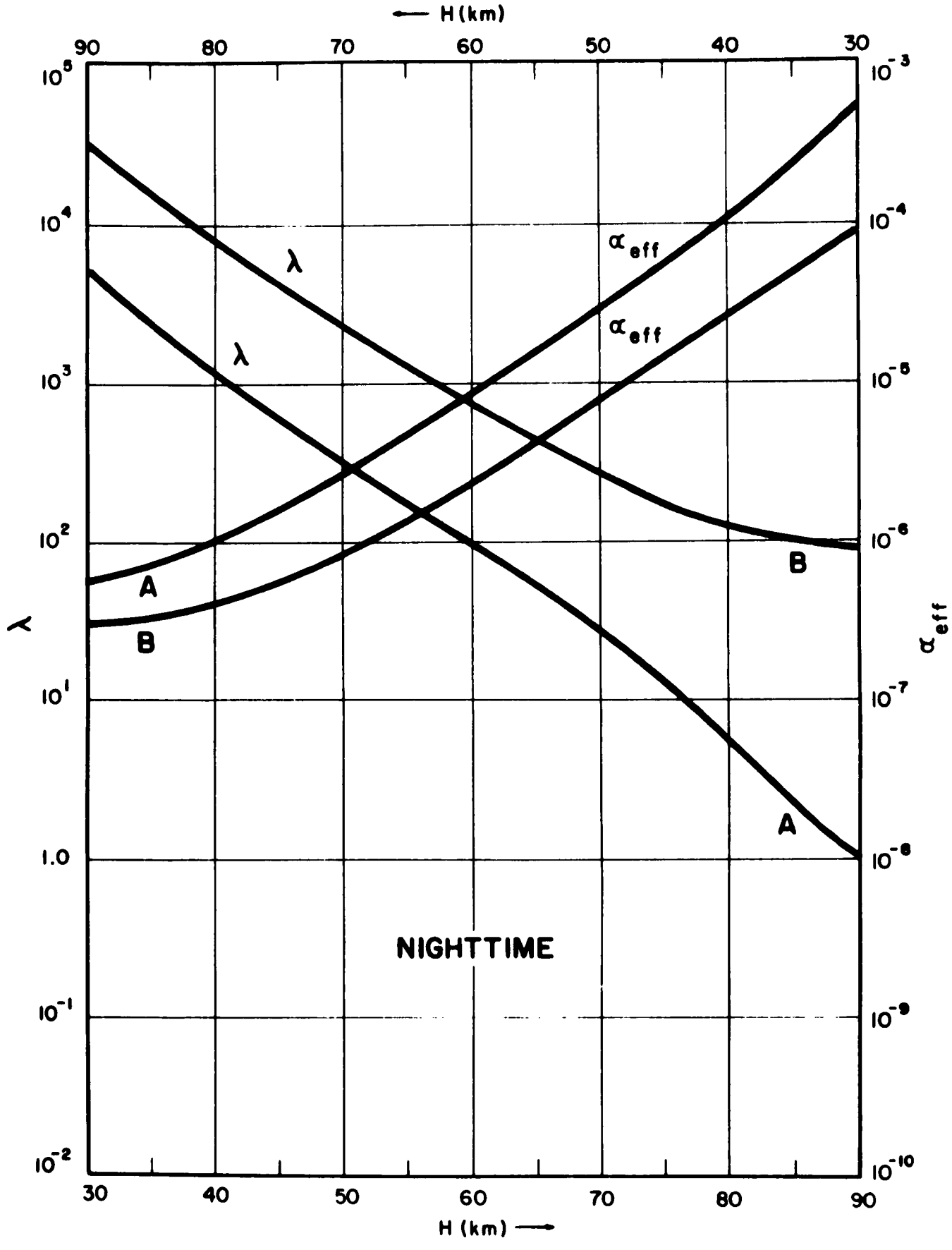
← H(km)
90
80
70
60
50
40
30
10^5
10^4
10^3
10^2
10^1
1.0
10^{-1}
10^{-2}
10^{-3}
10^{-4}
10^{-5}
10^{-6}
10^{-7}
10^{-8}
10^{-9}
10^{-10}
λ
α_{eff}
λ
α_{eff}
A
B
B
A
NIGHTTIME
30
40
50
60
70
80
90
H (km) →

FIGURE 6

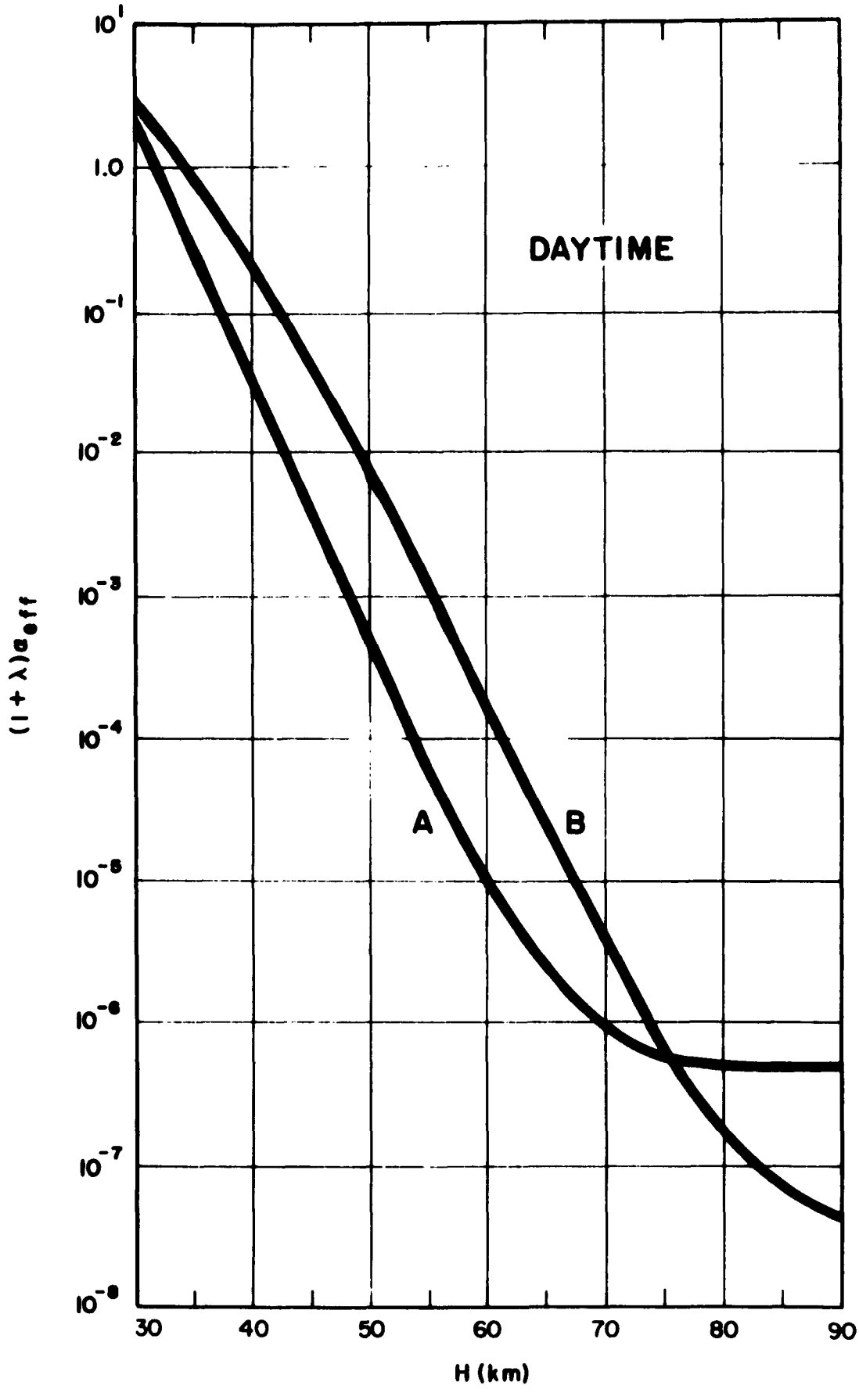
DAYTIME
A
B
10^{1}
1.0
10^{-1}
10^{-2}
10^{-3}
10^{-4}
10^{-5}
10^{-6}
10^{-7}
10^{-8}
$(1+\lambda)\alpha_{eff}$
30
40
50
60
70
80
90
H (km)

FIGURE 7

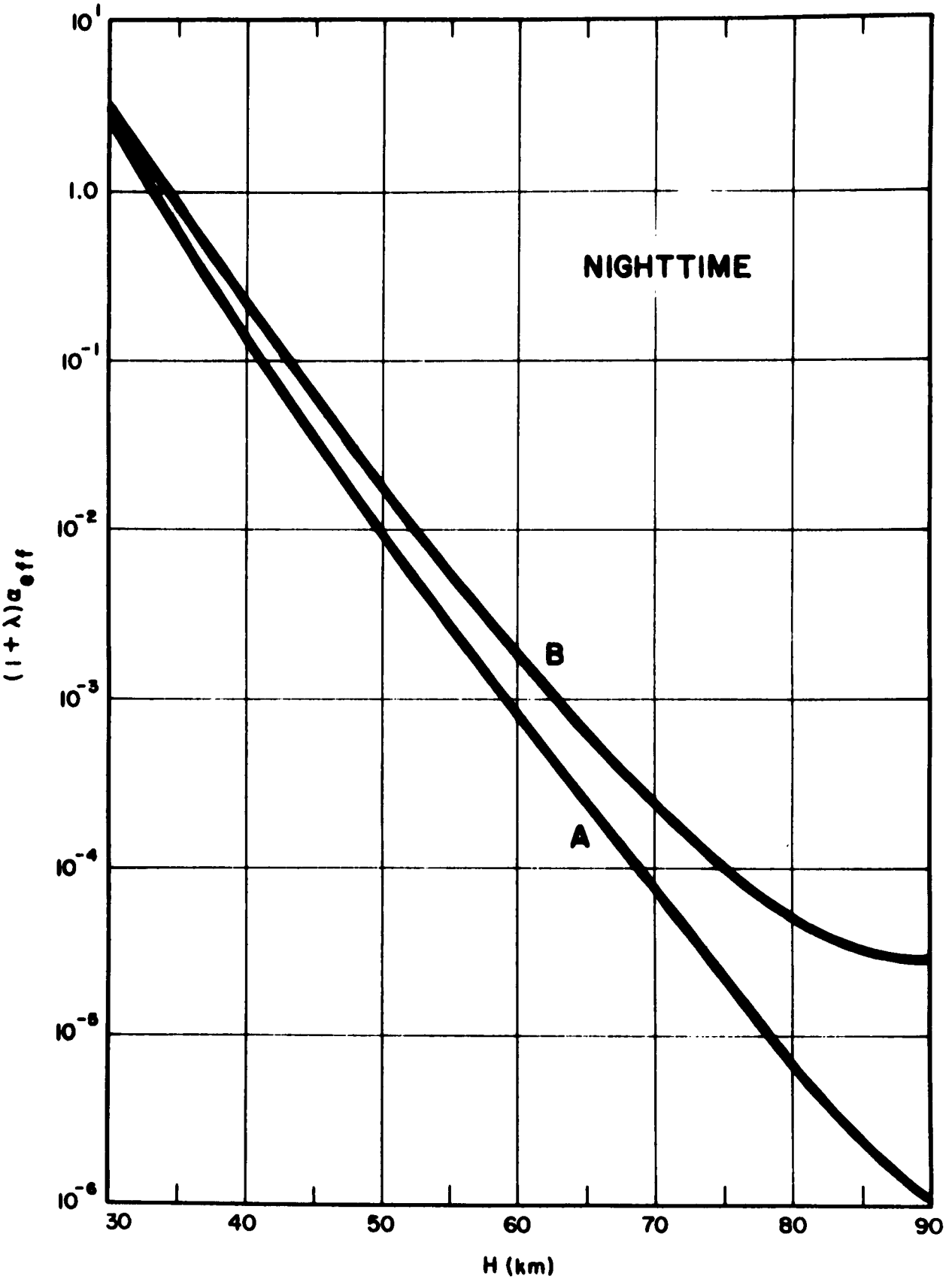
NIGHTTIME
B
A
10^{1}
1.0
10^{-1}
10^{-2}
10^{-3}
10^{-4}
10^{-5}
10^{-6}
$(1+\lambda)\alpha_{eff}$
30
40
50
60
70
80
90
H (km)

FIGURE 8

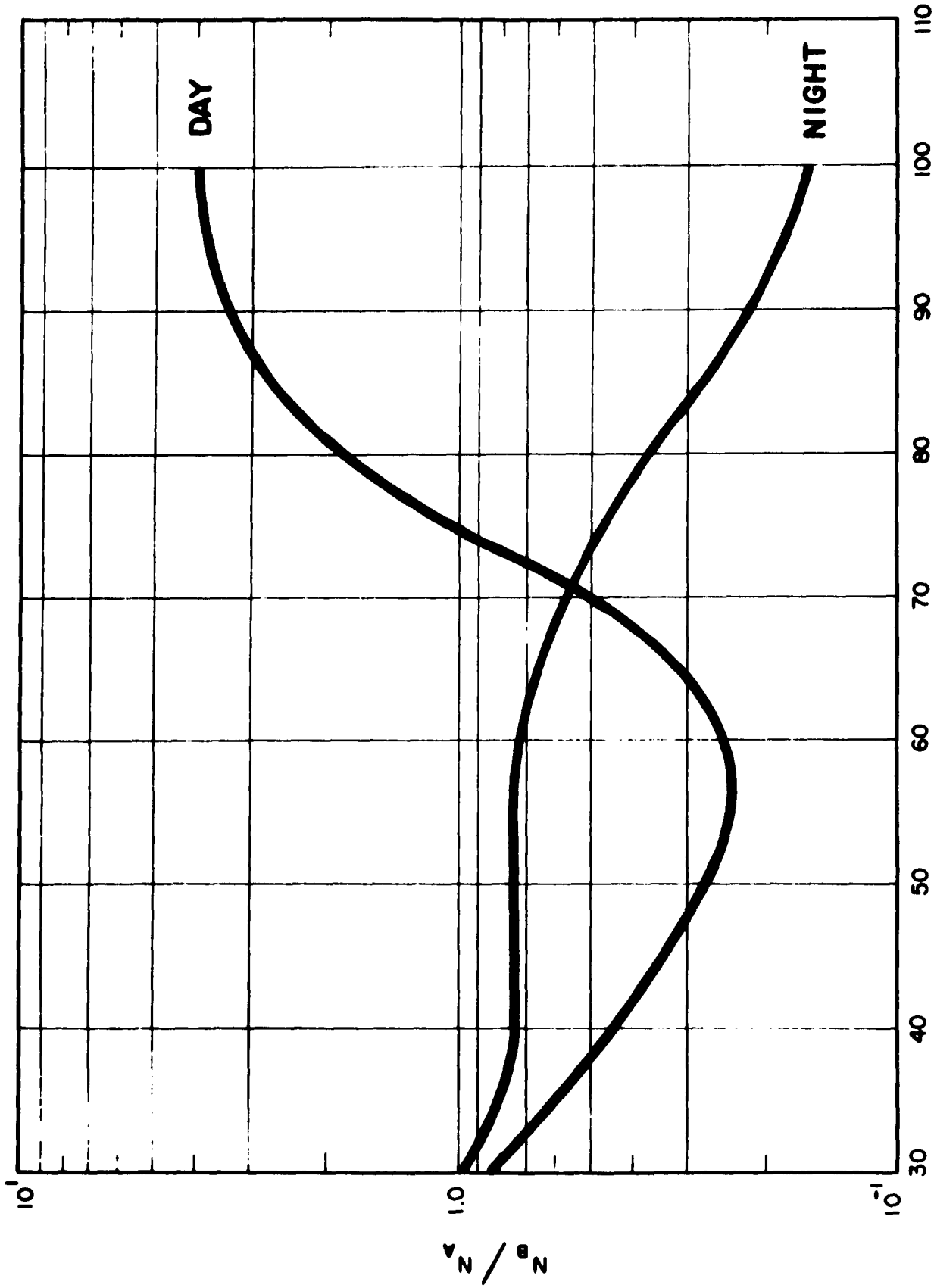

FIGURE 9

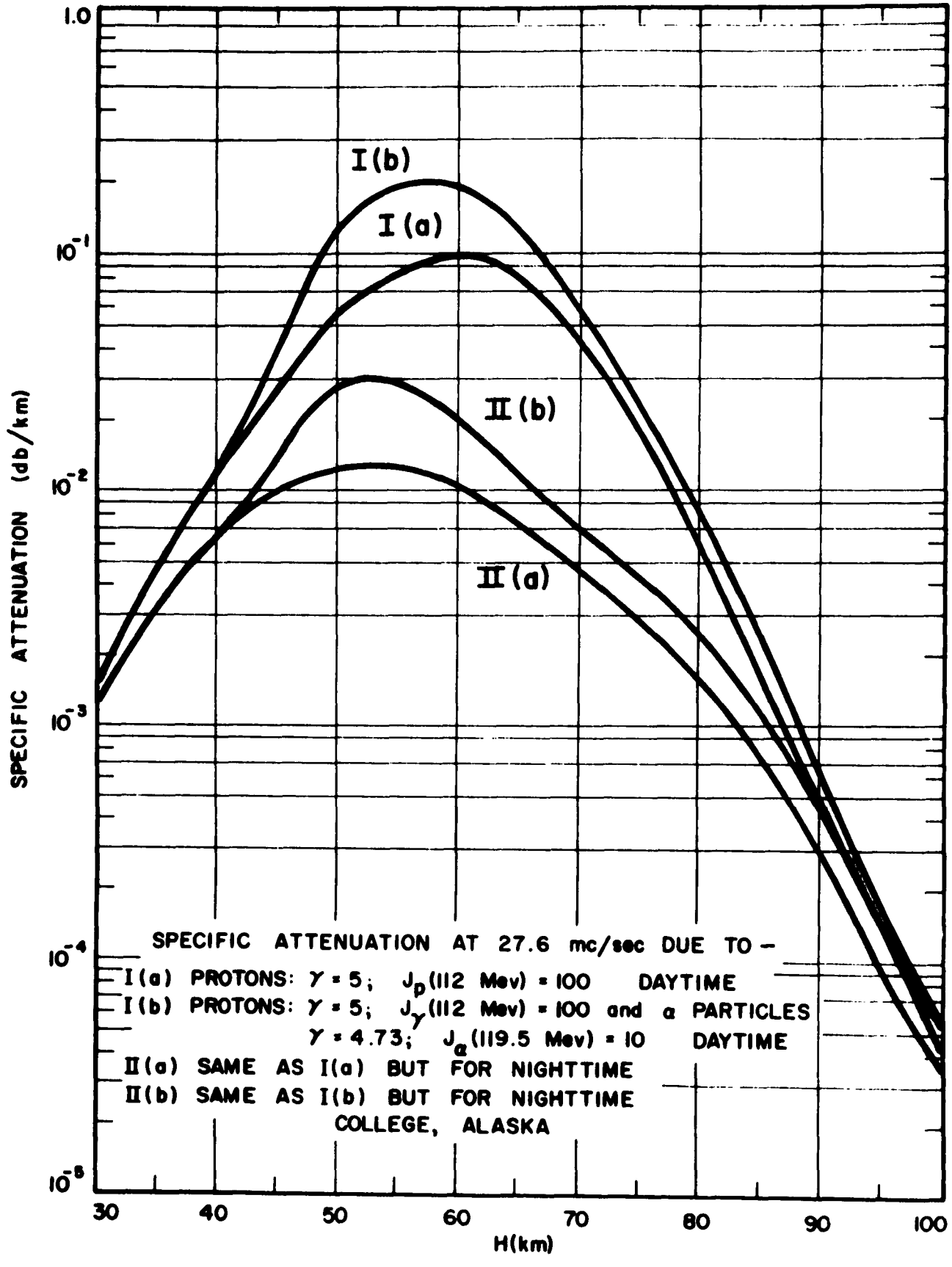
1.0
10^{-1}
10^{-2}
10^{-3}
10^{-4}
10^{-5}
SPECIFIC ATTENUATION (db/km)
I(b)
I(a)
II(b)
II(a)
SPECIFIC ATTENUATION AT 27.6 mc/sec DUE TO –
I(a) PROTONS: $\gamma = 5$; J_p(112 Mev) = 100 DAYTIME
I(b) PROTONS: $\gamma = 5$; J_γ(112 Mev) = 100 and α PARTICLES
$\gamma = 4.73$; J_α(119.5 Mev) = 10 DAYTIME
II(a) SAME AS I(a) BUT FOR NIGHTTIME
II(b) SAME AS I(b) BUT FOR NIGHTTIME
COLLEGE, ALASKA
30
40
50
60
70
80
90
100
H(km)

FIGURE 10

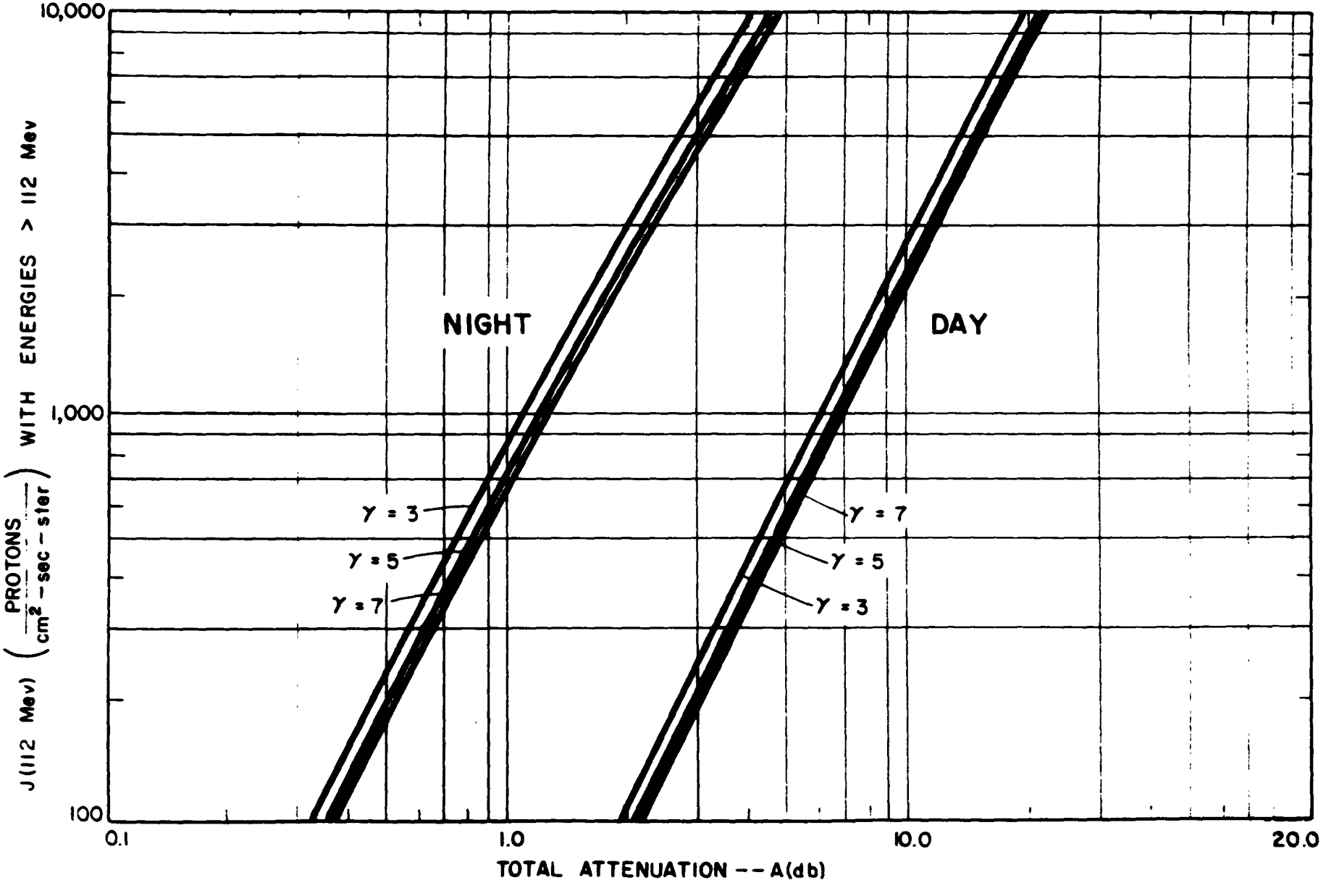
10,000
1,000
100
0.1
1.0
10.0
20.0
NIGHT
DAY
γ = 3
γ = 5
γ = 7
γ = 7
γ = 5
γ = 3
J(112 Mev) (PROTONS / cm² - sec - ster) WITH ENERGIES > 112 Mev
TOTAL ATTENUATION -- A(db)

FIGURE 11

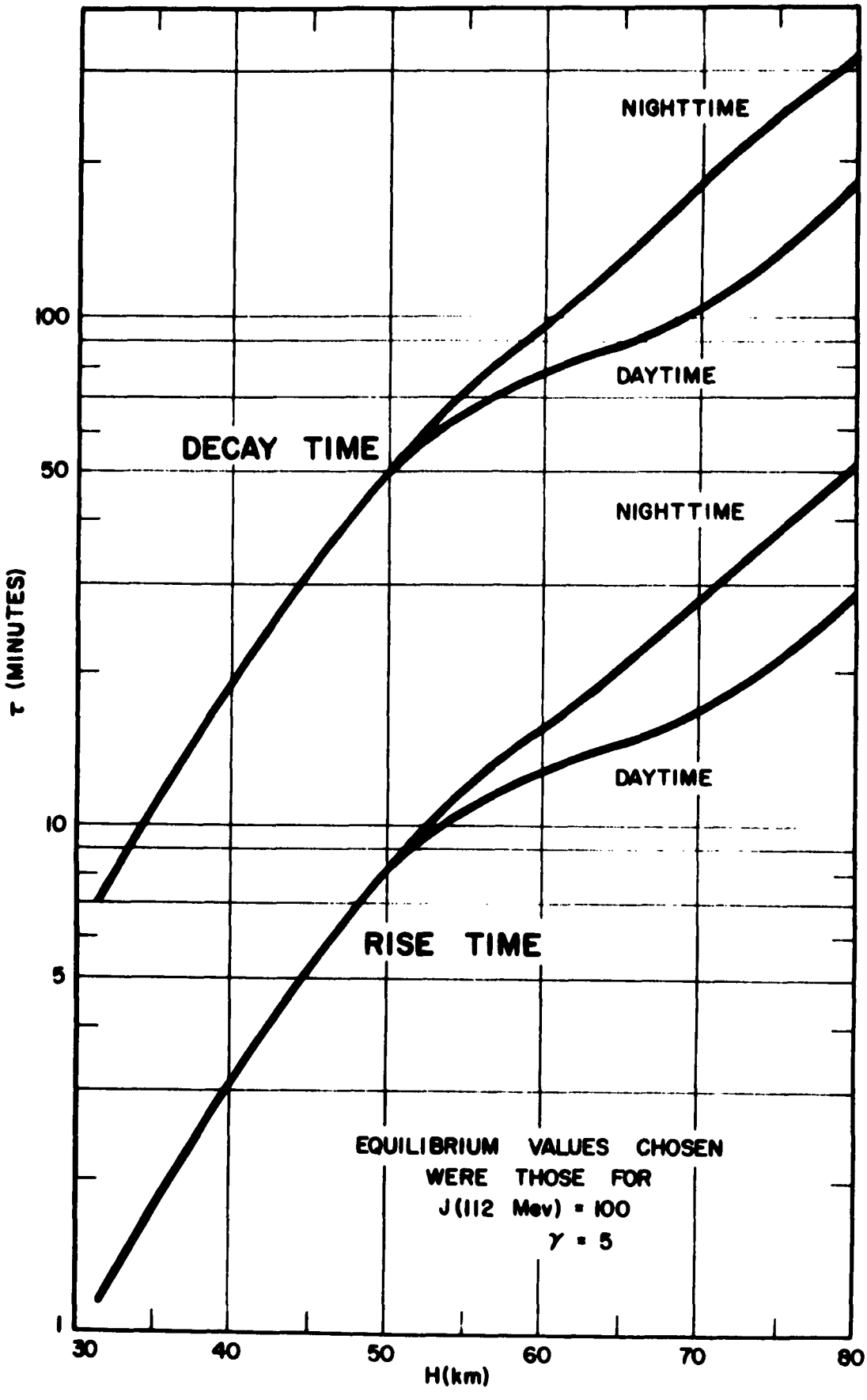
NIGHTTIME
DAYTIME
DECAY TIME
NIGHTTIME
DAYTIME
RISE TIME
EQUILIBRIUM VALUES CHOSEN
WERE THOSE FOR
J(112 Mev) = 100
γ = 5
τ (MINUTES)
100
50
10
5
1
30
40
50
60
70
80
H(km)

FIGURE 12

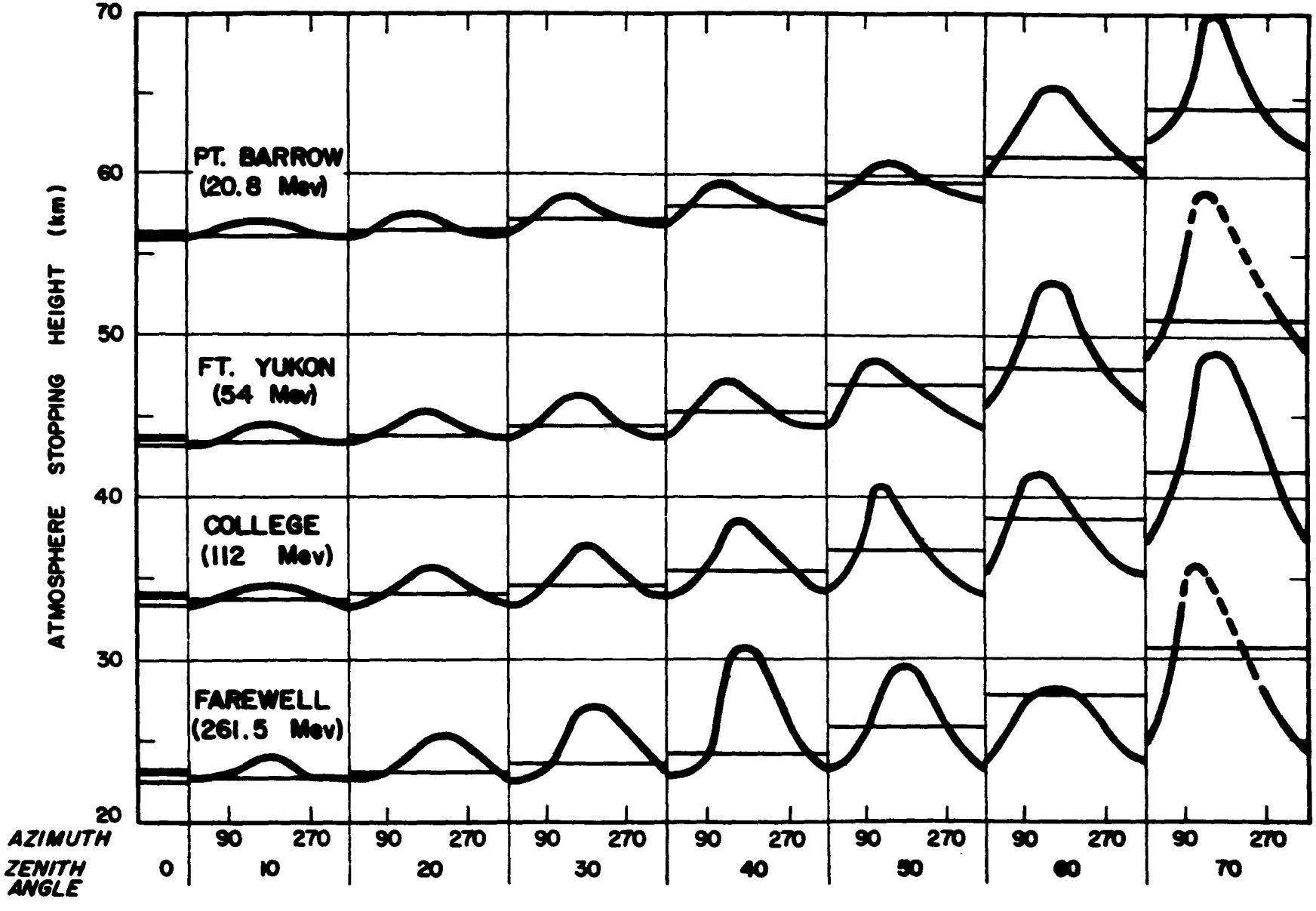
ATMOSPHERE STOPPING HEIGHT (km)
70
60
50
40
30
20
PT. BARROW
(20.8 Mev)
FT. YUKON
(54 Mev)
COLLEGE
(112 Mev)
FAREWELL
(261.5 Mev)
AZIMUTH
ZENITH ANGLE
90 270 90 270 90 270 90 270 90 270 90 270 90 270
0 10 20 30 40 50 60 70

FIGURE 13

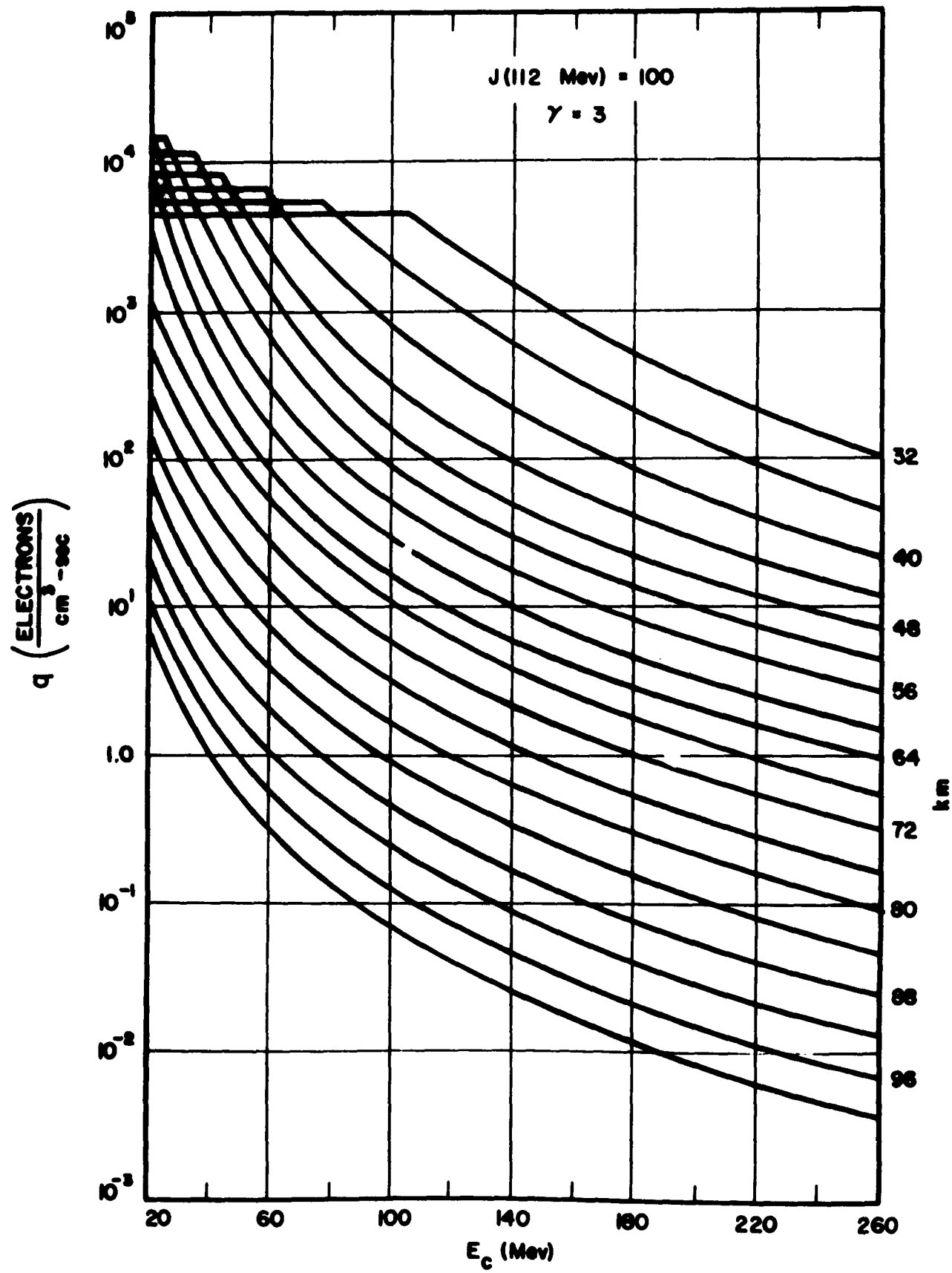
J(112 Mev) = 100
γ = 3
10^3
10^2
10^1
1.0
10^{-1}
10^{-2}
10^{-3}
$q\left(\frac{\text{ELECTRONS}}{\text{cm}^3\text{-sec}}\right)$
20
60
100
140
180
220
260
E_c (Mev)
32
40
48
56
64
72
80
88
96
km

FIGURE 14

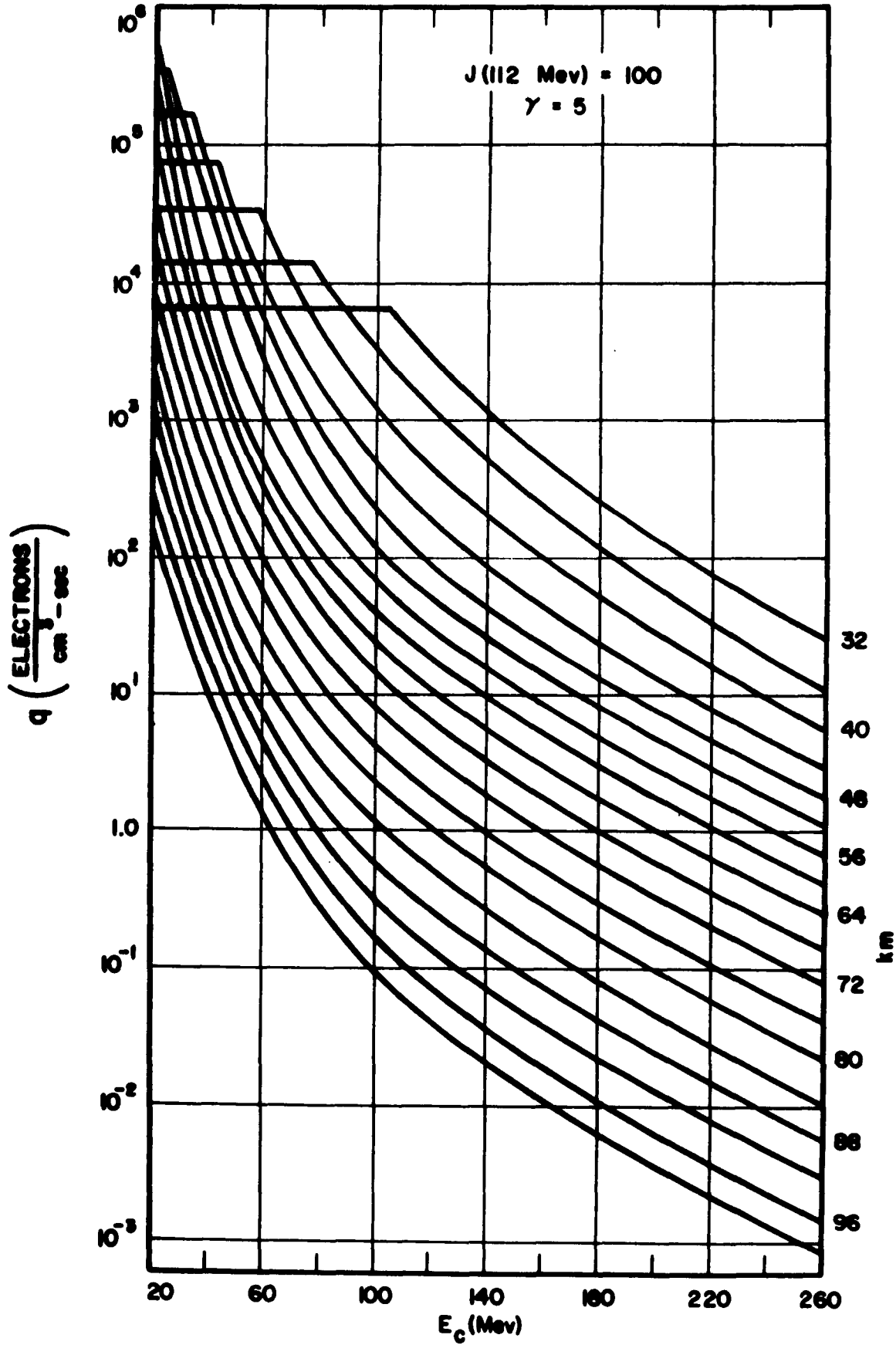
J(112 Mev) = 100
γ = 5
10^{6}
10^{5}
10^{4}
10^{3}
10^{2}
10^{1}
1.0
10^{-1}
10^{-2}
10^{-3}
$q\left(\frac{\text{ELECTRONS}}{\text{cm}^3-\text{sec}}\right)$
20
60
100
140
180
220
260
E_c(Mev)
32
40
48
56
64
72
80
88
96
km

FIGURE 15

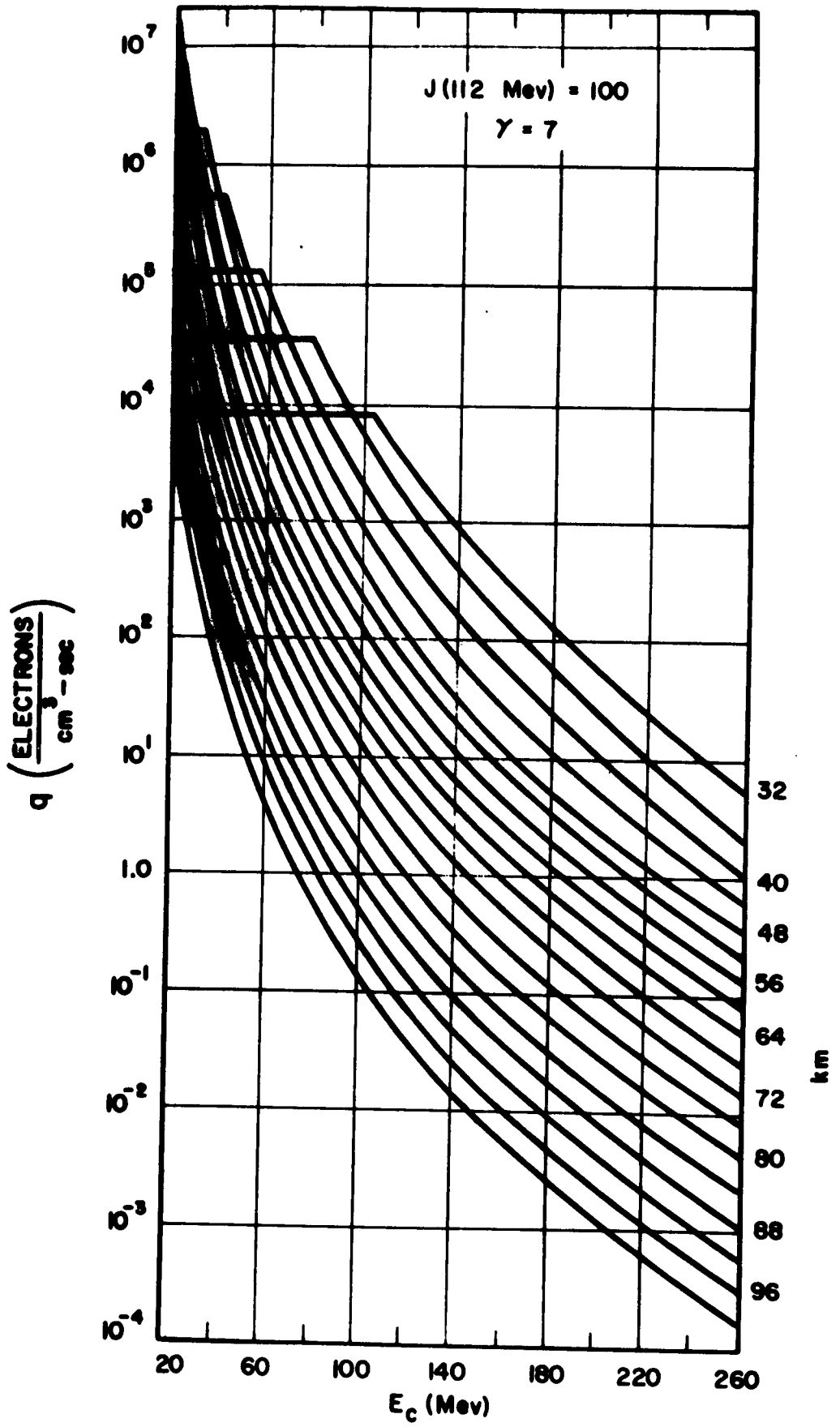
J(112 Mev) = 100
γ = 7
10^7
10^6
10^5
10^4
10^3
10^2
10^1
1.0
10^{-1}
10^{-2}
10^{-3}
10^{-4}
$q\left(\frac{\text{ELECTRONS}}{\text{cm}^3-\text{sec}}\right)$
20
60
100
140
180
220
260
E_c (Mev)
32
40
48
56
64
72
80
88
96
km

FIGURE 16

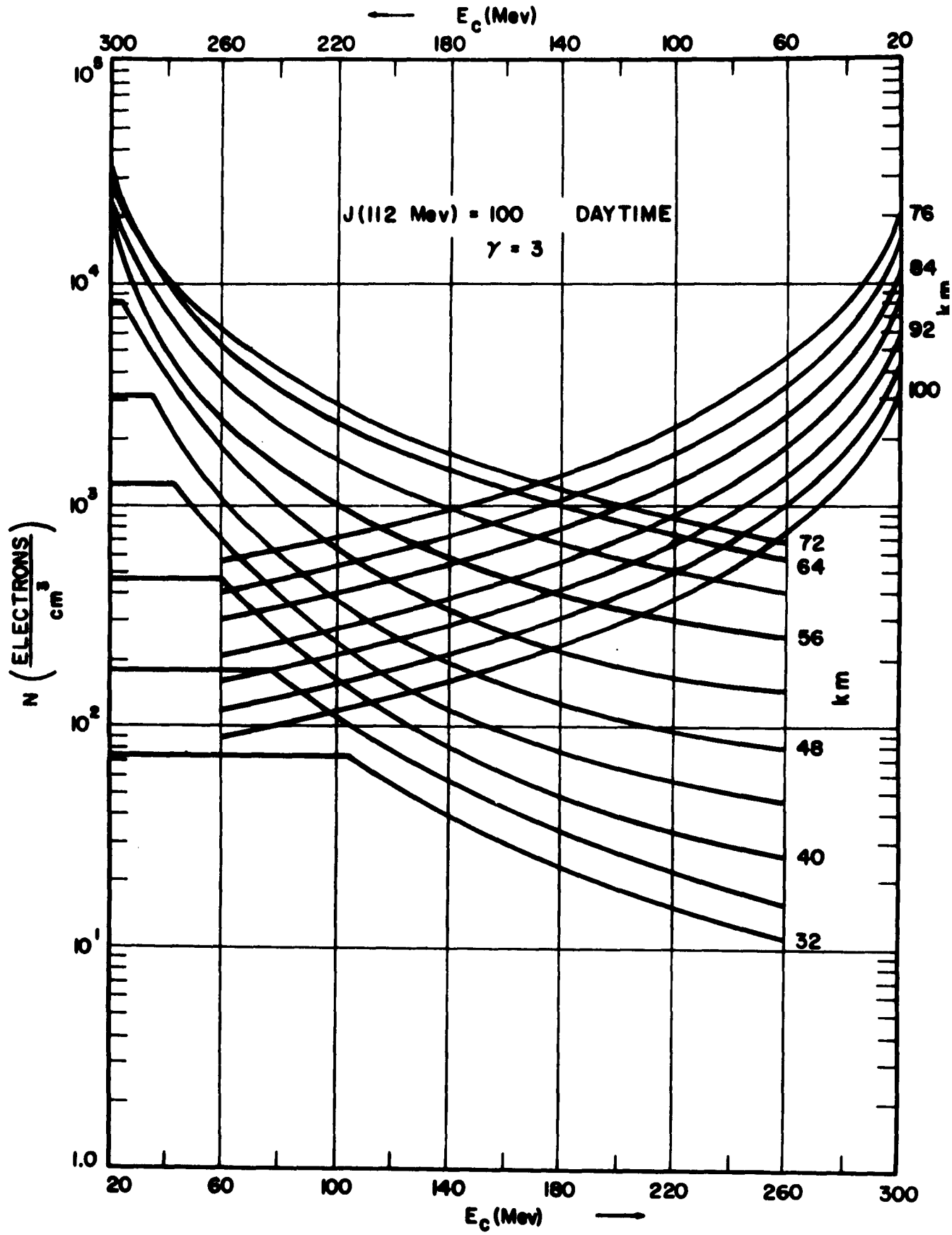
E_c (Mev)
300
260
220
180
140
100
60
20
J(112 Mev) = 100
DAYTIME
γ = 3
76
84
92
100
72
64
56
48
40
32
km
N (ELECTRONS / cm³)
10⁵
10⁴
10³
10²
10¹
1.0
20
60
100
140
180
220
260
300
E_c (Mev)

FIGURE 17

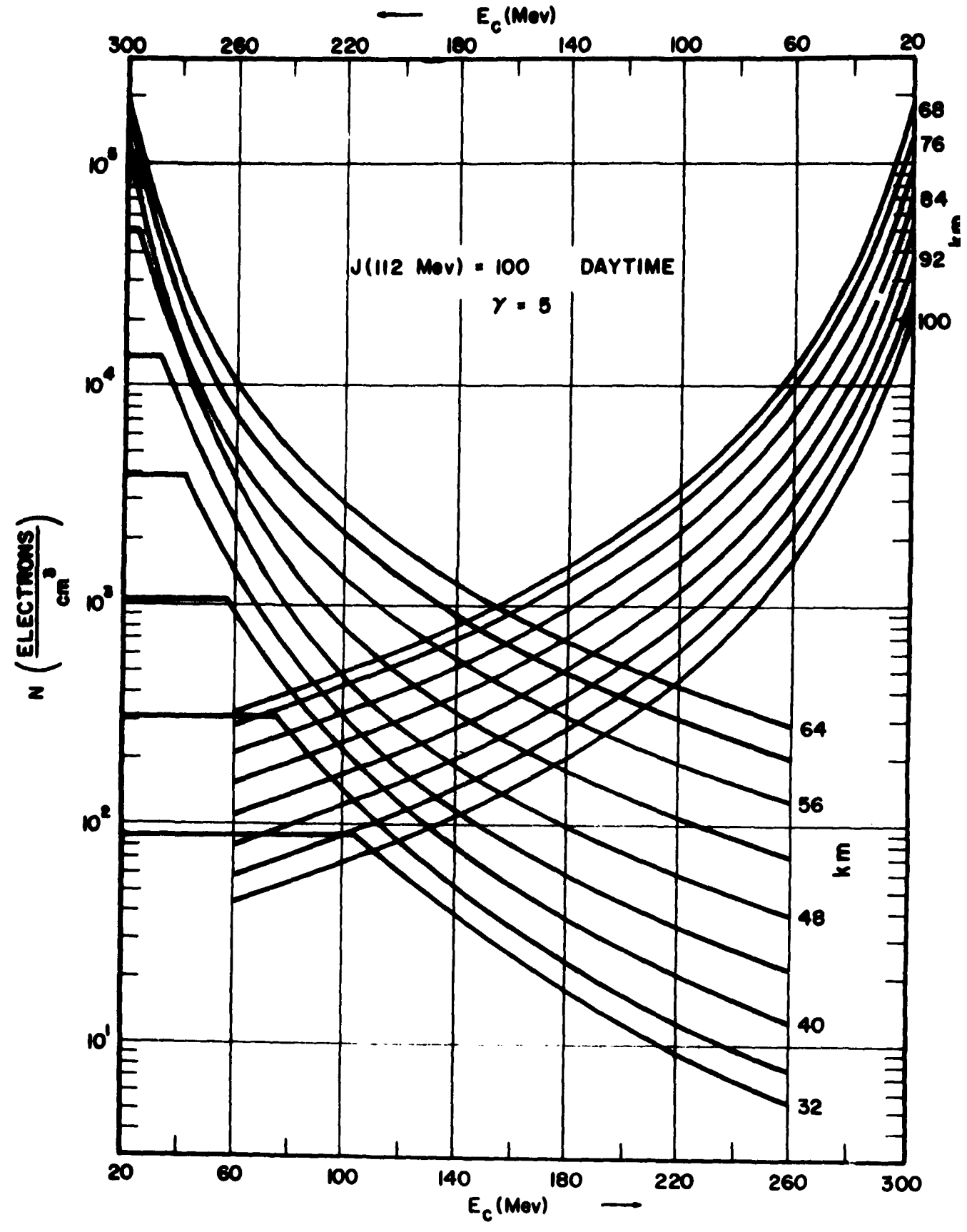
E_c (Mev)
300
260
220
180
140
100
60
20
J(112 Mev) = 100
DAYTIME
γ = 5
N (ELECTRONS / cm³)
10⁸
10⁴
10³
10²
10¹
68
76
84
92
100
64
56
48
40
32
km
20
60
100
140
180
220
260
300
E_c (Mev)

FIGURE 18

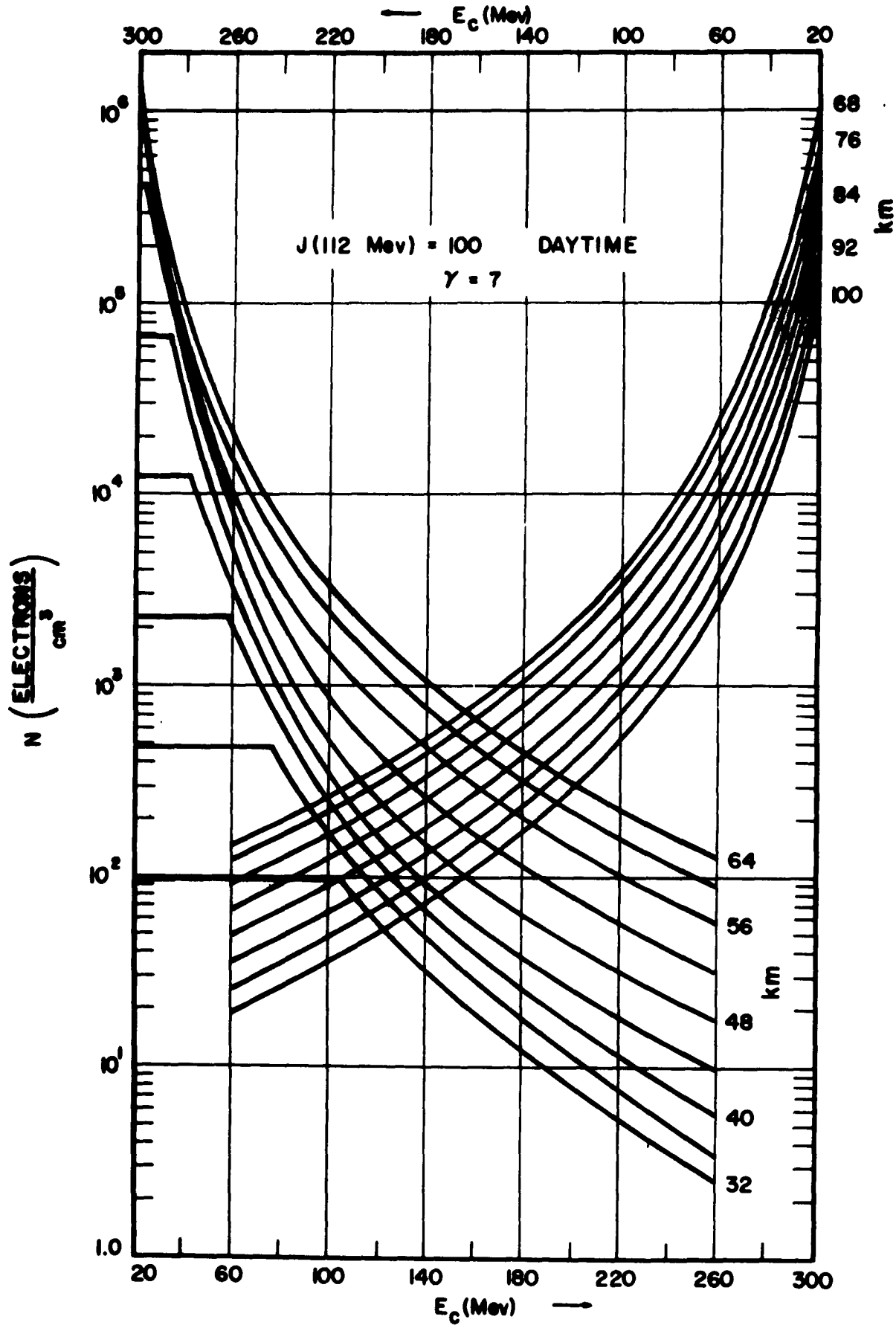
E_c (Mev)
300
260
220
180
140
100
60
20
J(112 Mev) = 100
DAYTIME
γ = 7
68
76
84
92
100
km
64
56
48
40
32
km
N (ELECTRONS/cm³)
10⁶
10⁴
10³
10²
10¹
1.0
20
60
100
140
180
220
260
300
E_c (Mev)

FIGURE 19

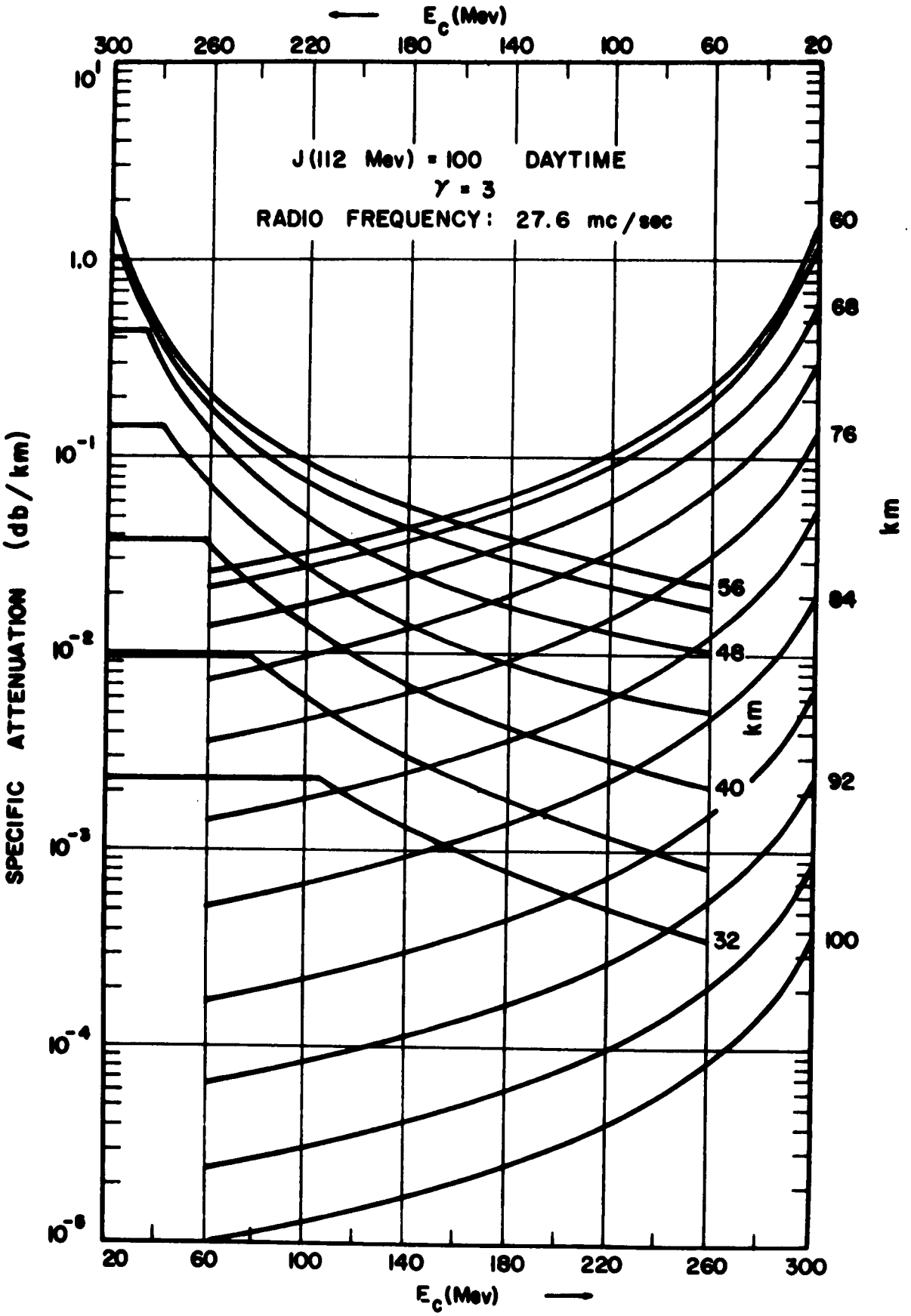
E_c (Mev)
300
260
220
180
140
100
60
20
J(112 Mev) = 100 DAYTIME
γ = 3
RADIO FREQUENCY: 27.6 mc/sec
SPECIFIC ATTENUATION (db/km)
10^1
1.0
10^-1
10^-2
10^-3
10^-4
10^-5
56
48
40
32
km
60
68
76
84
92
100
km
20
60
100
140
180
220
260
300
E_c (Mev)

FIGURE 20

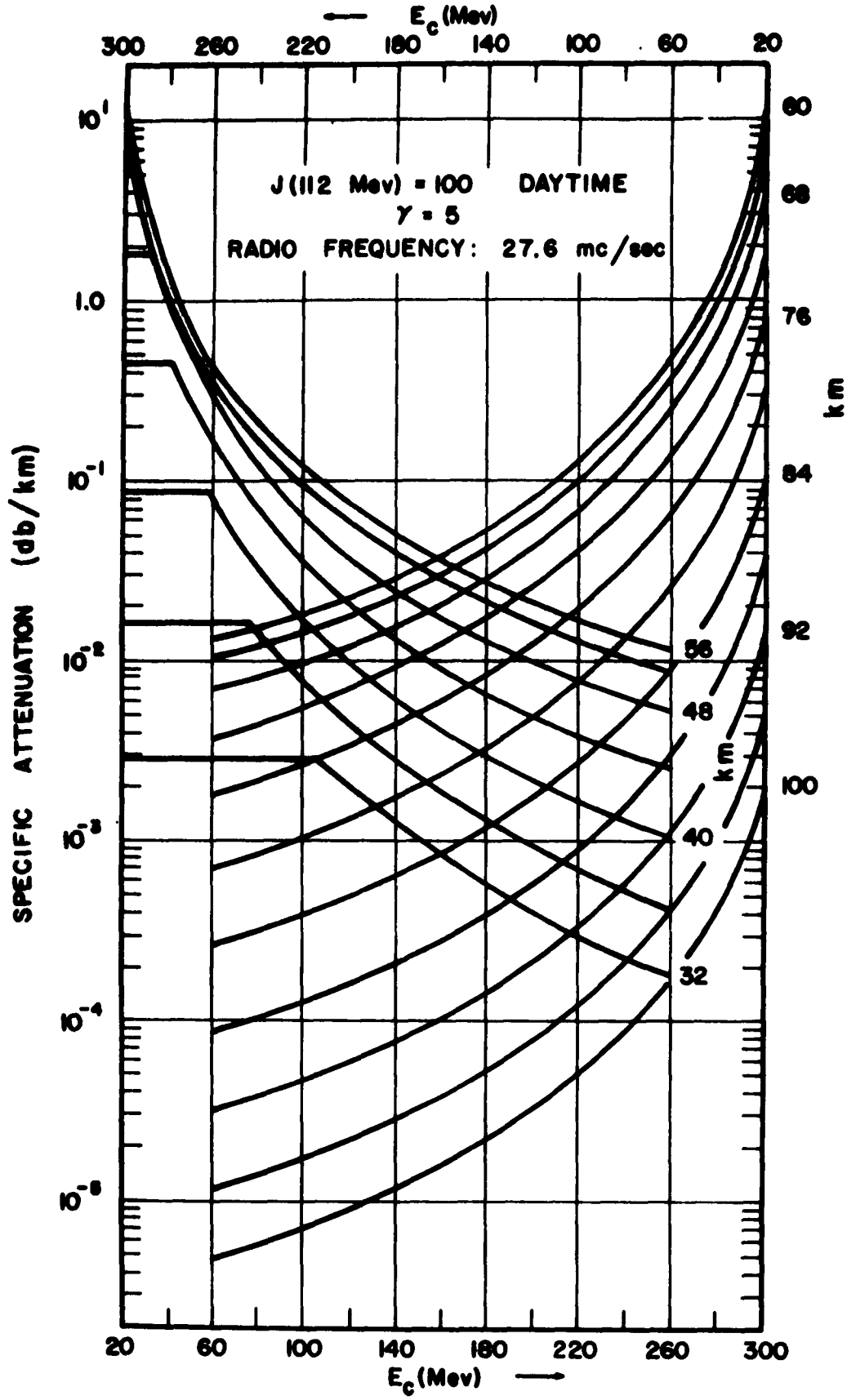
E_c (Mev)
300
260
220
180
140
100
60
20
J(112 Mev) = 100 DAYTIME
γ = 5
RADIO FREQUENCY: 27.6 mc/sec
SPECIFIC ATTENUATION (db/km)
10^1
1.0
10^-1
10^-2
10^-3
10^-4
10^-5
56
48
40
32
km
60
68
76
84
92
100
20
60
100
140
180
220
260
300
E_c (Mev)

FIGURE 21

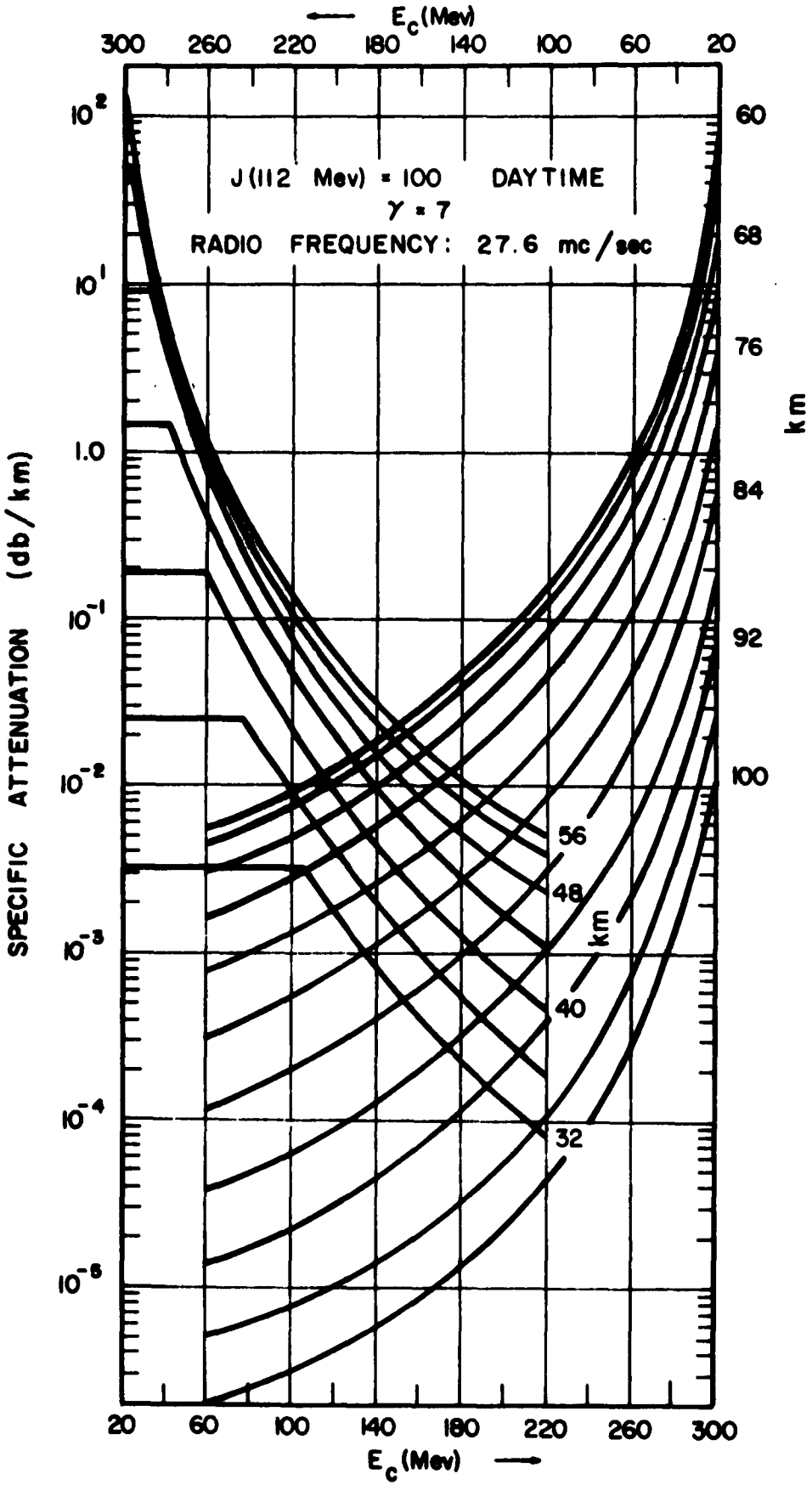
E_c (Mev)
300 260 220 180 140 100 60 20
J (112 Mev) = 100 DAYTIME
γ = 7
RADIO FREQUENCY: 27.6 mc/sec
SPECIFIC ATTENUATION (db/km)
10^2
10^1
1.0
10^-1
10^-2
10^-3
10^-4
10^-5
60
68
76
84
92
100
km
56
48
40
32
km
20 60 100 140 180 220 260 300
E_c (Mev)

FIGURE 22

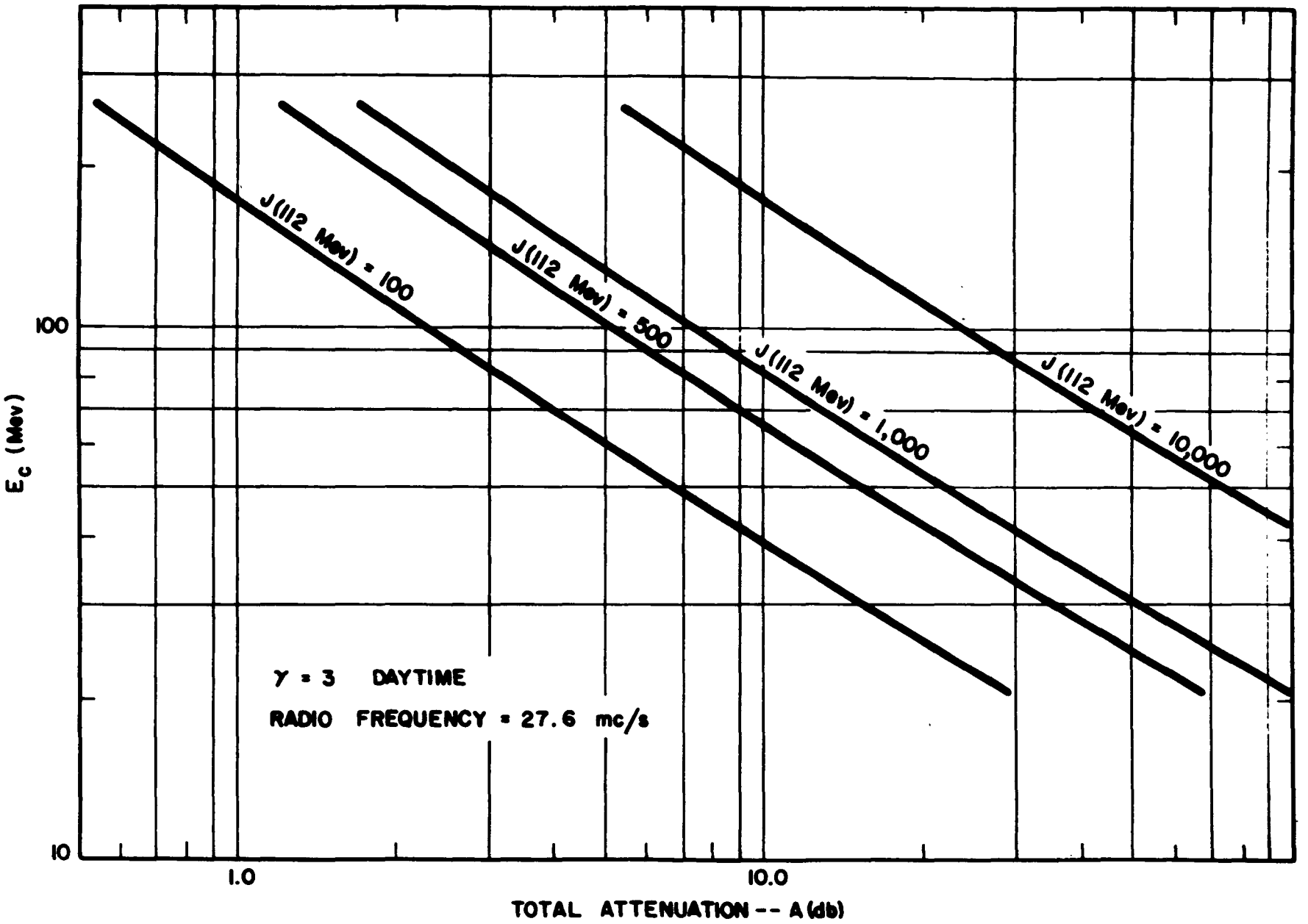
J(112 Mev) = 100
J(112 Mev) = 500
J(112 Mev) = 1,000
J(112 Mev) = 10,000
γ = 3 DAYTIME
RADIO FREQUENCY = 27.6 mc/s
100
10
E_c (Mev)
1.0
10.0
TOTAL ATTENUATION -- A (db)

FIGURE 23

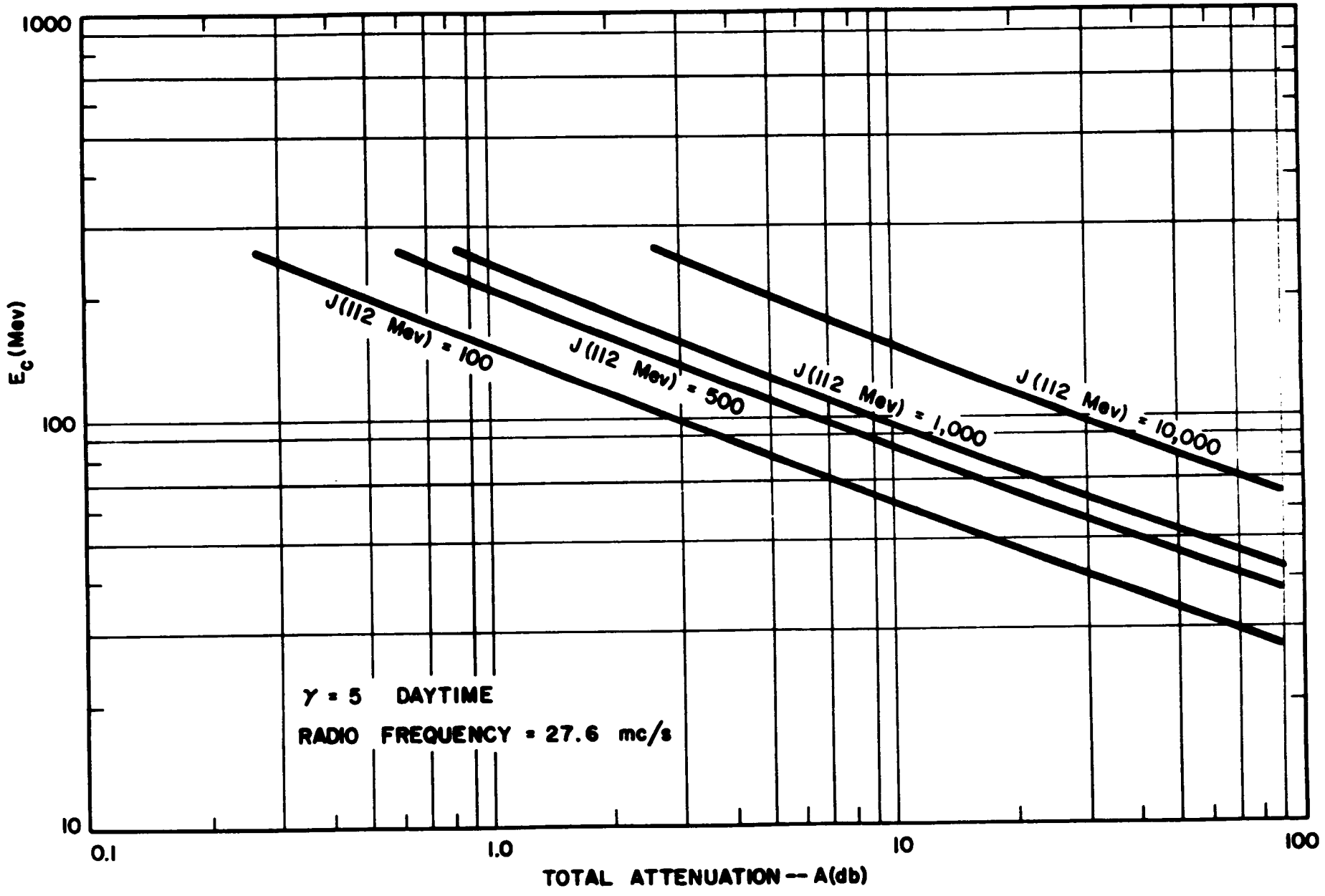
1000
100
10
E_c (Mev)
J(112 Mev) = 100
J (112 Mev) = 500
J(112 Mev) = 1,000
J (112 Mev) = 10,000
γ = 5 DAYTIME
RADIO FREQUENCY = 27.6 mc/s
0.1
1.0
10
100
TOTAL ATTENUATION — A(db)

FIGURE 24

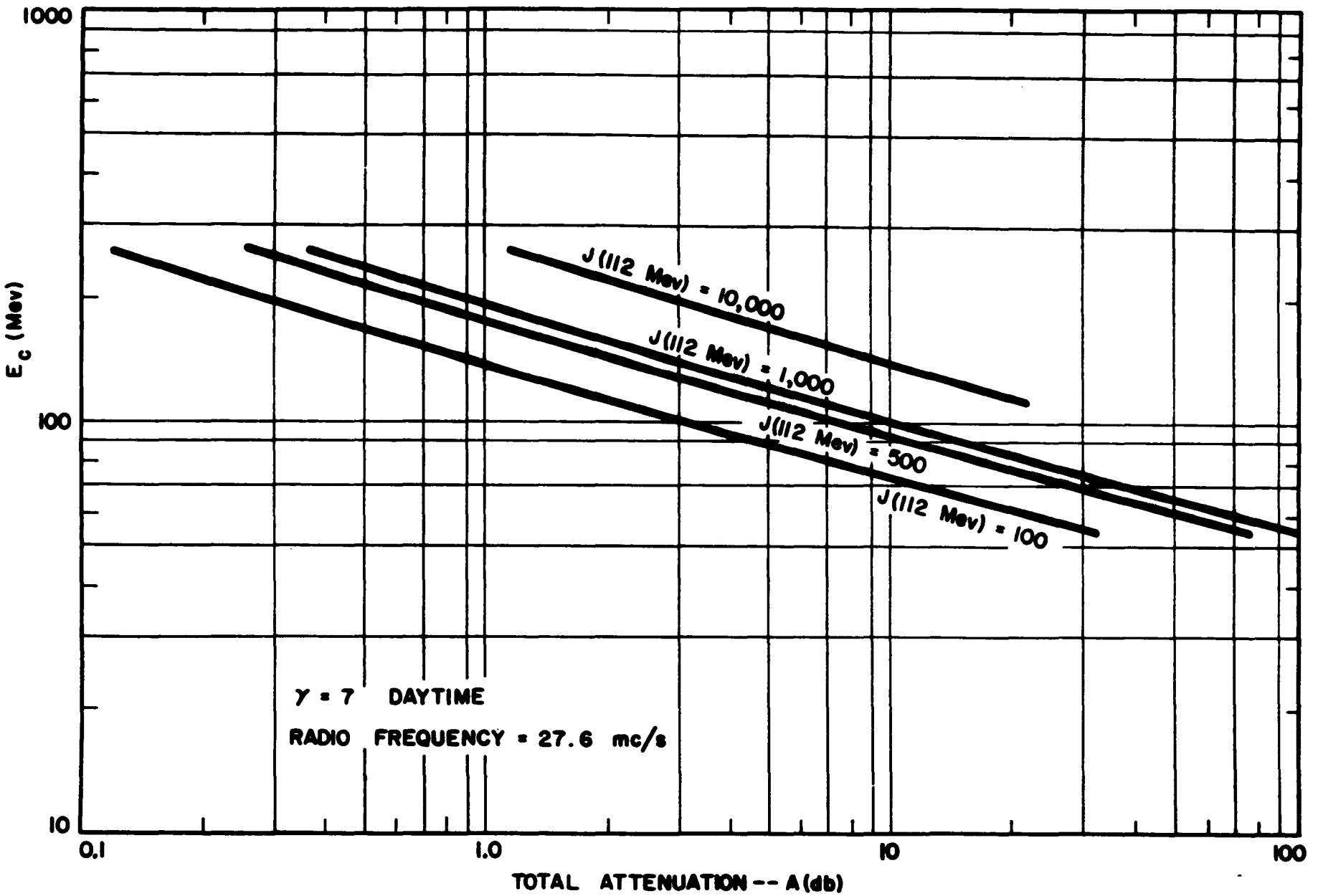
1000
100
10
E_c (Mev)
J(112 Mev) = 10,000
J(112 Mev) = 1,000
J(112 Mev) = 500
J(112 Mev) = 100
γ = 7 DAYTIME
RADIO FREQUENCY = 27.6 mc/s
0.1
1.0
10
100
TOTAL ATTENUATION -- A(db)

FIGURE 25

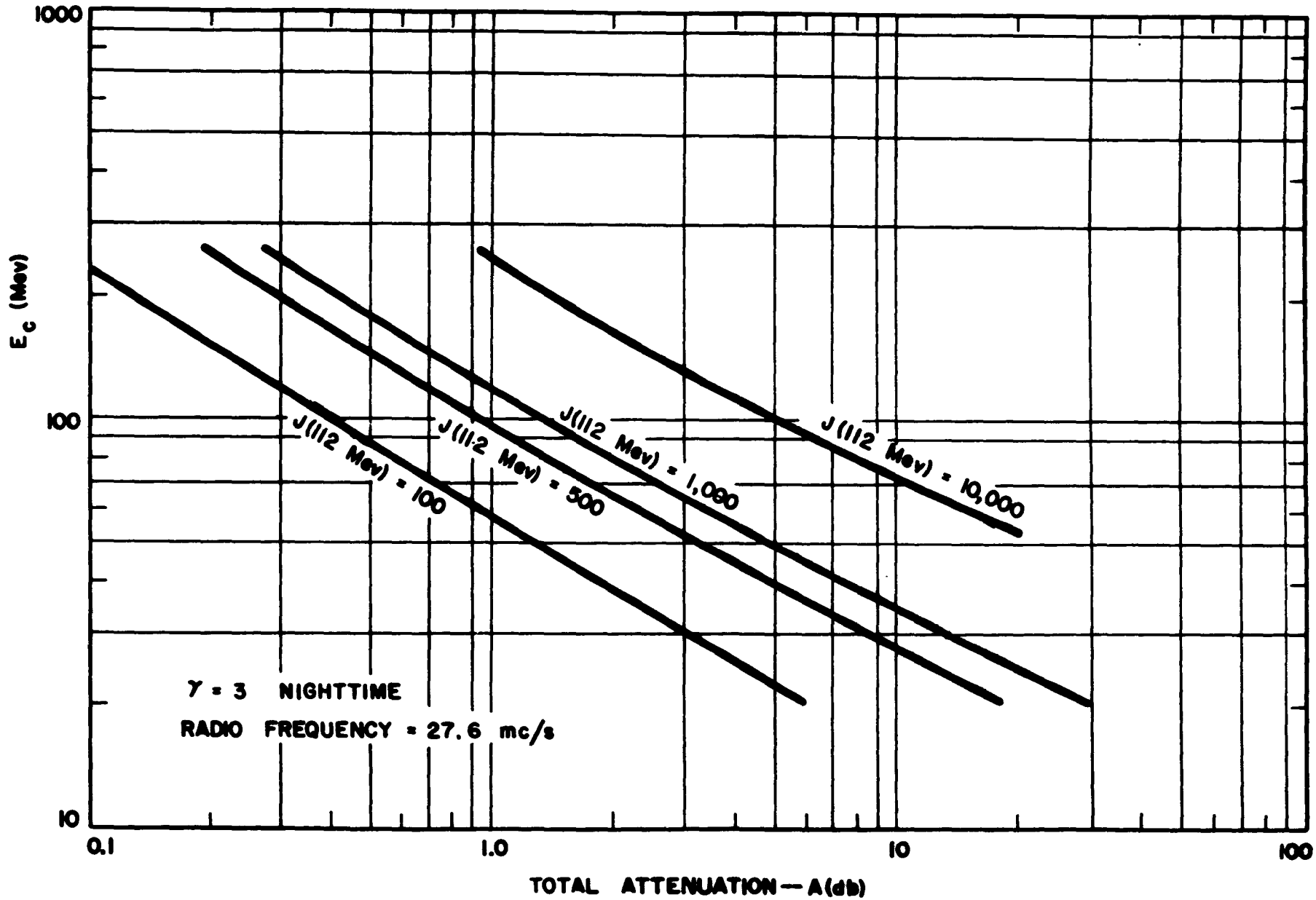
1000
100
10
E_c (Mev)
0.1
1.0
10
100
TOTAL ATTENUATION — A(db)
J(112 Mev) = 10,000
J(112 Mev) = 1,000
J(112 Mev) = 500
J(112 Mev) = 100
γ = 3 NIGHTTIME
RADIO FREQUENCY = 27.6 mc/s

FIGURE 26

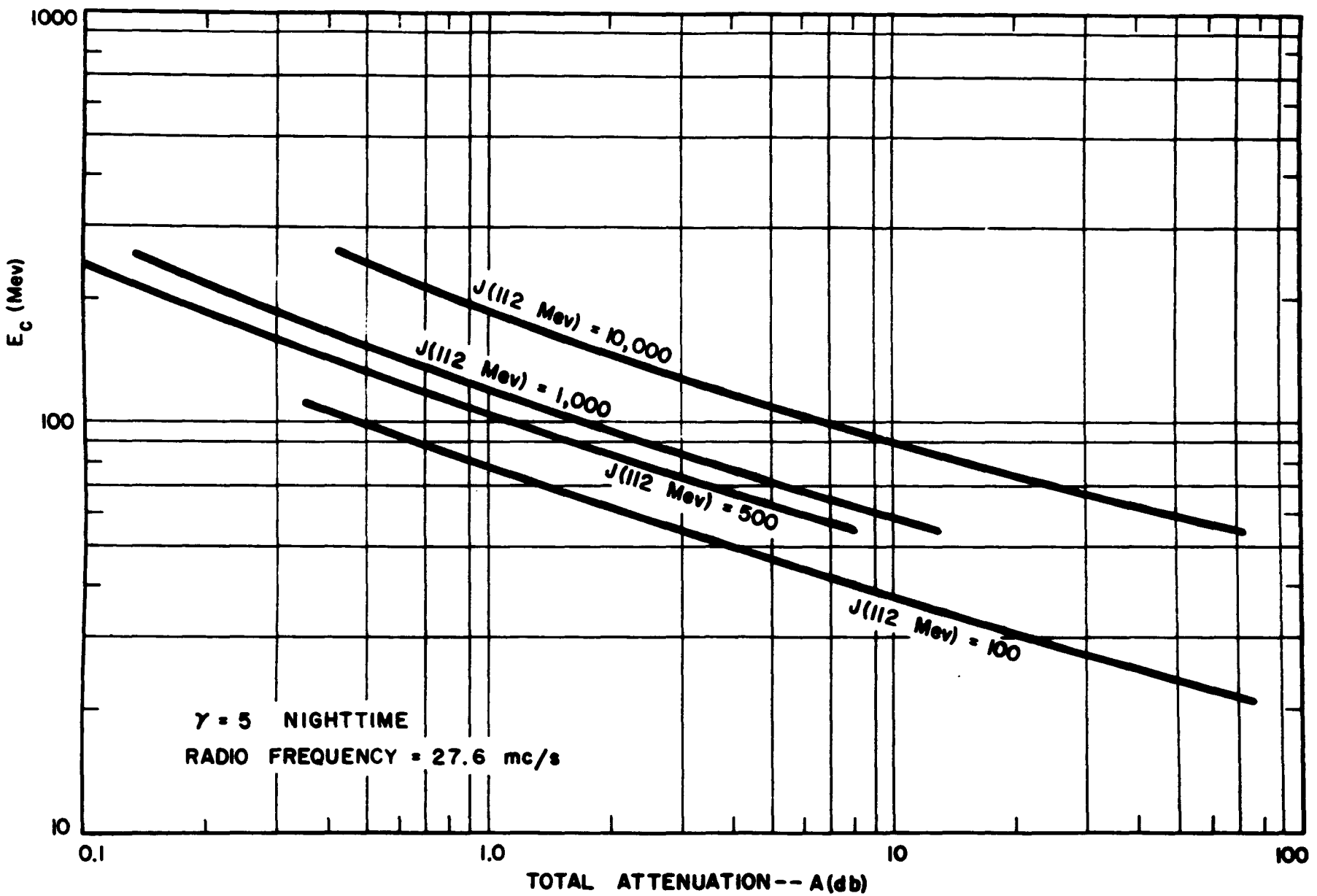
1000
100
10
E_c (Mev)
J(112 Mev) = 10,000
J(112 Mev) = 1,000
J(112 Mev) = 500
J(112 Mev) = 100
γ = 5 NIGHTTIME
RADIO FREQUENCY = 27.6 mc/s
0.1
1.0
10
100
TOTAL ATTENUATION -- A(db)

FIGURE 27

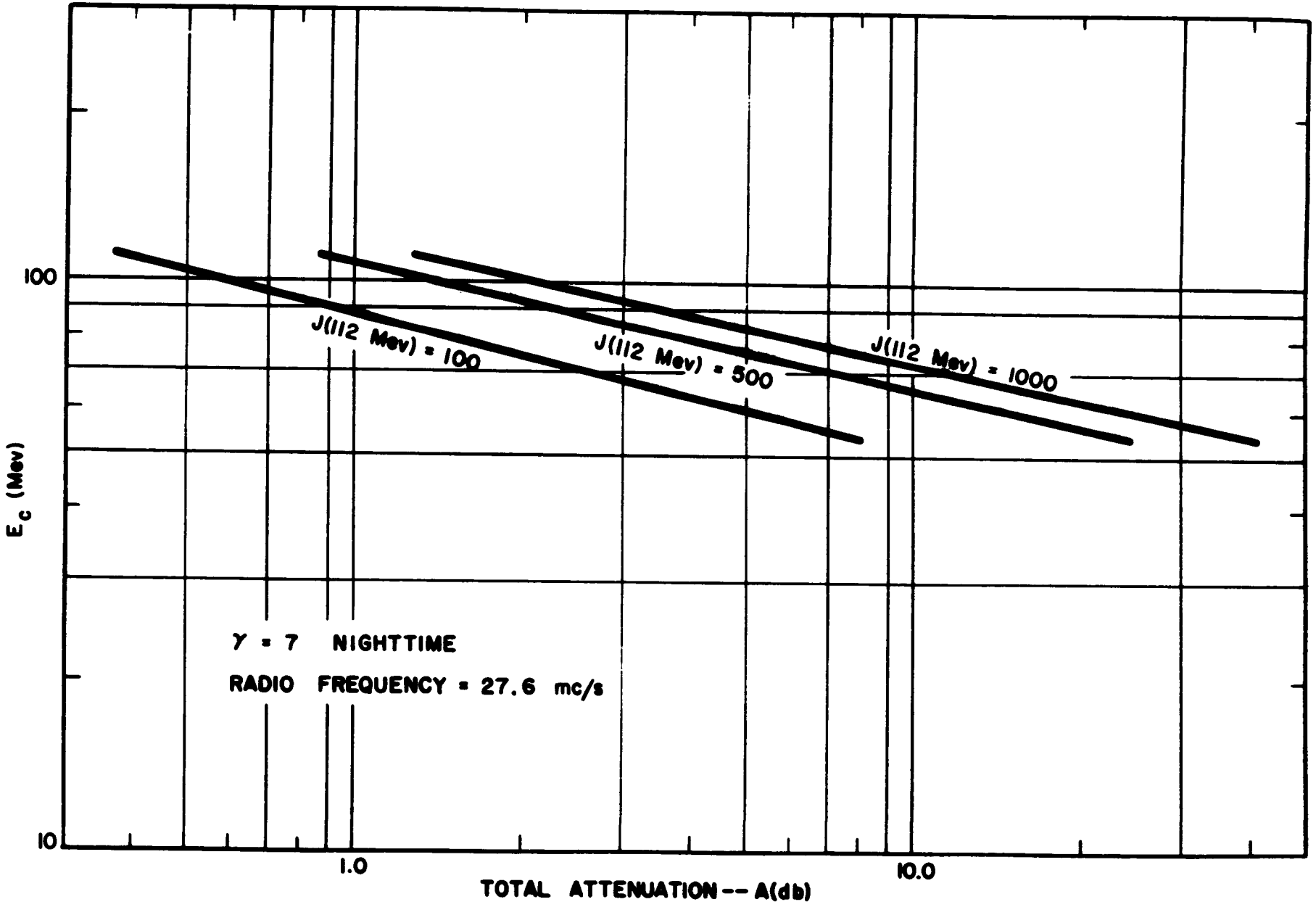
100
10
E_c (Mev)
J(112 Mev) = 100
J(112 Mev) = 500
J(112 Mev) = 1000
γ = 7 NIGHTTIME
RADIO FREQUENCY = 27.6 mc/s
1.0
10.0
TOTAL ATTENUATION -- A(db)

FIGURE 28

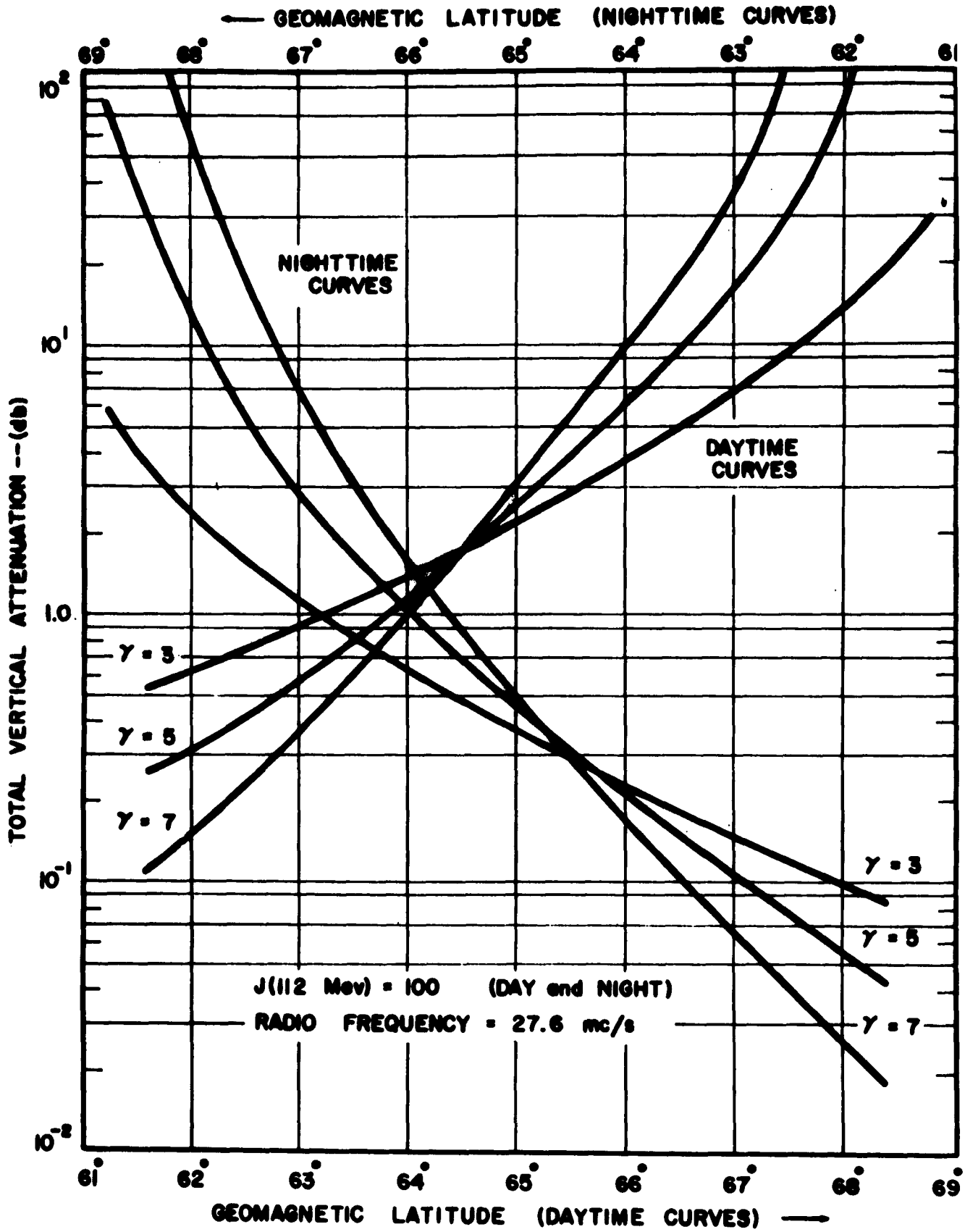
GEOMAGNETIC LATITUDE (NIGHTTIME CURVES)
69°
68°
67°
66°
65°
64°
63°
62°
61
10^2
10^1
1.0
10^{-1}
10^{-2}
TOTAL VERTICAL ATTENUATION --(db)
NIGHTTIME CURVES
DAYTIME CURVES
γ = 3
γ = 5
γ = 7
γ = 3
γ = 5
γ = 7
J(112 Mev) = 100 (DAY and NIGHT)
RADIO FREQUENCY = 27.6 mc/s
61°
62°
63°
64°
65°
66°
67°
68°
69°
GEOMAGNETIC LATITUDE (DAYTIME CURVES)

FIGURE 29

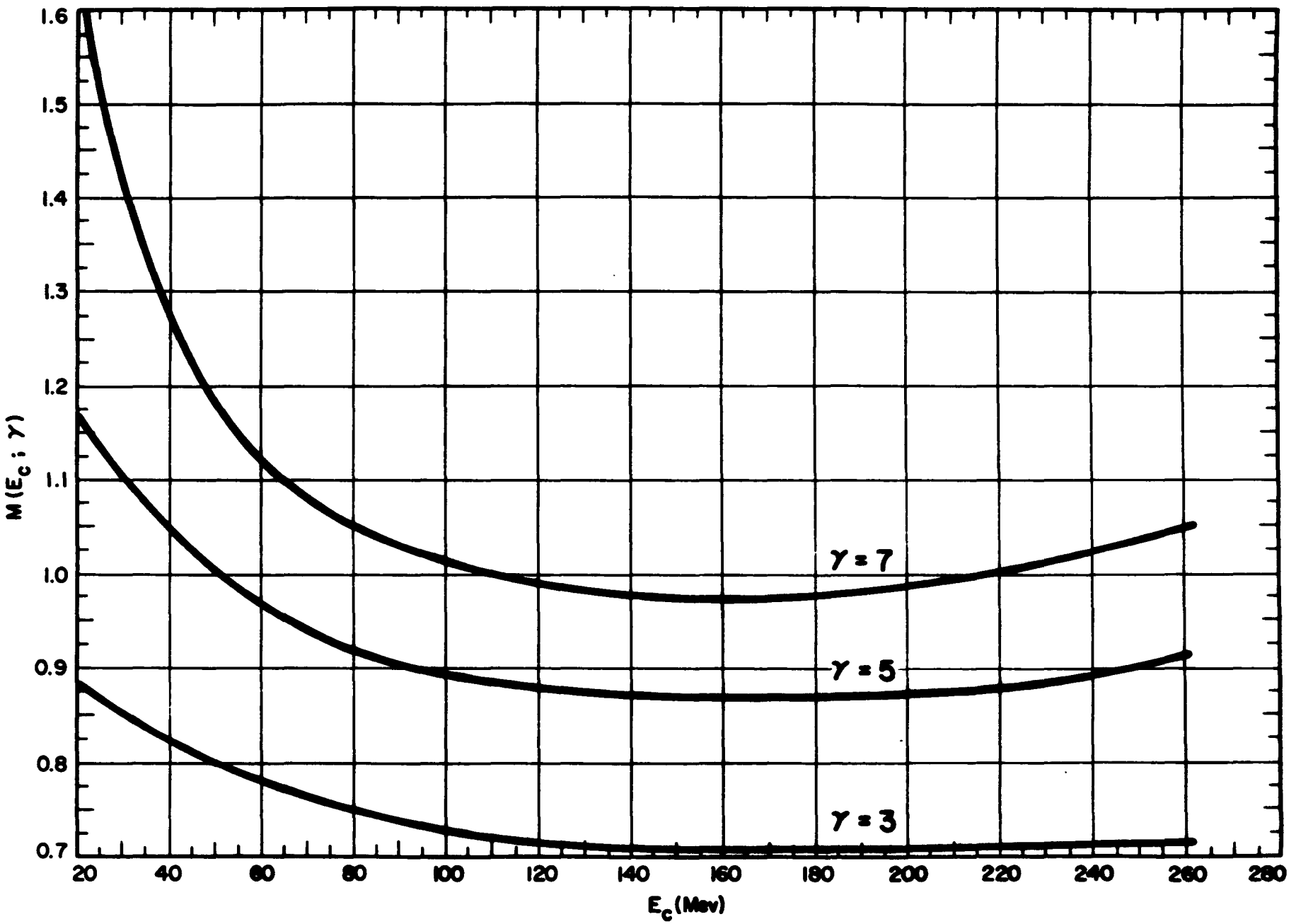
1.6
1.5
1.4
1.3
1.2
1.1
1.0
0.9
0.8
0.7
M(E_c ; γ)
γ = 7
γ = 5
γ = 3
20
40
60
80
100
120
140
160
180
200
220
240
260
280
E_c (Mev)

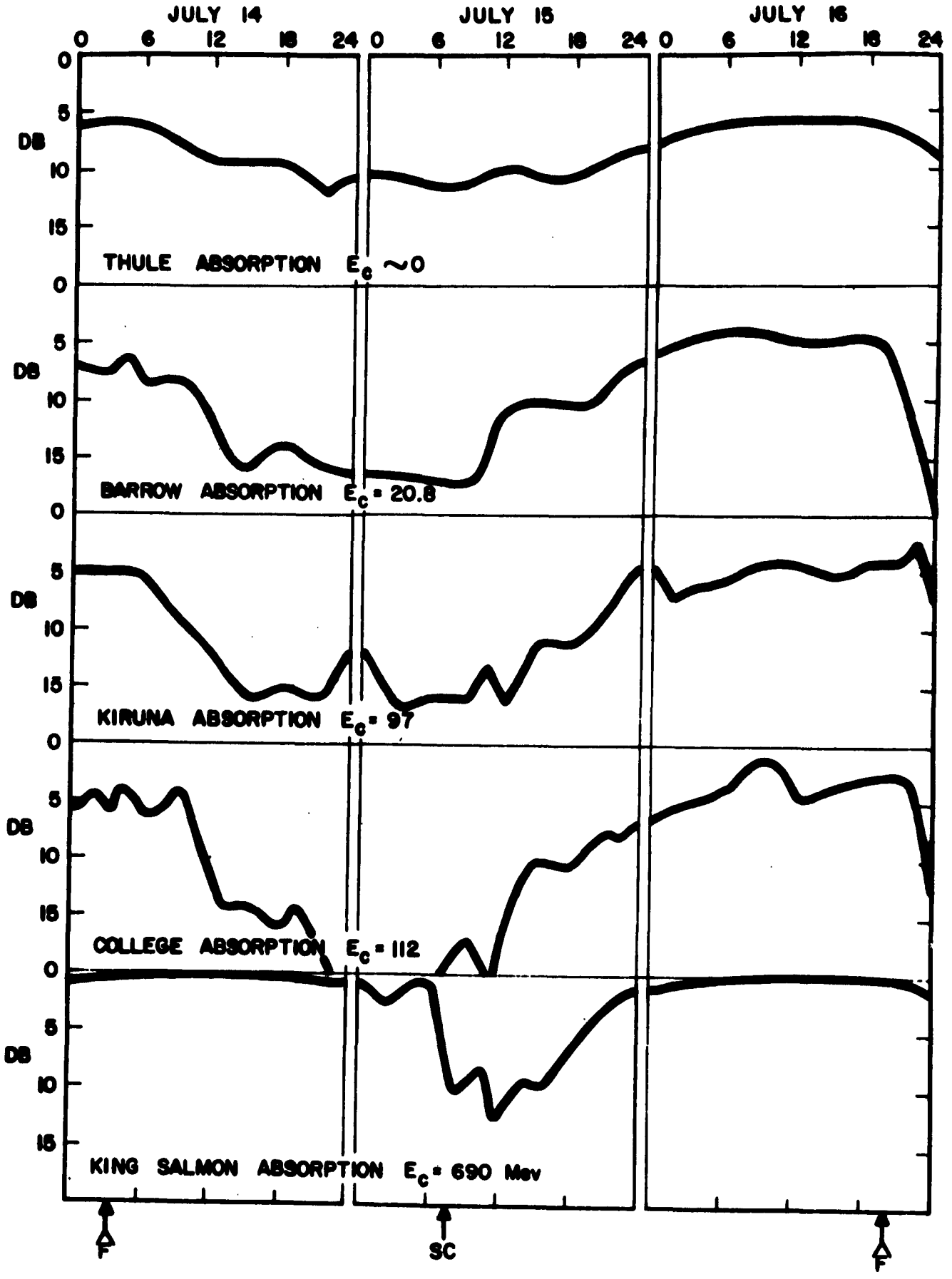
JULY 14
JULY 15
JULY 16
0 6 12 18 24 0 6 12 18 24 0 6 12 18 24
DB
0
5
10
15
THULE ABSORPTION $E_c \sim 0$
BARROW ABSORPTION $E_c = 20.8$
KIRUNA ABSORPTION $E_c = 97$
COLLEGE ABSORPTION $E_c = 112$
KING SALMON ABSORPTION $E_c = 690$ Mev
F
SC
F

FIGURE 31